



**Digital Image Correlation For Fatigue
Life Characterization Of
Ultrasonically Welded Lap Shear
Joints**

Ioan Bîrgăoanu-Acăei

Digital Image Correlation For Fatigue Life Characterization Of Ultrasonically Welded Lap Shear Joints

Ioan Bîrgaoănu-Acăei (4545249)

to obtain the degree of Master of Science

at the Delft University of Technology,

to be defended publicly on Tuesday September 12, 2022 at 10:00 AM.

Student number: 4545249

Thesis committee: Dr. ir. C. Rans, TU Delft, supervisor
Dr. ir. S. G. P. Castro, TU Delft, supervisor

An electronic version of this thesis is available at
<http://repository.tudelft.nl/>.

Contents

Contents	i
List of figures	iii
List of Symbols and Abbreviations	viii
Executive Summary	ix
1 Introduction	1
2 State Of The Art Challenges	2
3 Research Definition	6
3.1 Research objective	6
3.2 Research questions	6
3.3 Available experimental data	8
4 Methodology for single weld spot analysis	11
4.1 Creation of finite element database of simulations	12
4.1.1 Choice of finite elements	14
4.1.2 Choice of boundary conditions	14
4.1.3 Numerical representation of weld spot	15
4.1.4 Finite element implementation	16
4.1.4.1 Implementation limitations	16
4.1.4.2 Implementation verification	19
4.1.5 Choice of meshing technique	19
4.2 DIC to FEM strain field correlation	20
4.3 Measured reaction force to FEM reaction force correlation	20
4.4 Result analysis	22
5 Results for single weld spot analysis	24
5.1 Results displaying consistent agreement	24
5.1.1 Results for specimen 1 (0730-10)	24
5.1.2 Results for specimen 2 (0730-25)	28
5.2 Results displaying less agreement	30
5.2.1 Results for specimen 3 (0730-4)	30
5.2.2 Results for specimen 4 (0730-24)	35
6 Methodology for multiple weld spot analysis	38
6.1 Multiple spots fatigue experimental setup	38
6.2 Creation of finite element database of simulations	40
6.2.1 Choice of finite elements	40
6.2.2 Choice of boundary conditions	40
6.2.3 Numerical representation of weld spots	40
6.2.4 Finite element implementation	41
6.2.4.1 Implementation limitations	43

6.2.4.2	Implementation verification	44
6.2.5	Choice of meshing technique	44
6.3	DIC to FEM strain field correlation	44
6.4	Measured reaction force to FEM reaction force correlation	45
7	Results for multiple weld spot analysis	47
8	Discussion of results	62
8.1	Analysis of single weld spots	62
8.1.1	Comparison of results with previous research	62
8.1.2	Reflection on research questions	64
8.1.2.1	Surface strain field correlation research question	64
8.1.2.2	Increase in compliance analysis research question	65
8.1.3	Applicability of results	66
8.2	Analysis of multiple weld spots	66
8.2.1	Reflection on research questions	66
8.2.2	Applicability of results	66
9	Recommendations for future research	68
9.1	Single weld spot analysis recommendations	68
9.2	Multiple weld spot analysis recommendations	68
10	Conclusion	69
	Bibliography	70
	Appendix A Single Weld Spot Fatigue Evolution Results	72
A.1	Examples for specimen 0730-10 from [15]	72
	Appendix B Multiple Weld Spot Fatigue Evolution Enhancement Masks	73
	Appendix C Convergence study of finite element solution, single weld spot	76
	Appendix D Convergence study of finite element solution, multiple weld spots	78
	Appendix E Single wed spot specimen 2 (0730-25) analysis details	80
	Appendix F Single wed spot specimen 4 (0730-24) analysis details	84

List of Figures

- 2.1 Schematic drawings of the ultrasonic welding process. 2
- 3.1 Schematic of single lap shear joints welded through a single ultrasonic weld spot, and the fracture surfaces of the specimens presented in this report. Fracture surface pictures courtesy of [14]. 9
- 3.2 Schematic of single lap shear joints welded through a column of four ultrasonic weld spots, and the fracture surface of the specimen presented in this report. . . 10
- 4.1 Overview of the methodology presented in this thesis for assessing the damage state in a lap shear joint welded through ultrasonic spot welds. 12
- 4.2 Effect of disbonding criteria on the damage states simulated. 13
- 4.3 Sketch of specimen dimensions used for single weld spot testing in [15]. Picture courtesy of [15]. 15
- 4.4 Sketch of real boundary conditions used for single weld spot testing in [15]. Picture courtesy of [15]. 15
- 4.5 Sketch of boundary conditions used in FEM analysis. 15
- 4.6 Weld spot modelling representation through nodal tie constraints. 16
- 4.7 Simulated surface strain distributions for a perfectly round weld spot with continuum solid shell elements in Abaqus. 17
- 4.8 Simulated surface strain distributions for a perfectly round weld spot with the custom implementation of continuum solid shell elements. 18
- 4.9 Strains compared on the middle line of the overlap area pf the single weld spot specimens, extracted from figure 4.7 and figure 4.8 at the locations at the red lines. 18
- 4.10 Mesh used to model the lap shear test specimens, in its undeformed state in green and in its exaggerated deformed state, which is a result of the simulation, in red. 19
- 4.11 Simulated weld area influence on reaction force for a fixed displacement loading, specimen 0730-10 of [15]. 21
- 4.12 Reaction forces measured by the test machine during the fatigue test for specimen 0730-10 of [15], and the corresponding weld area matched by correlating simulated reaction forces. 22
- 4.13 Percentage of weld area disbonded, estimated throughout the test, with respect to the initially match weld area and with respect to the area of the fracture surface, traced by hand. The result corresponds to specimen 0730-10 of [14], which includes the analysis results of [15] [14]. 23
- 5.1 DIC to FEM strain field correlation results for specimen 1, loading cycle 50, longitudinal component (E11). 25
- 5.2 DIC to FEM strain field correlation results for specimen 1, loading cycle 2500, longitudinal component (E11). 26
- 5.3 DIC to FEM strain field correlation weld area results for specimen 1. 27
- 5.4 DIC to FEM strain field weld area results overlapped with measured reaction force to FEM reaction force correlation results for specimen 1. 27
- 5.5 Measured reaction forces and simulated dependency between weld area and reaction force for specimen 1. 28
- 5.6 DIC to FEM strain field correlation weld area results for specimen 2. 29

5.7	DIC to FEM strain field weld area results overlapped with measured reaction force to FEM reaction force correlation results for specimen 2.	29
5.8	Measured reaction forces and simulated dependency between weld area and reaction force for specimen 2.	30
5.9	DIC to FEM strain field correlation results for specimen 3, loading cycle 50, longitudinal component (E11).	31
5.10	DIC to FEM strain field correlation results for specimen 3, loading cycle 2500, longitudinal component (E11).	32
5.11	DIC to FEM strain field correlation results for specimen 3, loading cycle 2550, longitudinal component (E11).	33
5.12	DIC to FEM strain field correlation weld area results for specimen 3.	34
5.13	DIC to FEM strain field weld area results overlapped with measured reaction force to FEM reaction force correlation results for specimen 3.	34
5.14	Measured reaction forces and simulated dependency between weld area and reaction force for specimen 3.	35
5.15	DIC to FEM strain field correlation weld area results for specimen 4.	36
5.16	DIC to FEM strain field weld area results overlapped with measured reaction force to FEM reaction force correlation results for specimen 4.	36
5.17	Measured reaction forces and simulated dependency between weld area and reaction force for specimen 0730-24.	37
6.1	Geometry of square specimen successfully manufactured, picture courtesy of the authors of [15].	39
6.2	Geometry of column specimen successfully manufactured, picture courtesy of the authors of [15].	39
6.3	Weld spot modelling representation through nodal tie constraints.	41
6.4	Simulated surface strain distributions for a column of perfectly round weld spot with continuum solid shell elements in Abaqus.	42
6.5	Simulated surface strain distribution for a perfectly round weld spot with the custom implementation of continuum solid shell elements.	43
6.6	Mesh used to model the lap shear test specimens, in its undeformed state in green and in its exaggerated deformed state, which is a result of the simulation, in red.	44
6.7	Simulated weld area influence on reaction force for a fixed displacement loading.	45
6.8	Simulated weld area influence on reaction force for a fixed displacement loading.	46
7.1	DIC to FEM strain field correlation results, loading cycle 50, longitudinal component (E11).	49
7.2	DIC to FEM strain field correlation results, loading cycle 4500, longitudinal component (E11).	51
7.3	DIC to FEM strain field correlation results, loading cycle 6000, longitudinal component (E11).	54
7.4	DIC to FEM strain field correlation results, loading cycle 25050, longitudinal component (E11).	56
7.5	Strain fields measured through DIC after 25500 loading cycles.	57
7.6	DIC to FEM strain field correlation weld area results.	58
7.7	Correlated weld area, using the enhanced database of simulations for reaction force correlation.	58
7.8	Relative change in correlated weld area, using the enhanced database of simulations for reaction force correlation.	59
7.9	Reaction forces measured by the test machine during the fatigue test.	59

7.10	Correlated weld area.	60
7.11	Relative change in correlated weld area.	60
8.1	Comparison of the relative disbonding damage accumulation between the results obtained by strain field and reaction force correlation, proposed in this field, and the method of strain field analysis proposed by [15].	63
A.1	Various partly broken weld masks from the database of simulations.	72
B.0	Weld mask split into all combinations of individual welds.	75
C.1	Surface strain distribution, computed with the custom made finite element implementation. The red line represents the middle of the overlap, where surface strains are compared in the convergence study. 40x40x2 elements per plate over the overlap.	76
C.2	Influence of increasing the number of finite elements, through the thickness of the plates, on the simulated surface strain distribution at the mid-line of the joint overlap.	77
C.3	Influence of increasing the number of finite elements, along the length and width of the plates, on the simulated surface strain distribution at the mid-line of the joint overlap. The legend specifies the number of elements used to represent the plates over the 40x40mm overlap area	77
D.1	Surface strain distribution, computed with the custom made finite element implementation. The red line represents the middle of the overlap, where surface strains are compared in the convergence study. 145x40x2 elements per plate over the overlap.	78
D.2	Influence of increasing the number of finite elements, through the thickness of the plates, on the simulated surface strain distribution at the mid-line of the joint overlap.	79
D.3	Influence of increasing the number of finite elements, along the length and width of the plates, on the simulated surface strain distribution at the mid-line of the joint overlap. The legend specifies the number of elements used to represent the plates over the 40x40mm overlap area	79
E.1	DIC to FEM strain field correlation results for specimen 2, loading -cycle 50, longitudinal component (E11).	81
E.2	DIC to FEM strain field correlation results for specimen 0730-25, loading cycle 2500, longitudinal component (E11).	82
F.1	DIC to FEM strain field correlation results for specimen 0730-24, loading cycle 50, longitudinal component (E11).	85
F.2	DIC to FEM strain field correlation results for specimen 0730-24, loading cycle 2500, longitudinal component (E11).	86

List of Symbols and Abbreviations

Abbreviation	Meaning
NDT	Non-destructive measurement technique
DIC	Digital image correlation (NDT)
AE	Acoustic emission (NDT)
FEM	Finite element modelling
CSS8	Continuum solid shell element with 8 nodes, notation used by Abaqus
SC8R	Continuum solid shell element with 8 nodes and reduced integration, notation used by Abaqus

Executive summary

Before ultrasonic welding can be used to join composite components used in primary structural assemblies, their mechanical properties over the expected operational life need to be understood. While the main research effort of the ultrasonic welding community is oriented towards achieving welds of high quality, some research on modelling the fatigue life behavior of ultrasonic spot welds is already being conducted, in anticipation of the need to certify the use of ultrasonic welding technology, within the Aerospace Structures and Materials department at TU Delft [15][14]. In order to validate any numerical model used to predict the mechanical properties of an ultrasonically welded composite assembly, experimental measurements of the evolution of the state of damage associated with the welds is needed. Because the ultrasonic welds lie at the interfaces between composite parts, it is not possible to directly observe optically the state of the welds. Non-destructive direct measurements of the welds could only be conducted through techniques which can penetrate the composite parts, of which the most accurate and prohibitively expensive would be X-ray scanning, and a less accurate yet more affordable technique would be ultrasonic scanning. Although ultrasonic scanning would be a suitable technique for measuring the shape and area evolution of ultrasonic weld spots subjected to repeated loading, it is labor intensive to perform at regular intervals within fatigue lifetime tests. A more automatic means of gaining insight into the damage state of ultrasonic welds is needed for the fatigue life modelling research to become practical and productive. This thesis proposes the interpretation of surface strain fields, measured through digital image correlation, and the interpretation of the increase in compliance of a welded joint as fatigue damage progresses, recorded by the test machine as force-displacement relationships, as indirect methods of measuring the state of damage accumulated within the ultrasonic weld spots. A similar analysis has been done by [15] for lap shear joints containing a single ultrasonic spot weld, by interpreting the inflexions in the surface strain fields as an indication of load transfer at the weld location, with good agreement between the approximated weld area reduction and the measured increase in compliance. Within this thesis the interpretation of measured surface strain fields and of recorded load-displacement data is done by comparison to a collection of finite element simulations corresponding to ultrasonic weld spots containing various degrees of damage. This research aims to present a method of strain field interpretation that is more generalizable to the analysis of lap shear specimens containing multiple ultrasonic weld spots.

The research presented in this thesis is restricted to the study of composite lap shear joints, welded through either a single weld spot, or a column of four aligned weld spots. The surface strain fields were measured with two digital image correlation systems, on both sides of the overlap of the lap shear joint, at regular intervals within the fatigue test. The load-displacement relationship was recorded by the fatigue test machine at the peaks of each loading cycle. The finite element method was used to simulate the experimental conditions, with specimens containing ultrasonic welds containing various degrees of fatigue damage, represented only as weld disbonding damage. In order to represent the geometry and the mechanical properties of the welded plates, a regular mesh with continuum solid shell elements was used. The ultrasonic spot welds were modelled by using tie constraints between the nodes of the plates at the location of the weld. Disbonding damage within the welds was represented by eliminating the tie constraints at the nodal locations where the damage was located. For each pair of strain fields measured at a given loading cycle through digital image correlation, the closest matching pair of simulated strain fields is searched within the collection of finite element simulations. Strain field similarity is assessed through a weighed cross-correlation function. The modelled weld shape used to generate the best matching

pair of simulated strain fields is assumed to be representative of the real weld inside the tested lap shear joint, at the moment of the measurement. Correlating the compliance of the real specimen throughout the test, with the compliances of the simulated lap shear joints containing damaged welds, provides an indirect method of verifying that the results of strain field analysis are plausible.

The analysis results for specimens containing a single weld spot showed good agreement with the earlier results published by [15]. The analysis of single ultrasonic weld spots presented in this thesis extends the results beyond those obtained by [15], for the entire fatigue life of the specimens. Moreover, for the analysis of single weld spots, the method showed the capability of characterizing the weld area as well, rather than only the relative change in area.

Strain field interpretation is sensitive to the accuracy of the acquired digital image correlation data. The analysis of strain fields measured over the overlap of the larger specimen containing four ultrasonic weld spots in a column was much less accurate when compared to that of the strain fields measured over the smaller lap shear specimens containing a single weld spot, because the strain field measurements were less precise. The same digital image correlations were used in both test campaigns, but for the larger specimen containing multiple weld spots, the cameras had to be placed further away from the specimen in order to capture the overlapping area within the field of view, leading to a more coarse spatial resolution of results. The strain field analysis could only be used for a rough characterization of damage for each weld spot, into three levels: undamaged, significantly damaged and completely broken. Having said that, it was observed that the database of simulated strain fields corresponding to damaged weld spots contains the correct order of failure of the weld spots. If further experiments could validate this observation, it would mean that the simulations have already captured the correct order of weld spot failure, which is a starting point for further fatigue life modelling of ultrasonically welded lap shear joints.

The recommendation for future research is to conduct a test campaign of fatigue tests to include ultrasonic scanning of the weld spots at regular intervals throughout the fatigue life. Ultrasonic scanning would provide direct measurements of the disbonding damage accumulation within the weld spots. Direct measurements are needed to validate the results of the indirect measurement methods proposed in this thesis and by [15], before indirect methods of measurements are used to validate numerical predictions. Another recommendation is to exploit the usage of acoustic emission as a non-destructive measurement technique, alongside digital image correlation, to localize the accumulation of damage within the ultrasonically welded lap shear joints. Interpretation of surface strain fields has proven to be effective at characterizing the amount of disbonding damage accumulated, and acoustic emission has the potential to localize the damage within the weld spots more accurately.

1 Introduction

In the pursuit of reducing the carbon footprint of commercial aviation, the structural design of aircraft plays a significant role as one of the main subsystems of an airplane. Reducing the environmental influence of aircraft can in part be achieved by designing more efficient structures, that can carry more payload. Continuous fiber reinforced plastics, which for simplicity will be referred to as composites for the remainder of the thesis, with their directionally dependent mechanical properties, can potentially be used to create lighter structures when compared to the traditional metallic counterparts. This has incentivized research into replacing airframe components, traditionally made of metal, with composites.

Traditionally, metallic aircraft components are joined with mechanical fasteners, mainly rivets and bolts. Those joining techniques are not well suited for joining composite components, primarily because they involve drilling of holes which often damage the composite material beyond the intended perimeter of the hole. Therefore, composites are best joined by adhesive bonding and by welding, which avoids drilling holes in the components.

One of the emerging welding techniques for thermoplastic composites is ultrasonic welding. Ultrasonic spot welding has the potential to be composite counterpart of the widely used, highly automatized spot welding technique used to join metals. State of the art research on ultrasonic welding is focusing on the welding process itself in search of the process parameters that allow consistent manufacturing of high quality welds. To complement this effort, the research of this thesis looks ahead at assessing the durability of welded products, which is the next step after assuring a good weld was created. This research aims to support the study of damage progression in ultrasonically welded components subjected to repeated loading, by providing a method of comparison between the observed surface deformation of joined components under lab experiment conditions and expected deformations predicted for the experiment with numerical modelling techniques.

2 State Of The Art Challenges

Ultrasonic welding is an emerging joining technique for thermoplastic composites, in which two thermoplastic composite parts are melted locally and thus fused, through the application of vibration and pressure. Ultrasonic welding has the potential to automate at low cost the production of welds with optimized patterns that improve qualities such as durability and damage tolerance. The welding apparatus could be mounted on robotic arms and controlled with high precision to create efficient weld patterns. An overview of the ultrasonic welding machine and of the ultrasonic welding process is given in figure 2.1. Researchers are currently studying the process parameters of ultrasonic welding in order to achieve consistent, high quality welds. The works of [22], [25], [24] [1], [4], [5], [23], [7] are some of the significant recent contributions on the study of the ultrasonic spot welding and continuous welding process. Parameters such as weld energy, sonotrode size, applied pressure, applied displacement, application of energy director and boundary conditions can influence the outcome of the welding process. The current focus of the ultrasonic welding research community is to understand the interaction between the main parameters influencing the weld quality in order to achieve consistent quality in manufacturing.

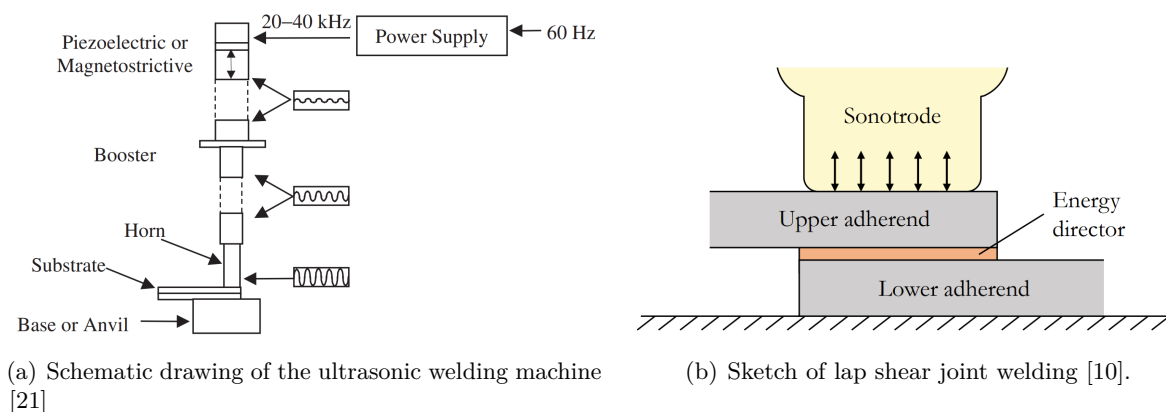


Figure 2.1: Schematic drawings of the ultrasonic welding process.

While research on the method of creating strong and uniform welds is crucial before any industrial applications of the process can be conceived, this is only the first step towards using ultrasonic welding on aircraft components. In order for ultrasonic welding to be accepted in the aviation industry, the parts manufactured by welding have to have predictable mechanical properties in order to ensure the safety of the structure. The durability of the welds under repeated flight loads has to be proven to certification authorities before ultrasonic welding can be used to help make aircraft lighter. To this end, studies into the fatigue life of such welds have to be conducted in order to allow to damage tolerant designs to be created, that can be proven to be safe by the acceptable means of compliance.

In order for any model describing the damage accumulation in an ultrasonic weld to be valuable, its accuracy has to be validated by experiment. This creates a need for efficient experimental quantification of damage accumulation in ultrasonic welds, which is not sufficiently addressed by existing research.

There are a number of non-destructive techniques that can be used to observe the accumulation

of damage in a composite part at different measurement scales. A comprehensive review has been published by [3]. Each non-destructive inspection technique has its domain of applicability, the best results being obtained when multiple techniques are combined at the same time to compensate each other's limitations. Among those, the most practical to be used to observe the failure of an ultrasonically welded spot weld, that do not require stopping the fatigue test and do not require extra measures to ensure health safety, are digital image correlation, infrared thermography and acoustic emission. Acoustic emission and digital image correlation are often combined effectively to obtain good damage localization and insight into the mechanism of damage progression, see [8], [13] [12] and [20]. Those techniques are well suited for tracking delamination and disbonding like defects. This study will focus on the usage of digital image correlation alone in order to explore its capabilities in quantifying weld fatigue damage modelled as disbonding.

Digital image correlation is a non-destructive measurement technique which tracks surface deformations of structure with the aid of pairs of cameras arranged in a stereo format. The method relies on the surface of the body to be highly textured, which is regularly achieved in laboratory conditions by painting the specimen with a fine speckle pattern. By tracking the motion of the textured features in subsequent pairs of images, the surface deformation field of a loaded structure can be approximated. From the surface deformations, measures of strain can be computed, which is often compared to the strains predicted through the use of numerical models for the purpose of model validation. It may be possible, however, to use the good match between the surface strains predicted by a numerical model and the surface strains measured with digital image correlation to gain insight about the state of hidden damage within a tested structure. Measurements made during fatigue tests of ultrasonically welded lap shear joints could be used, in conjunction with a numerical model, to gain insight into the accumulation of damage within the weld spots. Such insight would be valuable for understanding the mechanical properties of ultrasonic welds when subjected to cyclic loading, and will stand as validation data for future modelling efforts of the ultrasonic weld fatigue life.

Research is currently being conducted within the Aerospace Structures and Materials department at TU Delft on modelling the fatigue damage evolution of ultrasonic spot welds. These pioneering studies are restricted to ultrasonically welded lap shear specimens. From a fatigue response modelling perspective, lap shear test results have to be treated with caution because the test combines multiple failure modes, see the publication of [19]. The research only focuses on the fatigue life of spot welded lap shear test samples because they are easier to manufacture consistently with the available welding technology. Currently, to the best of the author's knowledge, only one conference paper study has been published on measuring the fatigue damage accumulation of ultrasonically welded lap shear joints [15]. In [15], inflections in the surface strain fields measured with digital image correlation are used to infer the state of damage in lap shear specimens welded ultrasonically through a single, approximately round spot. The rate of damage accumulation showed good agreement with the increase of compliance of the specimen, associated with gradual breaking of the weld spot, throughout the fatigue life of a specimen. Albeit successful in approximating damage evolution for over 75% of the fatigue life, the method presented in [15] is limited to the analysis of lap shear specimens containing a single ultrasonic weld spot. The search continues for a method that can be used to assess the damage state in lap shear specimens containing multiple ultrasonic welds.

In addition to [15], the conference publication discussing the first attempt to quantify the accumulation of damage in ultrasonically welded lap shear joints through the analysis of strain fields measured through the use of digital image correlation, the main author of [15] is also

working on a yet unpublished PhD thesis on the fatigue life modelling of ultrasonic welds. This thesis which will be referenced to as [14], within this research, until publication, as the authors kindly provided the data collected throughout the entire test campaign from which the data published in [15] originates. The data consists in surface strain fields, measured through digital image correlation, on both sides of the specimen as mentioned in [15], and in the reaction forces recorded by the test machine throughout the fatigue tests.

The measured surface strain fields provided by [14] can be formatted as digital image data, which is then suitable for analysis through image processing techniques. The literature on digital image processing is vast, ranging from analytical methods to methods based on artificial intelligence. Analytical methods of processing have the advantage of being completely understandable, it is possible to fully explain the result of analytical processing through the formulas used. Methods based on artificial intelligence have the potential of compensating for imperfect data, and are suitable when subjective, variable interpretation of the image data is required. At the start of a research path it is advantageous to build a basis of experience using available analytical methods, which can subsequently be used as a reference for comparison with other data-driven approaches, because the results obtained are fully transparent and repeatable. [18] covers comprehensively the most common image processing technique, and includes analytical functions for assessing the similarity of pairs of images, such as through the sum of absolute differences between the pixel values, or through cross correlation of image areas. If the measured and the simulated surface strain fields of the lap shear joints analyzed by [15] can be formatted as digital images, then those techniques can be applied to assess the similarity between measured strain fields and the simulated strain fields. The similarity between measurement and simulation could then be used to interpret the strain measurements on the surface of the lap shear joints to infer information about the state of damage inside each the weld spots at the interface between the welded plates. A comparison of measured and simulated surface strain fields, interpreted as digital images, may be suitable for the characterization of damage in lap shear specimens containing a multiple weld spots in any manufacturable configuration, as the method of strain field interpretation is relatively free of assumptions about the mechanical properties of the specimen. The physical behavior is included in the interpretation through the simulation methods used for generating comparison images of strain fields, rather than directly in the strain field interpretation method as in [15]. By updating only the simulations used in the comparison to be representative of the real tests on which measurements are made, the image same comparison method may remain applicable across any ultrasonically welded specimens. Such flexibility would be of great value to the ultrasonic welding modelling community, who would be able to validate their models on a large variety of ultrasonically welded lap shear joints using a consistent method of analysis.

Methods of inferring state of damage within a structure, by estimating the compliance of the structure from force-displacement data during laboratory tests, have been standardized within the fracture mechanics research community [17], [16]. The force-displacement curves throughout the fatigue life of each specimen tested by [14] could therefore be used as a secondary source of information about the total damage accumulated in a lap shear joint. [15] has already compared, with good results, the increase in compliance of lap shear joint specimens, welded through a single ultrasonic weld spot, to the estimated accumulated damage from the analysis of surface strain fields. The measured and simulated force-displacement data for each specimen may yield additional insight into the total amount of accumulated fatigue damage in the ultrasonic spot welds of a lap shear joint specimen. A comparison between compliance and rate of damage accumulation, as done by [15], serves as a validation of the rate of damage accumulation made through surface strain field analysis, because the interpretation of force-displacement data and of surface strain fields is done independently of each-other. A comparison between the total

damage estimations in an ultrasonically welded lap shear joint, made through force-displacement curve comparison and surface strain field comparison between real measurements and simulated results, would serve as a useful partial validation of more detailed damage characterization. The validation would be only partial, as both total damage estimations would be done by comparison to finite element simulations, yet still potentially useful to provide confidence in more detailed damage estimations. The more detailed the damage in ultrasonically welded lap shear joints can be characterized, the more validation data will be available for future fatigue life modelling efforts.

3 Research Definition

With the anticipated research need of quantifying the accumulation of disbonding damage in ultrasonically welded joints in sight, this section encapsulates the research goals of this thesis. The research objective will be stated. Questions and sub-questions will be noted that guide the research process towards achieving the research objective. An overview of the experimental data used to answer the research questions will be included.

3.1 Research objective

The main objective of this thesis is to quantify the accumulation of disbonding damage, due to repetitive loading, in ultrasonically spot welded lap shear specimens, by comparing surface strain measurements made with digital image correlation to simulated surface strains using the finite element method. The desired outcome of this thesis is a damage quantification procedure that remains effective when used on spot welded lap shear specimens of different sizes, with different number and arrangements of spot welds.

The secondary objective of this thesis is to investigate whether measured force-displacement data can be interpreted with the help of simulated force-displacement relationships to quantify the state of overall damage in an ultrasonically welded lap shear joint. Measured compliance reduction can be used as an indication of global damage accumulation within a structure [17] [16]. Correlation of compliance reduction with a finite element model may yield more information into the amount of disbonding damage accumulated at the weld locations of an ultrasonically welded lap shear joint.

3.2 Research questions

In order for the research objective of this thesis to be achieved, several questions have been formulated to guide the research process. The research questions have been split into questions about lap shear test specimens welded with a single spot, and lap shear test specimens welded with multiple spots, in different configurations. The research is therefore split into two phases: a phase about establishing a damage quantification procedure that works consistently for specimens welded with a single spot, and a phase about testing the applicability of the procedure in more general situations.

The distinction between quantifying the damage accumulation in a single weld spot, versus quantifying the damage accumulation in multiple weld spots simultaneously is relevant for this thesis for three reasons. First, the expected surface strain fields are better correlated to the state of a weld inside the lap joint when the weld provides a single load path consisting of a single weld spot. When multiple spot welds are created, each of them provides a load path between the plates of the lap shear specimen. The strain redistribution due to accumulated damage will depend not only on the extent of the damage within the welds, but also on the geometrical distribution of the weld points which provide alternative load paths. Such complexity is to be avoided in initial stages of research in order to ease the interpretation of results. The second reason for splitting the research into a single weld spot analysis phase and a multiple spot testing and analysis phase is related to state of the art manufacturing limitations. Manufacturing lap shear test specimens containing several high quality ultrasonic spot welds is still a difficult task actively

researched. There is the possibility that some ultrasonic spot weld configurations may not even be successfully manufactured within the scope of this thesis, and it is likely that there will be a larger variation in the shape of welds in specimens containing multiple spots. Correlating the surface strain fields of less uniform, more randomly shaped welds to simulations is more difficult as it requires a larger database of simulations to cover the variation in the mechanical and geometrical properties of the manufactured welds. The third reason for considering the analysis of specimens with multiple ultrasonic spot welds separately from that of specimens with a single spot weld is related to the accuracy of the available digital image correlation system. Specimens containing multiple weld spots need to be larger, in order to provide the surface area needed for welding. As the cameras used for digital image correlation need to fit in their common field of view a larger area containing welds, the measurement accuracy, partly related to spatial resolution, is expected to be lower, thus making any comparison with simulated data more difficult. The fourth reason for focusing the start of this research on an alternative method to that presented in [15] for quantifying the damage accumulation in single weld spot specimens, that can be subsequently extended to multiple weld spot specimens, is that the data set from the experimental campaign described in [15] is already available at the start of this thesis.

The questions for the single weld spot study phase of the thesis are:

- Can surface strain fields, simulated through a low fidelity finite element modelling technique, be correlated to surface strain fields, measured with digital image correlation, to characterize the state of disbonding damage in the weld spot of an ultrasonically welded lap shear joint?
- Can force-displacement curves, simulated with the finite element method, be correlated to measured force-displacement curves during a fatigue test, to characterize the state of disbonding damage in the weld spot of an ultrasonically welded lap shear joint?

The damage occurring in an ultrasonic weld spot during repeated loading will only be considered at a macro level, when the two welded plates have locally disbanded. The disbonding damage can be characterized at multiple degrees of detail, from the rate of weld area reduction throughout the fatigue test, to the weld area remaining intact at each loading cycle, to the evolution of the weld shape, which specifies where an ultrasonic spot weld is breaking in addition to its total area. The extent to which each proposed method can characterize the disbonding damage will be discussed in chapter 8.

The research questions for the study of lap shear joints welded through multiple weld spots are only a generalization of the questions asked for studying damage accumulation in lap shear joints ultrasonically welded through a single spot.

- Can surface strain fields, simulated through a low fidelity finite element modelling technique, be correlated to surface strain fields, measured with digital image correlation, to characterize the state of disbonding damage in each of the weld spots of an ultrasonically welded lap shear joint?
- Can force-displacement curves, simulated with the finite element method, be correlated to measured force-displacement curves during a fatigue test, to characterize the total state of disbonding damage in the weld spots of an ultrasonically welded lap shear joint?

The distinction from the single weld spot study lies mainly in the second research question, which generalizes from the characterization of damage in a single weld spot to an overall characterization of damage by correlating measured to simulated compliance reduction. The increase in compliance

of a specimen can be used as a global indication of damage within that specimen [17] [16]. The assumption is made within the analysis of this thesis that all damage leading to a decrease in stiffness of an ultrasonically welded lap shear joint occurs at the location of the weld spots.

Answering the research questions allows for the future development and validation of models to predict the mechanical properties, during the fatigue life, of ultrasonic spot welds in lap shear joints. The disbonding damage evolution quantification in single spot specimens, together with detailed modelling of the tested specimen, will allow for the first fatigue life predictions of ultrasonically welded lap shear specimens to be made. The predictive ability of such models could subsequently be validated by assessing their accuracy in lap shear joints with multiple weld spots. The classification of the weld spots damage states throughout the fatigue life of multiple spot specimens will provide the first validation data for assessing whether the fatigue models can predict correctly the sequence of spot failures.

3.3 Available experimental data

For the single weld spot part of the research, the experimental data has been provided by [14] [15]. Figure 3.1 gives an overview of the welded lap shear joint geometry and shows the fracture surfaces of the joints analyzed in this report. The fatigue loading was displacement controlled, with the displacement value obtained when loading each specimen to a set force, which was 80% of the average static failure load of the batch of specimens. The controlled displacement loading was determined individually for each tested specimen by first loading the specimen to a set force and measuring the displacement to be used for the fatigue test.

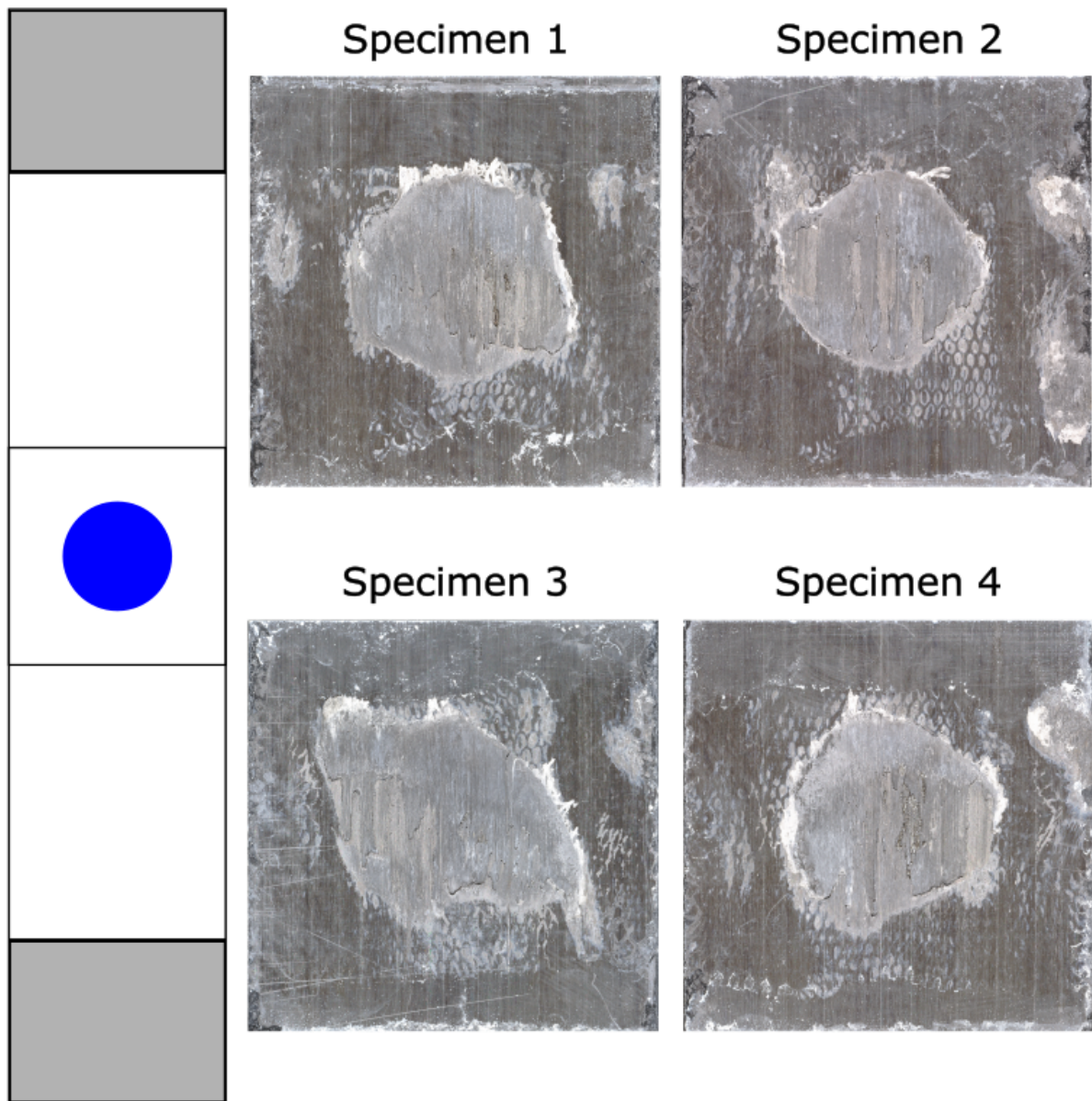


Figure 3.1: Schematic of single lap shear joints welded through a single ultrasonic weld spot, and the fracture surfaces of the specimens presented in this report. Fracture surface pictures courtesy of [14].

For the multiple weld spot phase of the research, the experimental data was created in collaboration with [14]. Figure 3.2 gives an overview of the geometry of the lap shear specimen successfully tested, and the fracture surface of the specimen analyzed in this report. Similarly to the single weld spot tests done by [14] [15] before, the controlled displacement loading was determined individually for each tested specimen by first loading the specimen to a set force and measuring the displacement to be used for the fatigue test.

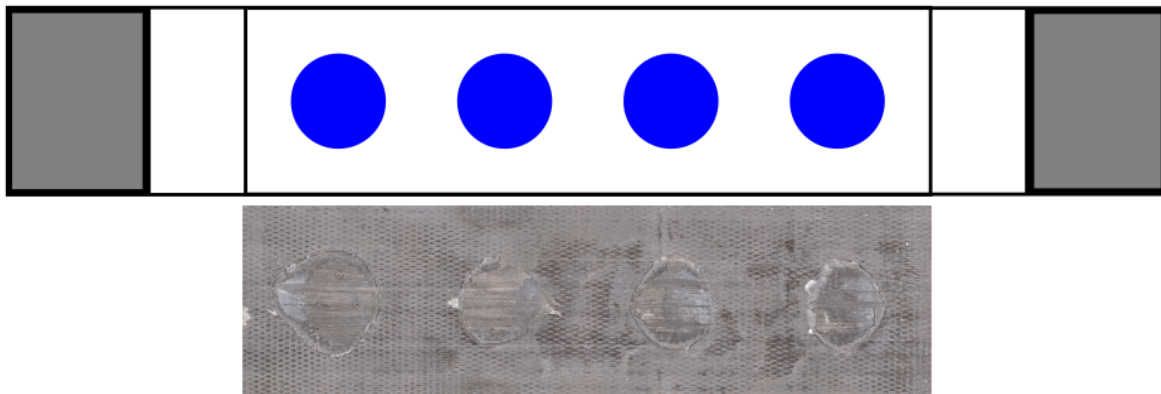


Figure 3.2: Schematic of single lap shear joints welded through a column of four ultrasonic weld spots, and the fracture surface of the specimen presented in this report.

4 Methodology for single weld spot analysis

In order to interpret the surface strain fields measured with DIC during fatigue experiments and the reaction forces measured during each loading cycle by the test machine, a finite element modelling technique is proposed in this chapter to generate a data base of reference simulations that can be used as comparison. The FEM analysis procedure used in this thesis is the standard one: choosing suitable finite elements to model the assembly of parts, meshing the parts to represent the geometry and the mechanical properties of the real specimens to an acceptable degree of accuracy, enforcing a set of boundary conditions on the FEM mesh that is sufficiently representative of the clamping and loading conditions during the fatigue experiment and solving the resulting system of equations. The modelling choices that were made in each step are presented subsequently in section 4.1.1, section 4.1.5, section 4.1.2 and section 4.1.3. The simulation results are then interpreted to imitate the real measurements made during the test campaign. A collection of such simulated results is compiled into a data base to cover a large number of possible weld shapes that could occur at any point during the fatigue tests. For every experimental measurement considered, a well matching simulation is searched for in the database. Under the presumption that the numerical model used to generate the matched simulation has mimicked the mechanical properties of the real specimen sufficiently accurately, and that the measurements taken during the experiment have captured the mechanical response of the real specimen sufficiently accurately, the representation of the weld used in the numerical model should correlate well with the real shape of the weld. The methods used for matching experimental data with simulated data, and for interpreting the result of the match are discussed in section 4.2 and section 4.3. An overview of the methodology is shown below in figure 4.1.

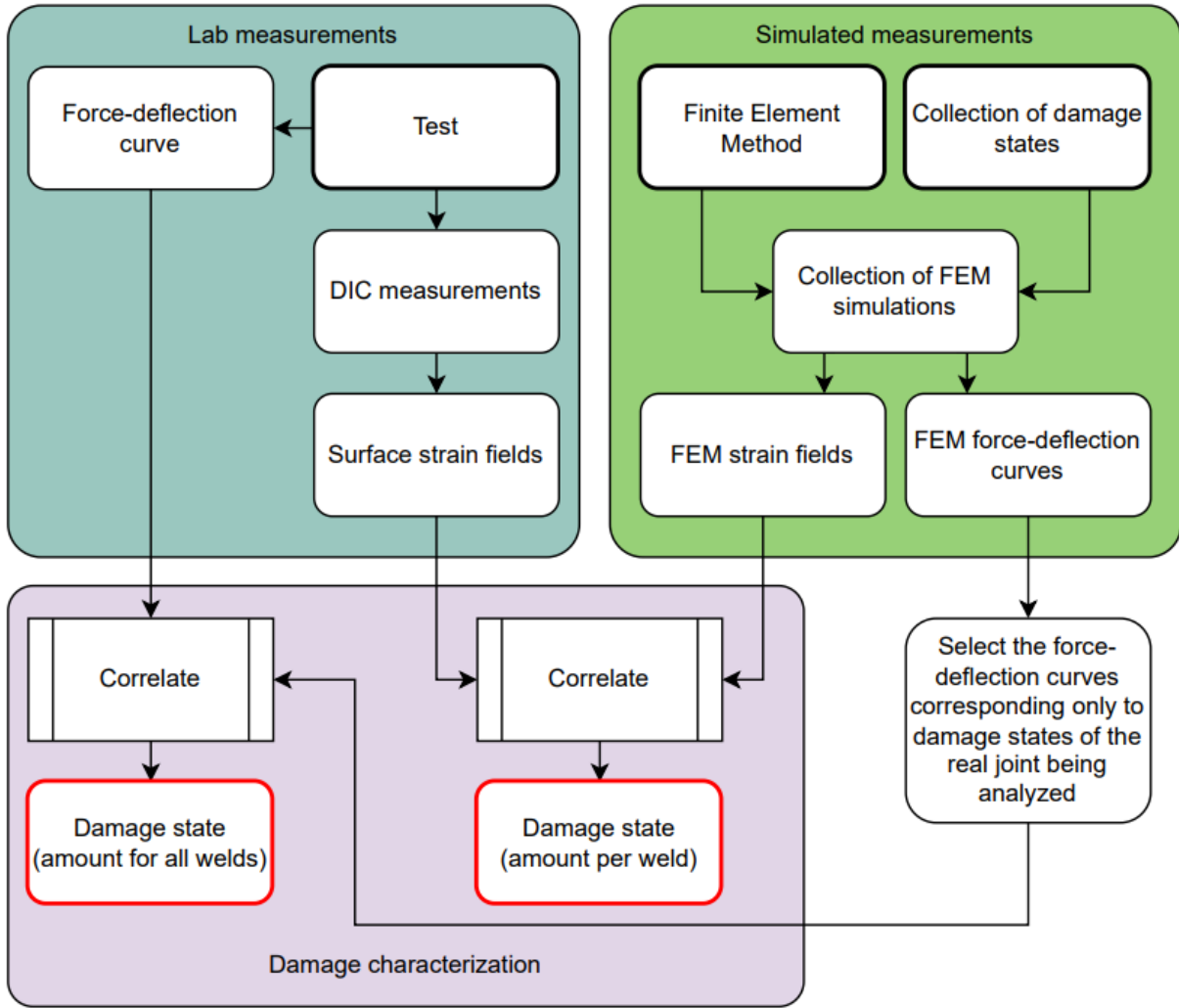


Figure 4.1: Overview of the methodology presented in this thesis for assessing the damage state in a lap shear joint welded through ultrasonic spot welds.

In order to enable a large degree of flexibility in setting up the FEM analysis and in processing the results, the finite element model used to generate the database of simulated experimental results was programmed from scratch. Important implementation choices, modelling limitations and verification of results are discussed in section 4.1.4.

4.1 Creation of finite element database of simulations

The database of simulations which is used for comparison to the test data is of high importance for the outcome of the interpretation. An ideal database would contain a model simulation for all possible shapes of the ultrasonic weld spot at the beginning of the test and throughout its fatigue life. The manufactured weld shapes divert from the desired perfectly round shape due to uncertainties in the current state of the welding process. Furthermore, each weld will fatigue in its slightly unique way, as no two specimens are exactly the same, and no test is perfectly identical. The larger the variation expected in the weld shapes after manufacturing, the more simulations need to be included in the database to cover the possible range of shapes. As the number of possible weld shapes, including their fatigued states, is very large, assumptions

need to be made to reduce the size of the needed database. Care must be taken such that the assumptions are not too restrictive, such that there remains a large pool of options to effectively test the performance of the algorithms interpreting the experimental data. The more restricted a database it, the more the assumptions made in restricting it influence the outcome of the interpretation. A balance needs to be reached between the computational cost of building a comprehensive database, and between restricting the variation included in the computations to the point of guiding the result towards an expected outcome.

The rules used to compile the database of reference simulations imply inherent assumptions about which cases are worth included and which are left out. The process of generating the database is exposed in relative detail to document those rules, which need to be considered when assessing the results of the analysis.

The single weld spot test campaign data created by [15] consisted in 13 tests. In order to build the database used to derive the results presented in this thesis, the 13 weld shapes tested were flipped and rotated vertically and horizontally to create a total of 104 initial weld shapes. Assumptions were then made about the shape evolution throughout the fatigue test of each weld. The welds were gradually broken by different rules based on the state of strain at the weld location. A total of 9 rules were used, by considering 3 breaking criteria at 3 different peak value thresholds. The criteria are to damage the weld at the nodal locations where the difference in: equivalent strain, axial strain and shear strain between the panels is the largest. The threshold considered for breaking are: top 95%, top 80% and top 65% of the maximum value for the current state of the weld, which means that the weld was disbonded gradually from the places where one of the criteria mentioned above had a value larger than the specified threshold value. More details about the breaking locations depend on the mesh used to represent the specimens, and are elaborated on in section 4.1.3.

The modelled weld shapes can be visualized by plotting the locations on the lap shear joint overlap where tie constrains are used to represent the weld (more details about modelling will be introduced in subsequent sections). The effect of each of the three weld disbonding criteria used to simulate different damage states can be visualized by averaging the weld representations created with each damage criterion. Figure 4.2 presents the result for the modelled weld of specimen 1. The brighter a point is in the figure, the more simulated weld shapes contain the point. It can be seen how considering different strain components to model damage accumulation influences the shapes of the damaged welds.

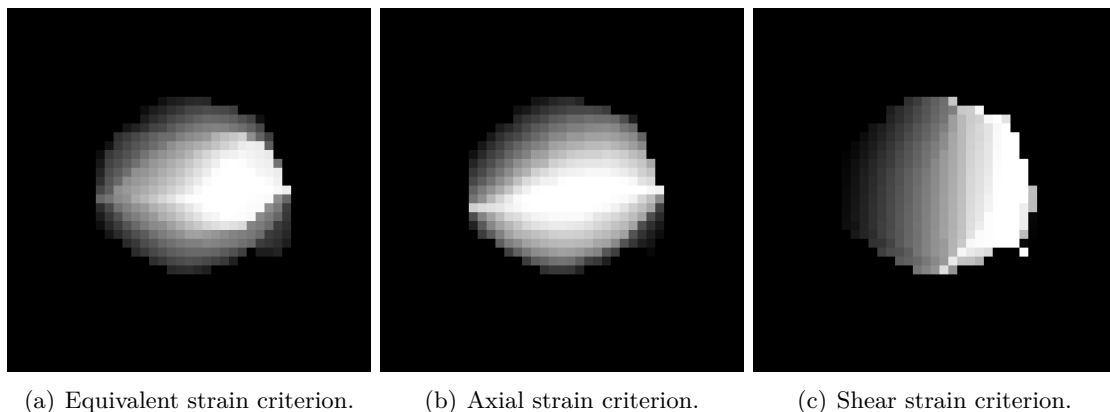


Figure 4.2: Effect of disbonding criteria on the damage states simulated.

The simulated weld generation criteria do not represent an attempt at simulating the real fatigue progression of specimens. The damaging criteria were rather conceived to generate a large variation in the resulting weld shapes, while maintaining the shape of the weld simply connected. Those damage creation criteria are not exhaustive, any random combination of them could be considered throughout the simulated fatigue breaking process to generate new shapes from the initial weld shapes.

Even though modelling the fatigue life of weld spots is not desired when generating the database of simulations, the assumptions made above do limit the weld shapes included in the database. Having said that, from the initial 13 specimens tested in the laboratory, using the techniques mentioned, a database of over 40000 finite element simulations was created. Through empirical experimentation with various sizes of databases it was concluded that this database covers enough variation to assess the correlating algorithms performance in terms of stability, consistency and accuracy. It was observed that the limits of accuracy of the correlating algorithms are reached sufficiently clearly on this database, as will be discussed in chapter 8. Including more analysis in the database will not further increase the confidence in the obtained results, because the bottleneck in accuracy is more related to the accuracy of the real life measurements than to the diversity of the set of simulations available for comparison.

4.1.1 Choice of finite elements

The finite elements chosen shall allow for the strain distribution on the surface of the plates to be accurately represented. There are multiple shell-like finite elements suitable for modelling the plates, with 4 to 8 nodes. The selection of any particular finite element is not overwhelmingly in favor of any particular element, each having their advantages either in terms of ease of modelling or in terms of claimed accuracy or in terms of computational effort. The choice was made to use continuum shell elements, even though arguments could be made in favor of regular shell elements as well.

Continuum shell elements are a mix between shell elements and continuum elements, with the advantage for this particular application of being able to represent more accurately the state of stress at the weld interface at a lower computational cost than solid elements require. The literature on continuum shell elements for composite panels spans three decades, with one of the most notable contribution being the work of [11] which integrates and refines the most successful previous element formulation attempts. The article of [11] is also the theoretical reference of the continuum shell elements implemented in Abaqus, a commercial finite element analysis software package tailored for the needs of the aerospace industry. In this thesis, the continuum shell finite element formulation described in [6] is followed. [6] presents an earlier formulation, identical to that of [11] for geometrically linear analysis. In this thesis, the numerical model is kept linear in order to reduce the computational costs required to create a large database of simulations, with the presumption that the error made by assuming linearly elastic behavior remains small, or can be effectively compensated for by tuning the model parameters to address model shortcomings. This is done by comparing the results of the linear analysis to that of a fully converged non-linear analysis with continuum shell elements in Abaqus. The modelling limitations are further discussed in section 4.1.4.

4.1.2 Choice of boundary conditions

The dimensions of the real specimens used in the single weld spot test campaign carried out by [15] are shown in figure 4.3, and the boundary conditions enforced on the specimen by the test

machine are depicted in figure 4.4.

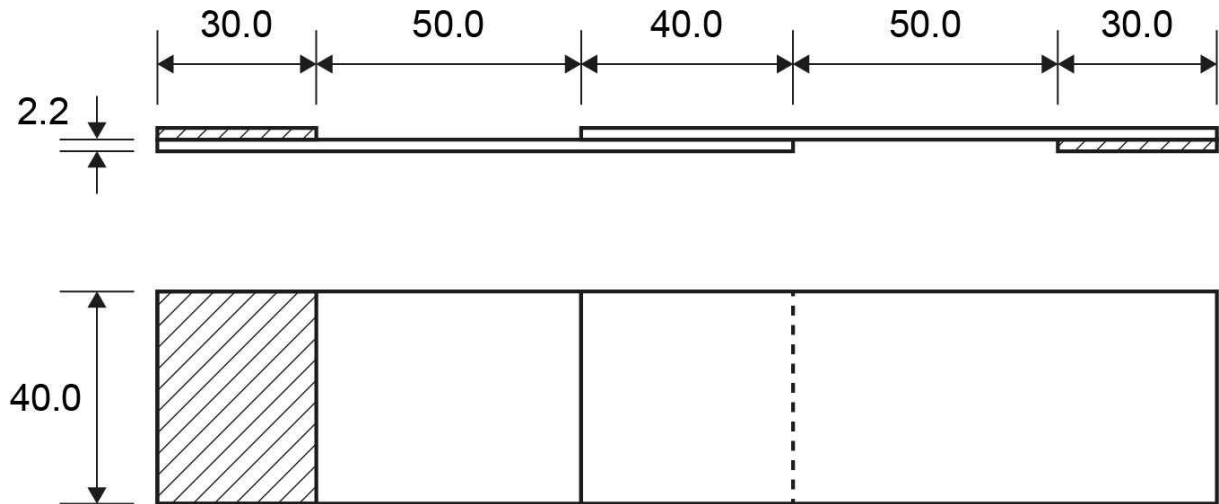


Figure 4.3: Sketch of specimen dimensions used for single weld spot testing in [15]. Picture courtesy of [15].



Figure 4.4: Sketch of real boundary conditions used for single weld spot testing in [15]. Picture courtesy of [15].

The influence of the boundary conditions enforced in the FEM analysis on the surface strain distributions over the specimen overlap areas was studied. A comparison was made between the boundary conditions depicted in figure 4.4 and the simpler boundary conditions shown in figure 4.5. It was thus experimentally found that directly clamping the edge of the specimen at the start of the vice of the machine produces almost identical strain fields over the overlap area compared to the more realistic boundary conditions where the loads at the vice of the machine are introduced through surface shear over the clamped area, even for very fine meshes with 6 elements through the thickness of each plate. The simulations were subsequently carried out using the simpler boundary conditions with the loads introduced directly on the end surfaces of the specimens, as fewer finite elements are required which saves computation time.



Figure 4.5: Sketch of boundary conditions used in FEM analysis.

4.1.3 Numerical representation of weld spot

The weld spots were modelled through single point tie constraints between the nodes within the weld perimeter, enforced with the penalty stiffness method as described in [9]. Starting from

pictures of the weld fracture surfaces, masks of the main initial fracture surface were traced by hand and then rotated and flipped as described in section 4.1 to augment the set of simulations in a way that is representative of the real manufacturing deviations in the set of specimens used for testing by [15]. The nodes of the mesh on each plate, at the contact surface between the plates, located within the perimeter of the traced weld, were considered as part of the weld and tied in pairs with the penalty stiffness method. The stiffness given to the weld constrains was 1000 times larger than the largest stiffness of the material properties, as suggested by [9]. Figure 4.6 gives an example of one of the weld masks created, with a mask of the associated tie constrains at mesh nodal locations.

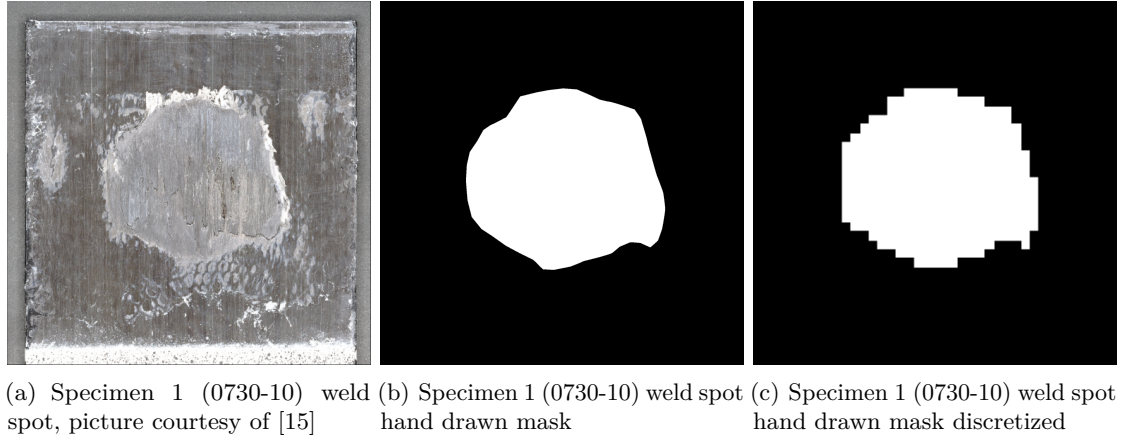


Figure 4.6: Weld spot modelling representation through nodal tie constraints.

A study was made into the influence of the weld FEM representation on the surface strain distributions simulated. It was found that the penalty stiffness chosen has a negligible influence, as long as it is not lower than the polymer stiffness of the material. Introducing another layer of elements to represent the weld alone resulted in similar surface strain distributions, with smoother gradients. Smoother gradients could also be obtained by using more finite elements through the thickness with the penalty stiffness method, but at a higher computational cost. As tens of thousands of simulations were run, the decision was made to use the simple penalty stiffness method as it keeps the systems of equations smaller, thus saving solving time.

4.1.4 Finite element implementation

A custom made FEM implementation was written to build the database of simulations required in this project. The implementation was written in Python, following the programming framework of [2] and the mathematical description of [6]. The implementation was written to enable easy parametric descriptions of the lap shear tests carried out in this research, with the specimen geometric definition, material properties and meshing parameterized to suit this purpose.

4.1.4.1 Implementation limitations

The main implementation limitation is that the analysis done are linear. Continuum solid shell elements require iterative updates of augmented strain fields to pass the bending patch test [11]. Without the enhanced strain fields, the elements are too stiff as a result of the shell bending kinematic assumptions. Comparing figure 4.7(a), which shows the resulting surface strain distribution for a perfectly round weld using fully nonlinear implementation of the continuum

solid shell elements described in [11], and figure 4.8(a) surface strain distributions simulated with the custom, linear only implementation written for this research, it can be observed that the strain distribution is largely similar, except on the bottom of the overlaps. At the overlap bottom the surface strains differ between the linear and the non-linear simulations, with the linear one not showing the small area of tensile strains (represented in blue). This is because the specimen plates modelled with the linear elements have a slightly different elastic curve in bending, as the elements are more stiff. As will be explained in section 4.2, the distribution of simulated surface strains matters most in comparison with the strain distributions measured during the real experiments with digital image correlation. In order to improve the correlation between real data and simulated data, a solution was sought to modify the bending response of the specimens simulated with linear elements to bring the surface strain distributions over the overlapping area closer to those obtained with the more accurate, fully non-linear implementation of Abaqus, without increasing the computational cost of the analysis. The best solution reached through experimentation was to shorten the plates, such that their bending curve over the overlapping area becomes similar to that of the Abaqus simulations. The resulting strain field of a specimen with planes 65mm long instead of 90mm long is shown in figure 4.8(b), which shows a strain distribution similar to figure 4.7(a), with the added benefit of using even less finite elements and therefore further decreasing the computational effort.

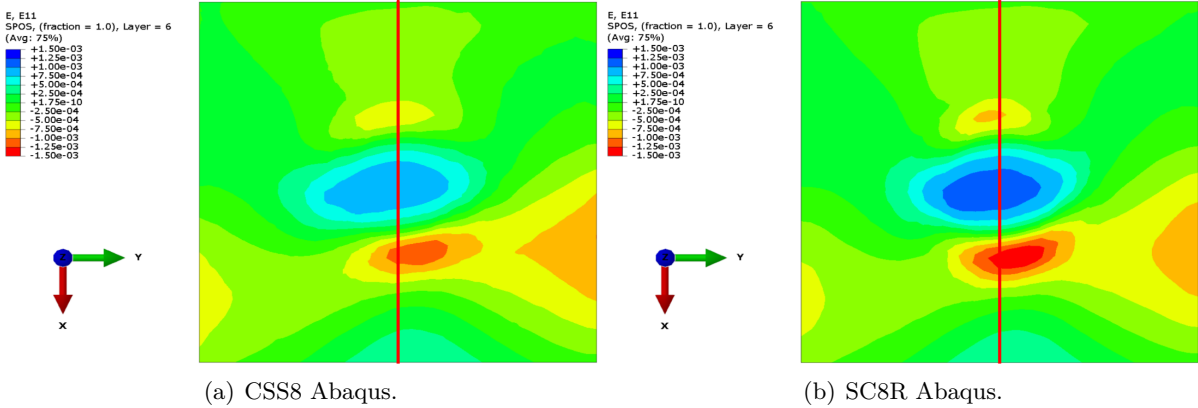


Figure 4.7: Simulated surface strain distributions for a perfectly round weld spot with continuum solid shell elements in Abaqus.

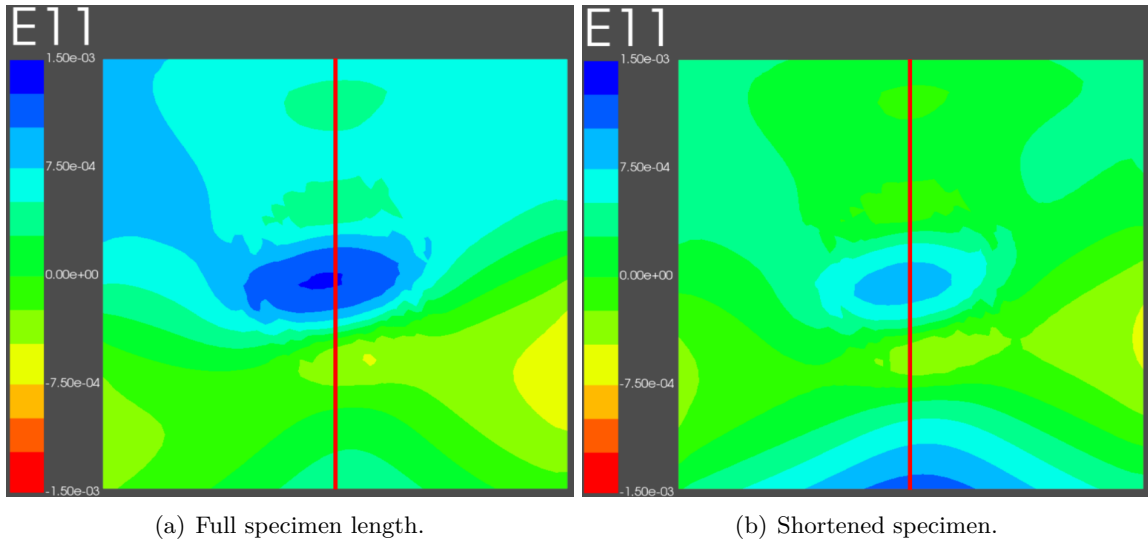


Figure 4.8: Simulated surface strain distributions for a perfectly round weld spot with the custom implementation of continuum solid shell elements.

For a better comparison of the surface strain fields shown in figure 4.7 and in figure 4.8, figure 4.9 overlaps the strain fields extracted along the mid-lines of the overlap, indicated through a red line in each corresponding simulation result. It can be seen that shortening the length of the plates simulated with the custom, linear only continuum shell elements, indeed brought the simulation results closer to the simulations made with Abaqus.

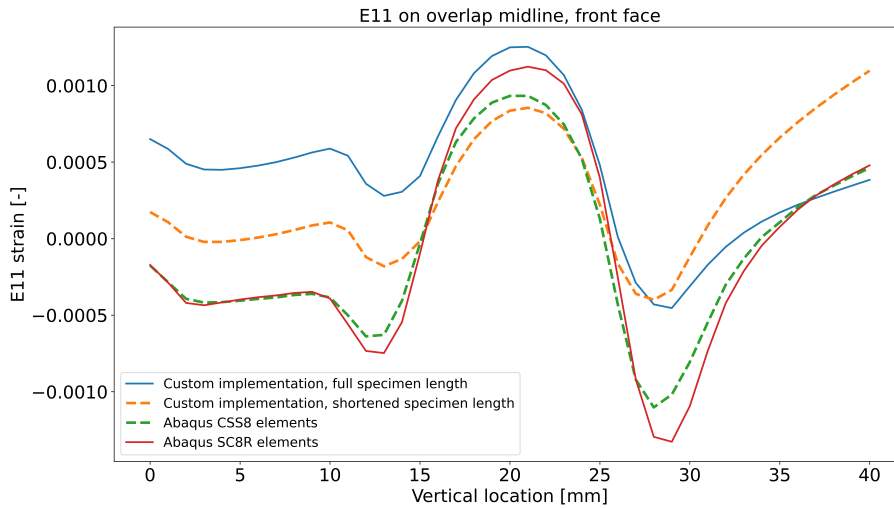


Figure 4.9: Strains compared on the middle line of the overlap area of the single weld spot specimens, extracted from figure 4.7 and figure 4.8 at the locations at the red lines.

The Abaqus simulation shown in figure 4.7(a), with continuum solid shell elements, runs in approximately 3 minutes. When using continuum solid shell elements with reduced integration (SC8R) in Abaqus, which simulate the strain fields shown in figure 4.7(b), the running time is of approximately 40 seconds. By comparison, the custom FEM implementation, which produces the strain field shown in figure 4.8(b), is solved in under 10 seconds, which shows the benefit of

customizing software for a particular purpose.

4.1.4.2 Implementation verification

In order to verify the correctness of the implementation, the membrane patch test and the plate bending test described in [11] were used. The bending patch test can not be passed by a linear formulation of the continuum shell elements. Good agreement between the surface strain fields produced by Abaqus continuum shell elements and the custom implementation made in this thesis stand as further verification that the implementation performs correctly for the simulations carried out.

4.1.5 Choice of meshing technique

Since the specimens used in the single ultrasonic weld spot test campaign carried out by [15] are rectangular and with constant thickness, a uniform mesh with right rectangular prisms is used, see figure 4.10.

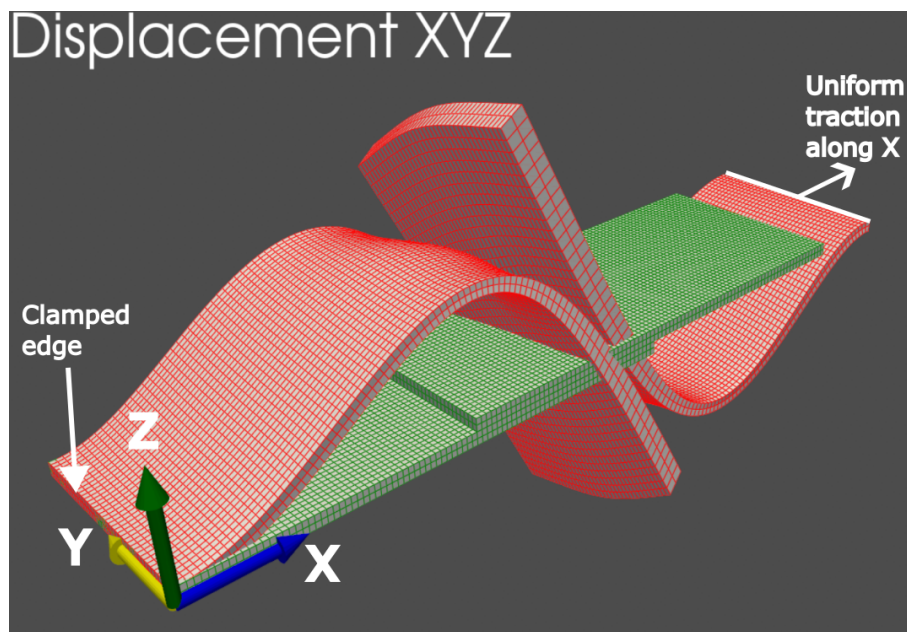


Figure 4.10: Mesh used to model the lap shear test specimens, in its undeformed state in green and in its exaggerated deformed state, which is a result of the simulation, in red.

Through a convergence analysis, shown in appendix C, it was found that a mesh with a refinement of one element per millimeter along the length and the width of the specimen plates, and two elements over the thickness of each plate, gives converged results at a low computational cost. Further mesh refinements do not change the results sufficiently to outweigh the disadvantage of generating larger systems of equations that take longer to solve. As it is desirable to have many thousands of simulations in any database used for interpreting experimental data, the computing time for each analysis is an important factor in deciding the mesh refinement.

4.2 DIC to FEM strain field correlation

The strain fields measured with digital image correlation over both outer surfaces of the overlapped specimens area are compared to the simulated strain fields over the overlap in order to find the most similar simulation from the database to the measured strain fields. The strain fields over the overlaps are formatted as digital images. The similarity of two image matrices is quantified with the cross correlation measure shown in equation (4.1).

$$CCOR = \frac{\sum image1 \cdot image2 \cdot GK}{\sqrt{\sum image1^2 + \sum image2^2}} \quad (4.1)$$

where *image1* and *image2* are the matrices of the two images, and *GK* is a gaussian kernel used to give more importance to the good agreement closer to the center of the images, where the weld spots are. The normalized cross correlation score is computed between each DIC strain field pair (front and back of specimen) and surface strain field from the database of simulations. The matching scores of the front and back strain fields are summed for each DIC strain field pair, which gives each set of strain fields from the FEM database a score of how well it correlated to the set of measured strain fields. The pair of strain fields with the highest correlation score is picked as the best fit. Attempts to use the strain fields corresponding to only one of the DIC systems generally resulted in less stable, less accurate matching results. When the data from both DIC systems is combined in the correlation, the most consistent results are obtained.

Other analytical image comparison techniques mentioned in [18] were tried, either in the spatial domain or in the frequency domain, with worse results. It was found by trial and error that cross correlation works best, likely because it scores higher the correct match of data distribution where the values are high, therefore matching well the peaks and valleys in the strain fields.

It is possible to constrain the evolution of the matched strain fields of the simulated weld shapes, such that the matched weld shapes remain geometrically consistent with the real fracture surface, and such that their evolution has to be a monotonous degradation. The decision was made to leave the result of each match independent from that of previous matches. The main advantage of not imposing further assumptions about the weld evolution on the matching algorithm is to avoid the risk of manufacturing a desired result, of fulfilling expectations about what the result ought to be to the detriment of real measurement. If the correlations are made purely on the basis of the available data, a more accurate indication of the validity of the method can be obtained. Leaving the matches independent from each other also has the advantage of not propagating errors in matching throughout the test.

4.3 Measured reaction force to FEM reaction force correlation

During the fatigue experiments, the test machine recorded the reaction force at the peak of each loading cycle. The measured reaction forces can be compared to the reaction forces computed through the finite element simulations, from the database of simulations, which modelled the tested specimen, to get an indication of the increase in compliance of the specimen. The increase in compliance of a composite specimen is commonly used as a global indication of damage accumulation within the specimen. The purpose of this analysis is to provide a rough validation, independent of DIC data, to the correlation results obtained with the help of DIC data.

It was found that the computed reaction force in a displacement controlled simulation for a

given weld spot correlates well with the area of that weld. Figure 4.11 shows the relationship between weld area and the simulated reaction force for the test conditions of specimen 0730-10 ran by [15]. Every data point in the graph corresponds to a FEM simulation representative of the real specimen, picked from the data base. The colors correspond to different criteria used to gradually reduce the area of the simulated weld, as explained in section 4.1. The legend summarizes the effect the different weld disbonding criteria have on the resulting average weld shapes. By averaging the weld shapes simulated through each main disbonding criterion, the distinct trends in the resulting shapes, which influence the simulated compliance of the specimens, can be visualized. Further examples of the effect different disbonding criteria have on the shapes of the simulated welds can be found in appendix A. At the beginning, the way in which the specimen breaks has little influence on the measured reaction force. As the weld area keeps being reduced, more spread can be observed as the shape of the weld spot varies more and has a larger influence on the reaction force for a given total area. The reason for selecting the subset of simulations from the database associated with that specimen is because each specimen was loaded under displacement control, with a different displacement as explained by [15]. Therefore a different weld area to reaction force correlation, as the one plotted in figure 4.11, will be done for each of the specimens tested by [15] analyzed in this report.

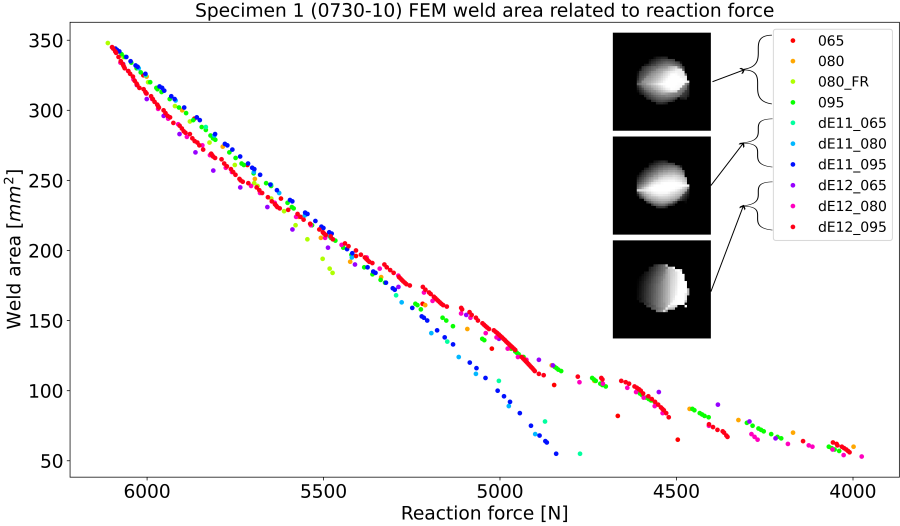


Figure 4.11: Simulated weld area influence on reaction force for a fixed displacement loading, specimen 0730-10 of [15].

Figure 4.12(a) shows the reaction forces measured by the test machine at the peak of each displacement controlled loading cycle for specimen 0730-10, which will be referred to as "Specimen 1" for ease of tracking in this report. For each reading of reaction force in figure 4.12(a), the closest matching reaction force in figure 4.11 is searched for, and the corresponding weld area found for that reaction force is plotted in figure 4.12(b). Through consistent usage of colors between figure 4.12(b) and figure 4.11 it is possible to follow which weld disbonding criterion lead to which weld area estimation. Each data point in figure 4.12(a) corresponds to the reaction force measured at the peak of a loading cycle by the test machine.

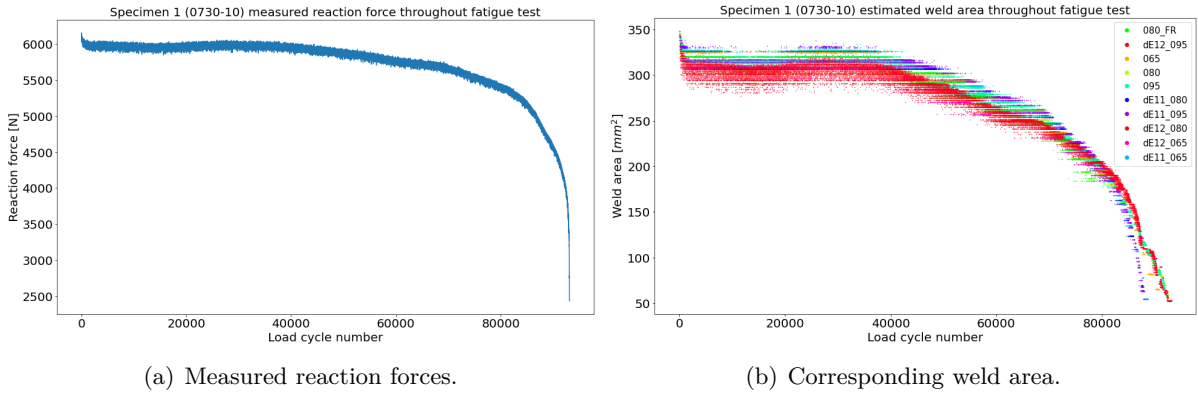


Figure 4.12: Reaction forces measured by the test machine during the fatigue test for specimen 0730-10 of [15], and the corresponding weld area matched by correlating simulated reaction forces.

The vertical spread in the data points shown in figure 4.12(b) is a consequence of the white noise in the reaction force data shown in figure 4.12(a). The horizontal white bands in the plot, where data points are not located, are due to the discrete nature of the data shown in figure 4.11. The weld area is discretized by the mesh into multiples of the area of a finite element, which leaves the horizontal gaps in correlated weld area in figure 4.12(b). The data could be interpolated and filtered to produce a smooth plot, but it was left more raw in order to display the real spread in data as an indication of the accuracy of the method. The larger the white noise in the reaction force measurement, the larger the vertical spread in figure 4.12(b). The larger the influence of the fatigued shape of a weld on the reaction force, the larger the spread in data in figure 4.11 and the larger the vertical spread in figure 4.12(b). The fewer finite element simulations included in figure 4.11, the larger the horizontal gaps in data in figure 4.12(b).

4.4 Result analysis

The weld areas estimated through surface strain field correlation and through interpretation of measured reaction force will be presented for each specimen for a comparative analysis. A high quality result will show good agreement between the weld areas estimated through both methods.

From a fracture mechanics perspective, the rate of damage growth is often the parameter of choice for modelling purposes, correlated with the strain energy release rate. In this report, the relative change of estimated weld area is presented both with respect to the initial area of the hand traced fracture surface used to model the welds and with respect to the initial area estimation obtained through each method. The advantage of using the area of the weld contour drawn by hand as reference, rather than the area of the first estimations, in comparing the measurement results in this report, is that initial area estimations do not influence the interpretation of results throughout the test when a fixed reference is used. Relative area changes with respect to initial matched area are also included to allow for a comparison with the earlier study results of [14], partly publicised already in [15].

The formulas used for computing the relative area changes are:

$$Reduction = 1 - \frac{A_{matched}}{A_{traced}}, \quad (4.2)$$

and

$$Reduction = 1 - \frac{A_{matched}}{A_{matched_0}} \quad (4.3)$$

where reduction is the computed weld area reduction, $A_{matched}$ is the value of the estimated area at each point in the test, $A_{matched_0}$ is the first match result and A_{traced} is the area of the fracture surface, traced by hand to model the welds, as explained in section 4.1.3. A negative reduction value corresponds to an estimated weld area larger than the initial weld area, which may happen in the area estimation process. A typical result is shown in figure 4.13, which also includes overlapped the results of [15] and [14] for comparison. Such results will be presented in more detail in chapter 5.

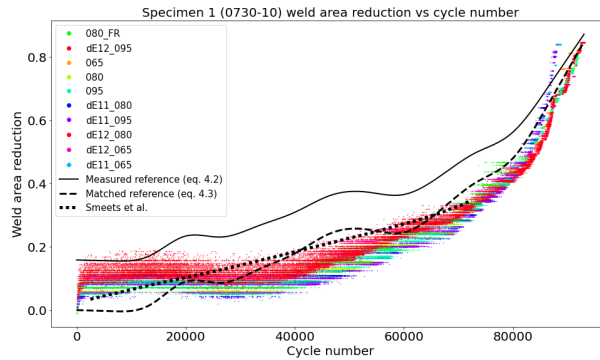


Figure 4.13: Percentage of weld area disbonded, estimated throughout the test, with respect to the initially match weld area and with respect to the area of the fracture surface, traced by hand. The result corresponds to specimen 0730-10 of [14], which includes the analysis results of [15] [14].

5 Results for single weld spot analysis

The results of the analysis of experimental data, collected during fatigue tests of lap shear joints welded with single ultrasonic weld spots are presented in this chapter. The methods used for analysis are those presented in chapter 4. In this chapter the results are presented with little qualitative judgment, the discussion being reserved for chapter 8.

For some tested specimens, there is good agreement between both methods of characterizing the spot weld area inside the lap shear joints, while for other specimens there is less agreement. The results presented in this section are therefore split into two main groups: results for which the weld area characterization is in good agreement between the method of correlating measured surface strain fields to a set of simulated strain fields, presented in section 4.2, and the method of correlating the reaction force measured by the fatigue machine to the reaction force estimated through simulations of a given specimen spot weld, described in section 4.3. The analysis results for two different specimens are presented in each group, with a total of 4 specimens analyzed in this section of the thesis. The results presented aim to be illustrative of all important points of discussion observed throughout analyzing the single weld spot fatigue data collected by [14].

The reasons for lesser coherence can be identified by analyzing the weld shapes, the strain field matching results, and the reaction forces measured. The corresponding reasoning explaining the distinctions will be included in a discussion for each of the specimens presented in this section. The figures shown in the corresponding subsections below aim to enable an objective discussion about the extent to which the research objective for the single weld spot analysis part of the thesis have been reached.

For ease of presentation, the four specimens presented will be simply named from "Specimen 1" to "Specimen 4", with the specimen names assigned and used by [14] given in parenthesis for each specimen. Including in brackets the specimen nomenclature used by [14] allows for easily tracking the results in future publications based on the same test campaign.

5.1 Results displaying consistent agreement

For some of the specimens tested, the strain fields measured with digital image correlation look very similar and correlate well to the simulated strain fields. For those specimens, the characterization of weld area by strain field correlation is more consistent and corresponds better to the observed fracture surfaces and to the measured reaction forces. For the latter to be true, the reaction forces measured during the experiment must also be accurate. Errors in reaction force measurement, either due to temperature fluctuations which cause the tested specimen and the test machine itself to expand or contract at different rates, which influences the loading in a displacement controlled test, or due to the specimen settling within the clamps of the test machine as a result of repeated loading, also lead to less agreement between DIC to FEM and reaction force to FEM characterizations of weld area. For the specimens presented in this section, both methods of weld area characterization show similar and largely overlapping trends.

5.1.1 Results for specimen 1 (0730-10)

The left side of figure 5.1 shows real measurements of surface strain fields for specimen 2 after 50 loading cycles, and a photograph of the fracture surface. After only 50 loading cycles, when the

first set of pictures were taken by the DIC systems, it is expected that the weld shape remained almost identical to the pristine shape of the weld, which can be approximated by the outer contour of the fracture surface. The right side of figure 5.1 shows correlated surface strain fields from the database of simulations, and the modelled weld surface which created them.

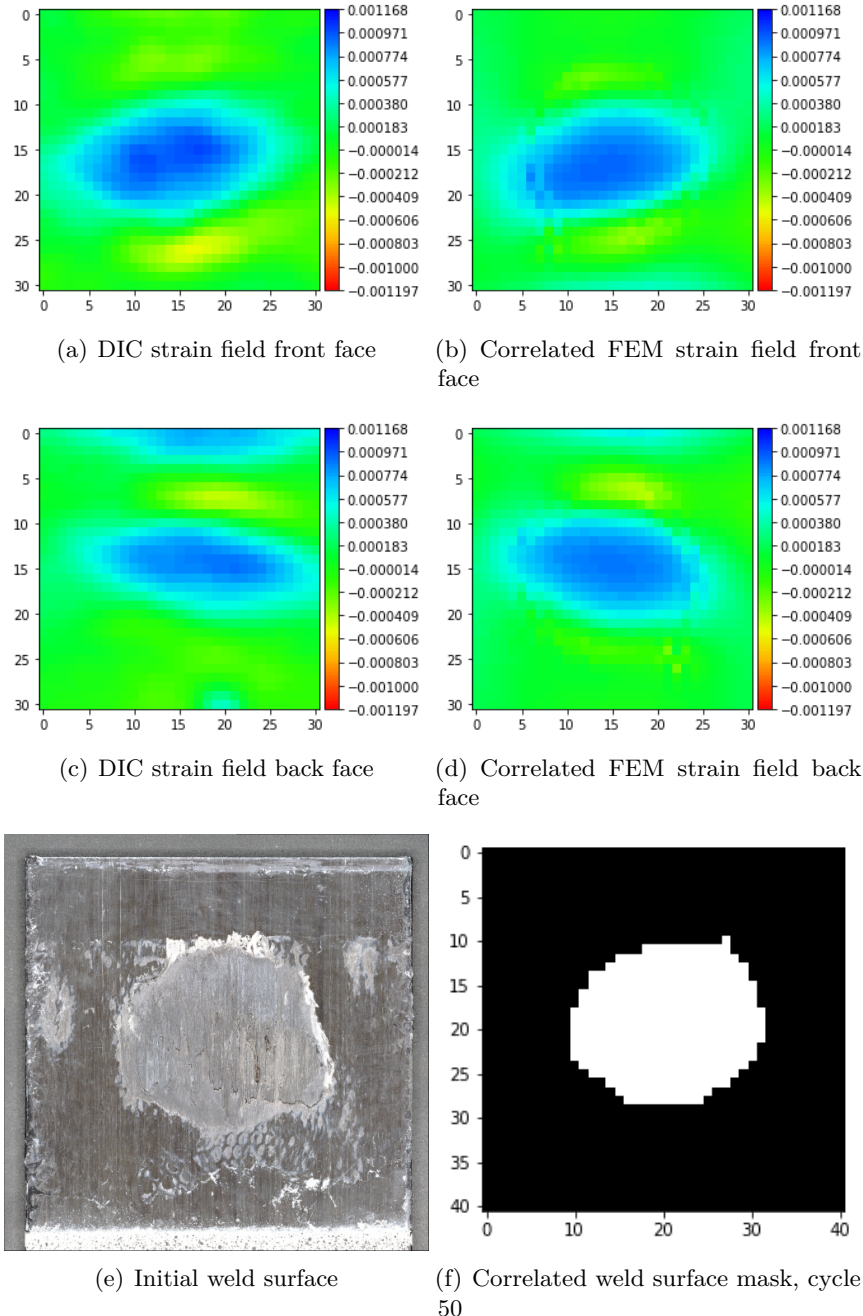


Figure 5.1: DIC to FEM strain field correlation results for specimen 1, loading cycle 50, longitudinal component (E11).

The left side of figure 5.2 shows real measurements of surface strain fields for specimen 2 after 2500 loading cycles, and a photograph of the fracture surface to aid in assessing the matched result. The right side of figure 5.2 shows correlated surface strain fields from the database of

simulations, and the modelled weld surface which created them.

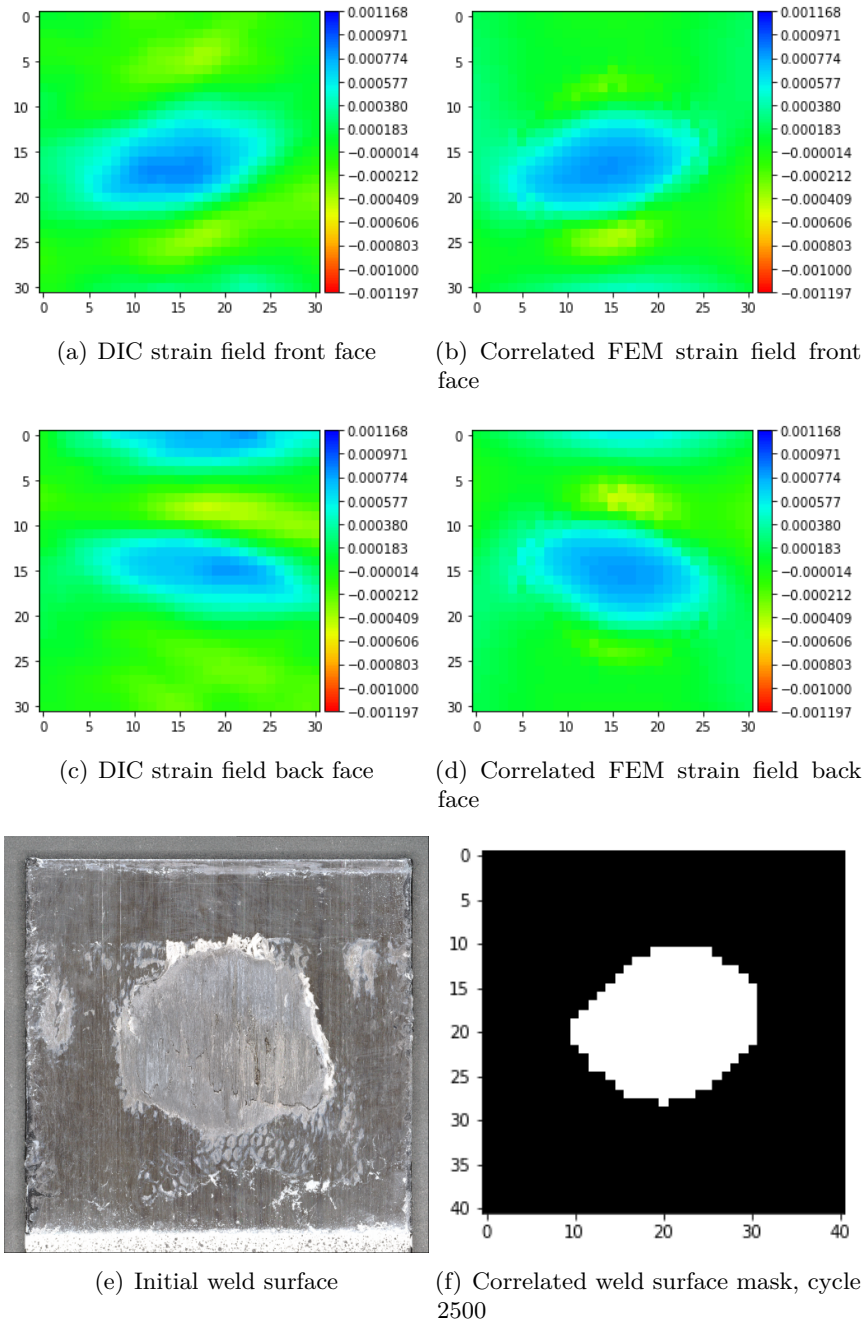


Figure 5.2: DIC to FEM strain field correlation results for specimen 1, loading cycle 2500, longitudinal component (E11).

Figure 5.3 shows in blue dots the results of DIC matching for the entire fatigue life, in terms of weld area and change in weld area with respect to the first matched area. The spread in the blue dots is due in part to inaccuracies in measured strain fields, which are not perfectly consistent with a degrading weld between adjacent measurements, and in part due to there being multiple simulations of weld slightly different weld shapes with very similar surface strain fields, because the strain at the weld surface diffuses through the thickness of the welded plates. In solid black

is a spline fitting of the data, which is later used for comparison to the weld area evolution based on reaction force correlation.

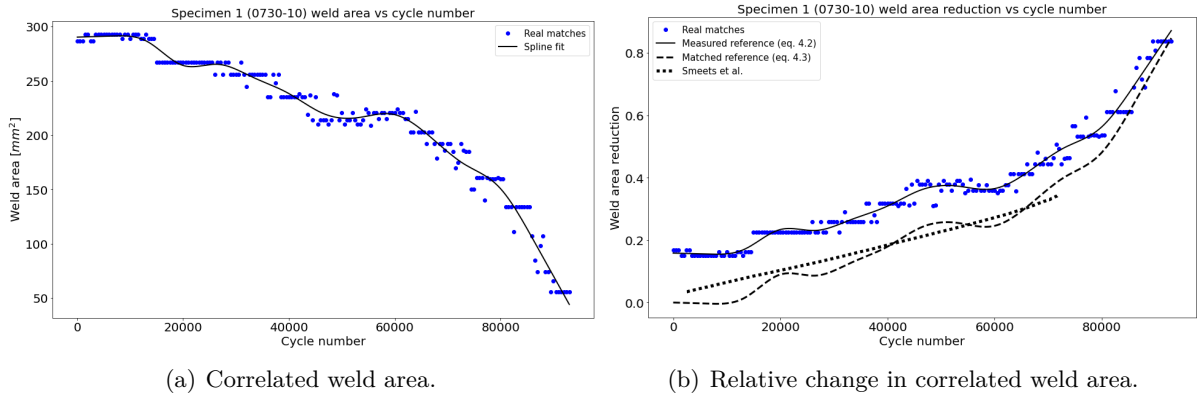


Figure 5.3: DIC to FEM strain field correlation weld area results for specimen 1.

The dashed black lines in figure 5.3 are the changes in estimated weld areas, expressed with respect to the first match result, obtained through the strain field analysis method presented in this thesis, and by [14] through the analysis method published in [15]. By comparing the dashed lines it is possible to contrast the results obtained by both methods of measured strain field analysis.

Figure 5.4 shows the weld area evolution based on reaction force correlation. Each dot in the picture corresponds to the reaction force measured during a loading cycle. The color of dots correspond to the criterion used to gradually disbond the welds, as explained in section 4.3. Overlapped in solid black are the results of strain field correlation from figure 5.3, and overlapped in figure 5.4(b) in dashed black lines are the relative area changes presented in figure 5.3(b).

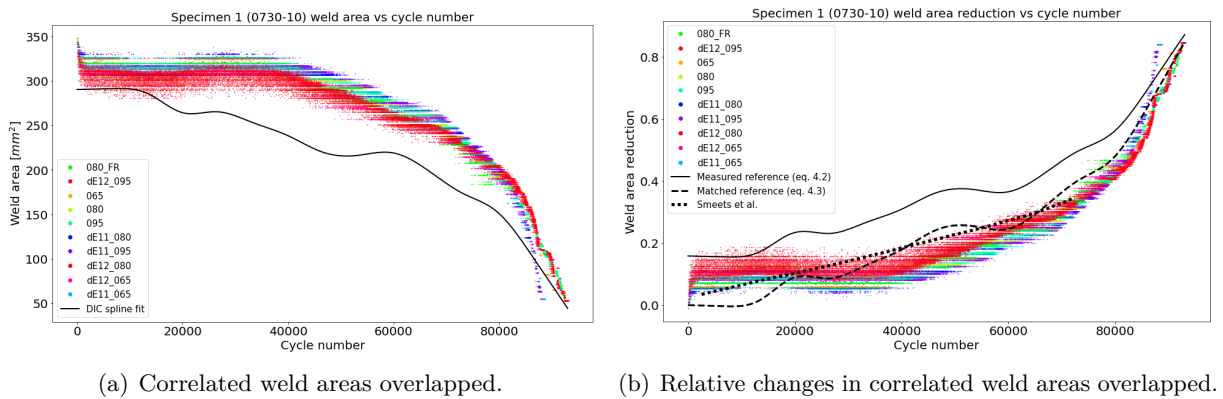


Figure 5.4: DIC to FEM strain field weld area results overlapped with measured reaction force to FEM reaction force correlation results for specimen 1.

To aid in understanding how the data points are placed in figure 5.4, figure 5.5 shows again the reaction force measured during the experiment, and the simulated relationships between the reaction force and the weld areas for this specimen from the database of simulations. The same figures were used as example in the explanation from section 4.3, where more explanations can

be found. In subsequent sections, more examples from other tests are included, which can be referred to by the reader for comparison.

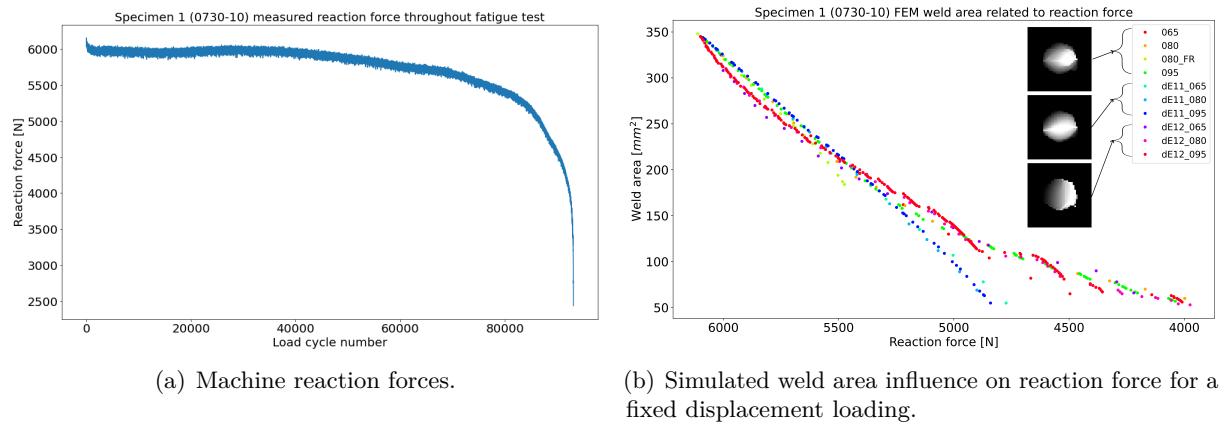


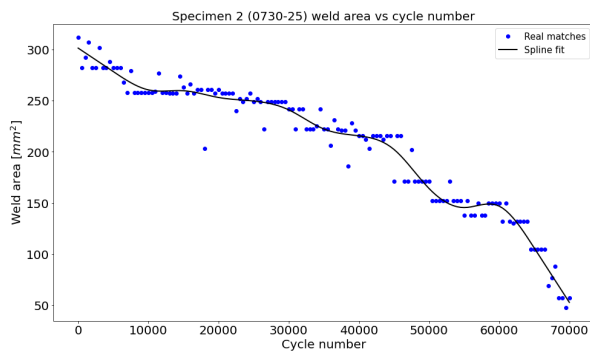
Figure 5.5: Measured reaction forces and simulated dependency between weld area and reaction force for specimen 1.

There is a slight disagreement between the estimated weld areas made with the two methods, possibly because of the lesser accuracy of DIC measurement on the back side of the specimen for this test in this data set. It was observed that the strain fields measured on the back of the specimen tend to be "squeezed" vertically when compared to the strain fields measured on the front of the specimen. This can also be seen both in figure 5.1 and in figure 5.2. As a result of the strain fields on the back side being narrower for this specimen, and the matching algorithm giving equal weight to both the front and the back side correlations, the matched weld areas overall were slightly smaller than that obtained through reaction force correlation. Figure 5.4(b) shows the change in predicted weld area relative to the initial weld area, approximated by the area of the weld mask traced by hand. An area reduction higher than 0 for the prediction made through strain field correlation confirms that indeed the approximated area, at least at the start of the fatigue test when the weld should have been intact, is underestimated.

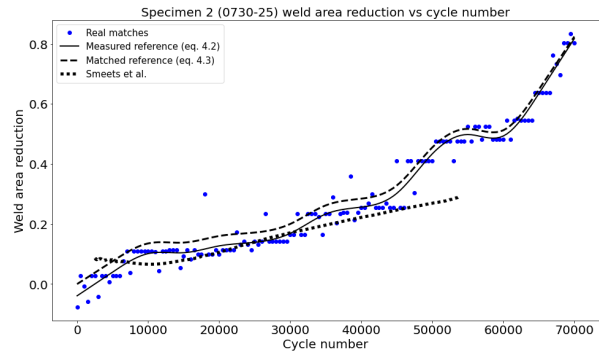
5.1.2 Results for specimen 2 (0730-25)

For the second specimen presented in this thesis, the strain field correlation analysis showed consistently accurate results. The strain field matching results details are included in appendix E, in a structure similar to that used in section 5.1.1. The conclusion of the analysis results are presented below.

Figure 5.6 shows in blue dots the results of DIC matching for the entire fatigue life, in terms of weld area and change in weld area with respect to the first matched area. In black is a spline fitting result of the data, which is later used for comparison to the weld area evolution based on reaction force correlation. In dashed black lines in figure 5.6(b) are the changes of damaged weld areas relative to the first matching results through the strain field correlation method of presented in this thesis and through the method of analysis proposed by [15].



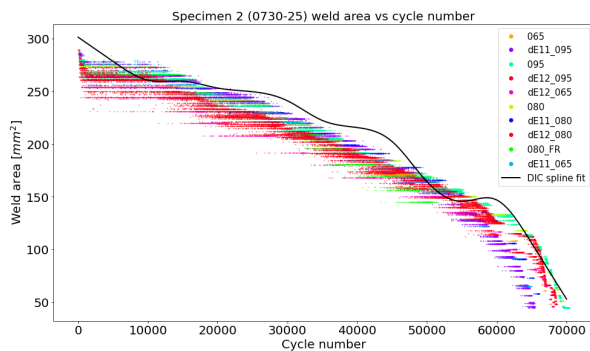
(a) Correlated weld area.



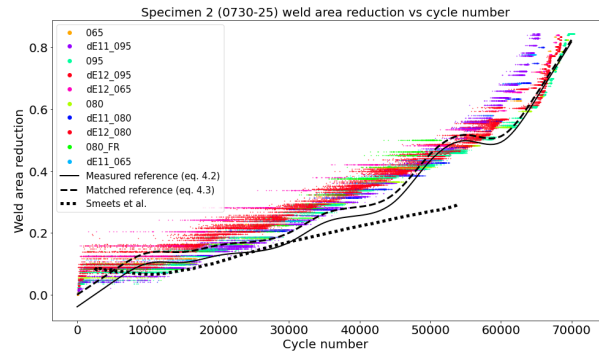
(b) Relative change in correlated weld area.

Figure 5.6: DIC to FEM strain field correlation weld area results for specimen 2.

Figure 5.7 shows the weld area evolution based on reaction force correlation. Each dot in the picture corresponds to the reaction force measured during a loading cycle. The color of each dot corresponds to a particular criterion used to disbond the simulated welds to create the database of simulations. Overlapped in black are the results of strain field analysis from figure 5.6.



(a) Correlated weld areas overlapped.



(b) Relative changes in correlated weld areas overlapped.

Figure 5.7: DIC to FEM strain field weld area results overlapped with measured reaction force to FEM reaction force correlation results for specimen 2.

The data used to create figure 5.7 is displayed in figure 5.8. On the right is the reaction force measured during the displacement controlled experiment by the test machine, and on the left are the simulated relations between the reaction force and the weld area, for different weld shapes generated through the color coded fatigue criteria.

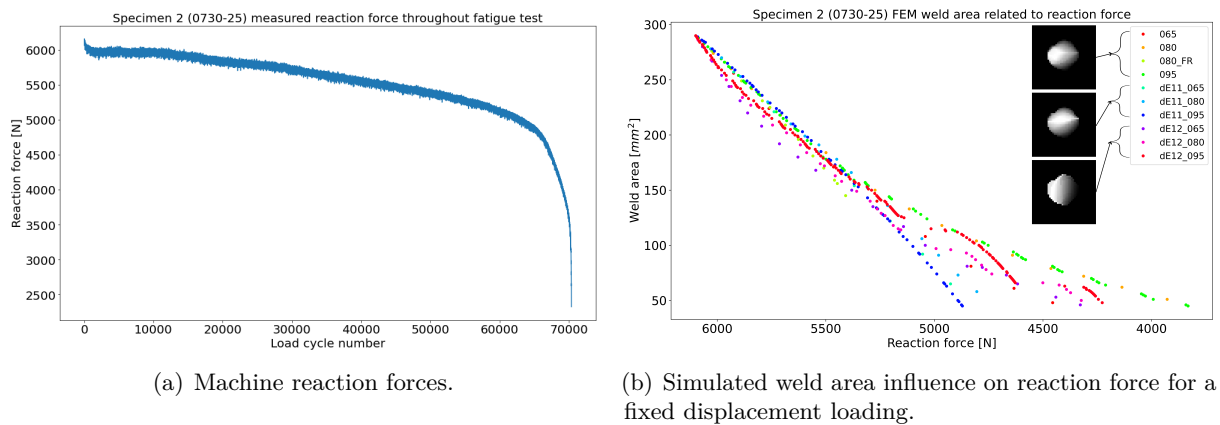


Figure 5.8: Measured reaction forces and simulated dependency between weld area and reaction force for specimen 2.

The weld area estimated by strain field correlation remains slightly higher than that estimated through reaction force correlation. The real weld area was likely in between, as the increase in compliance after the secondary welds broke would also lead to an underestimation of weld area through reaction force matching, because in order for the reaction force to drop by the same amount in the simulations, the weld had to be disbanded more. Figure 5.7(b) shows that the DIC spline fit starts at a value lesser than 0, which supports the observation that the weld area estimated by strain field correlation is slightly over-estimated, as the starting weld area was larger than the area of the manually traced weld profile.

5.2 Results displaying less agreement

Errors in reaction force measurement, inaccuracies in strain fields computed through DIC and limiting assumptions in the FEM simulations are the main sources of error for the specimens analyzed in this report. For specimens other than those on which the current database of FEM simulations was based, the limited choice of simulations for comparison may be another important limiting factor in the accuracy of the obtained results. Last but not least, the strain correlation criterion may over-emphasize matching of areas where the measurement errors are large, as it has no notion of which part of a measurement correspond best to physical behavior.

5.2.1 Results for specimen 3 (0730-4)

The left side of figure 5.9 shows real measurements of surface strain fields for specimen 3 after 50 loading cycles, and a photograph of the fracture surface. After only 50 loading cycles, when the first set of pictures were taken by the DIC systems, it is expected that the weld shape remained almost identical to the pristine shape of the weld, which can be approximated by the outer contour of the fracture surface. The right side of figure 5.9 shows correlated surface strain fields from the database of simulations, and the modelled weld surface which created them.

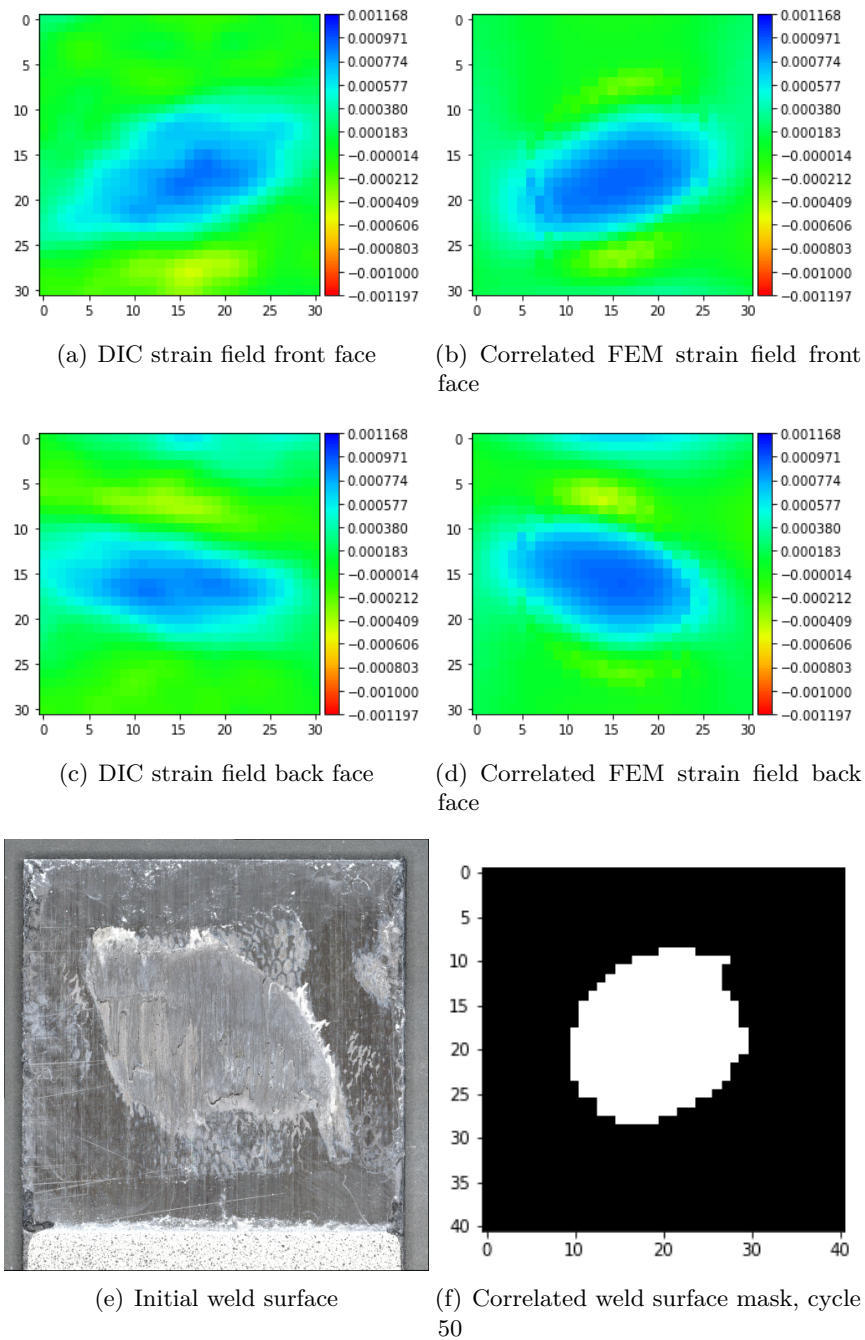


Figure 5.9: DIC to FEM strain field correlation results for specimen 3, loading cycle 50, longitudinal component (E_{11}).

The shape deviation of this manufactured weld spot from the desired circular shape was significant. Having said that, the measured strain distributions are not different enough from that of other simulated weld shapes to allow for a more accurate match. The confusions in matching that occur due to similarity is illustrated below. This is a limitation of the method, as strains at the surface of the weld diffuse through the thickness of the plate, and are only measured with limited accuracy. In order for the matching result to be more unequivocal, more accurate strain field measurements are required.

The left side of figure 5.10 shows real measurements of surface strain fields for specimen 3 after 2500 loading cycles, and a photograph of the fracture surface to aid in assessing the matched result. The right side of figure 5.10 shows correlated surface strain fields from the database of simulations, and the modelled weld surface which created them.

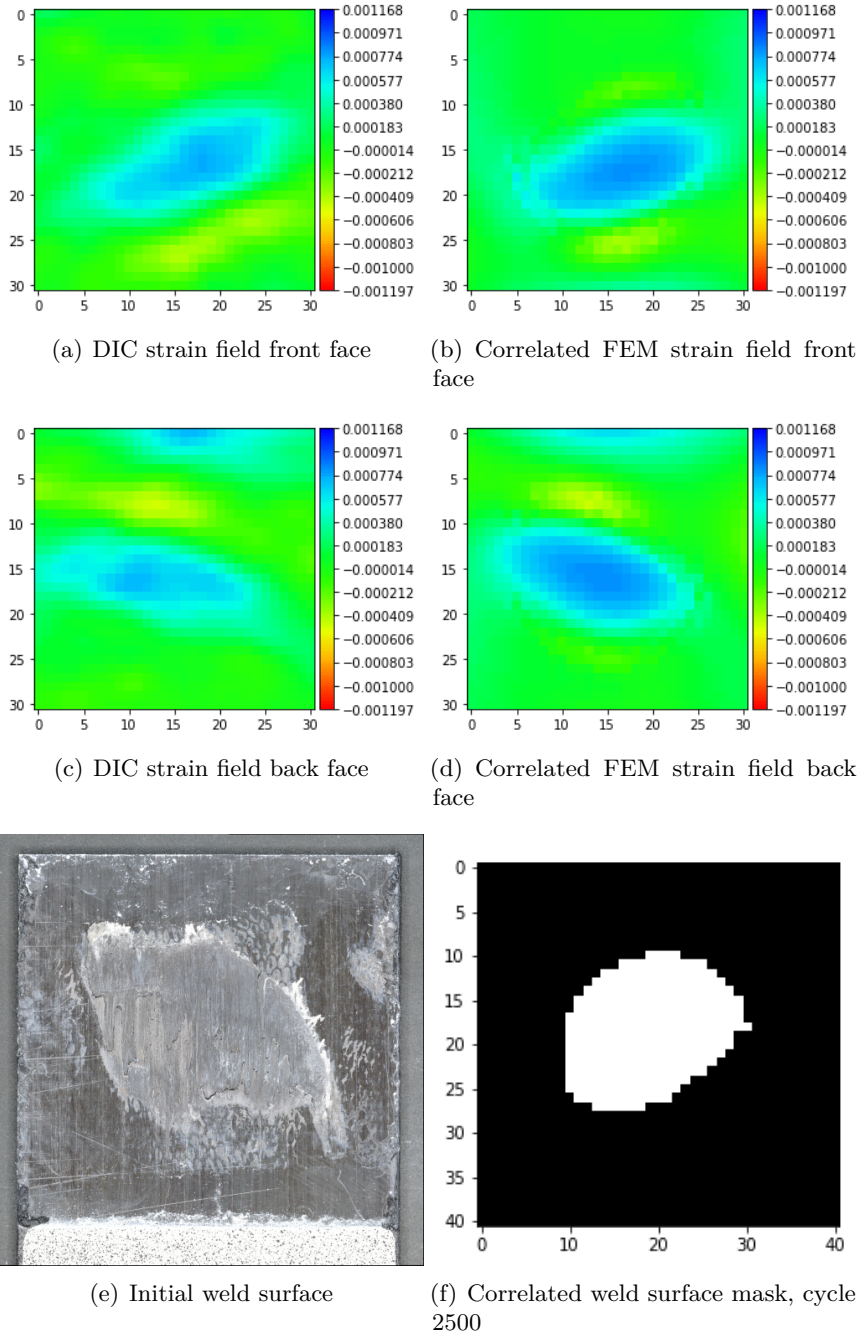


Figure 5.10: DIC to FEM strain field correlation results for specimen 3, loading cycle 2500, longitudinal component (E11).

To showcase the effect of inaccuracies in measured surface strain fields through DIC, the results for the very next set of DIC strain fields, measured 50 loading cycles later, is shown in figure 5.11.

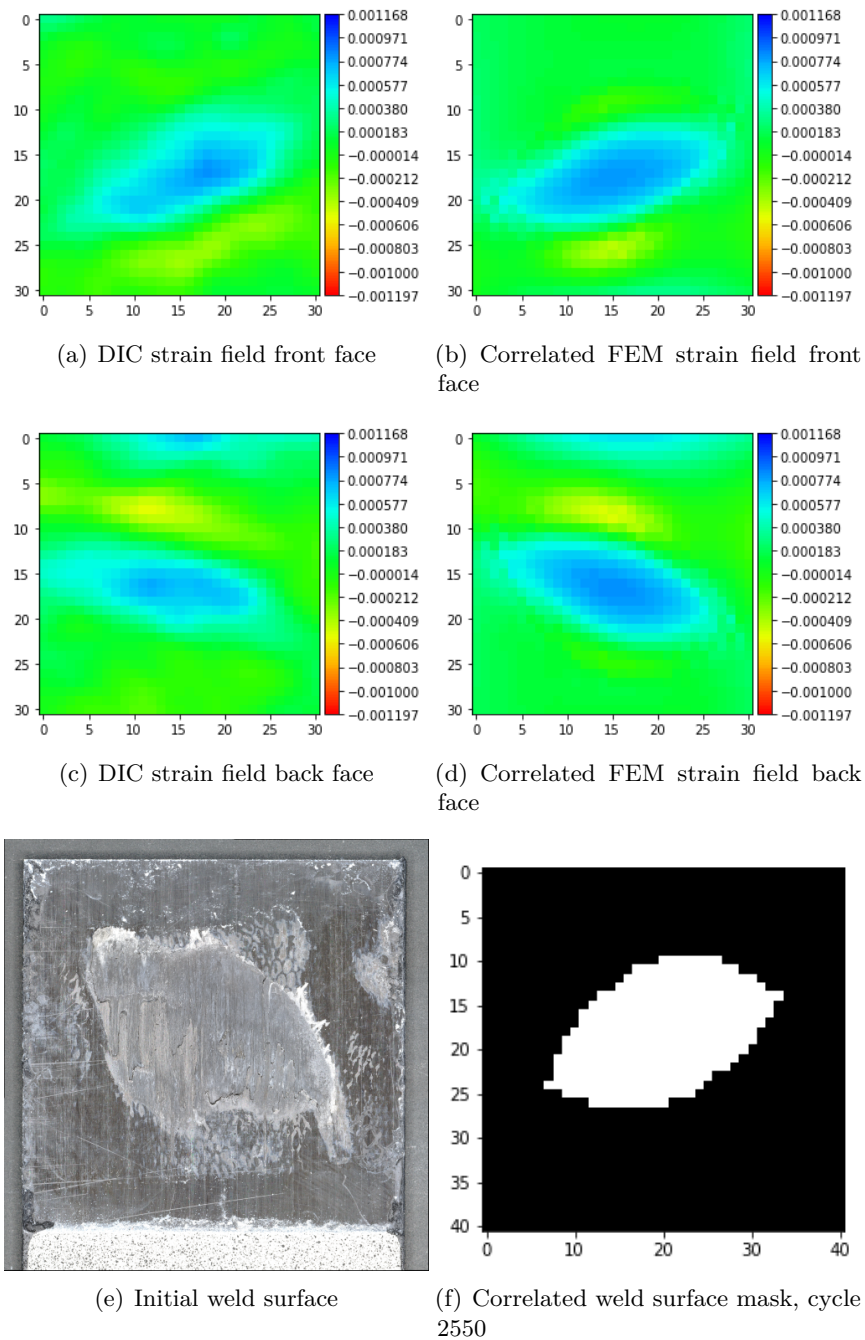


Figure 5.11: DIC to FEM strain field correlation results for specimen 3, loading cycle 2550, longitudinal component (E11).

Comparing the measured strain fields shown in figure 5.10 and figure 5.11 emphasizes how a slightly different measurement due to errors, can lead to a different optimal matching result from the database of simulations. The correlated weld surface masks, shown in figure 5.10(f) and in figure 5.11(f), respectively, are an example of the ability of the method to conclusively characterize the shape of a weld in the presence of a large enough set of simulations, for which the errors in consecutive measurements can breach the distinction between two different simulations.

The large oscillations in strain field correlation results are visible through the large spread in matched modelled weld areas shown in blue in figure 5.12, particularly for the first 6000 loading cycles. Overlapped in black is a spline fit over the data used to smoothen it for further comparison. The dotted black lines in figure 5.12(b) help in comparing the relative changes obtained through the method proposed in this thesis with the earlier results of [14].

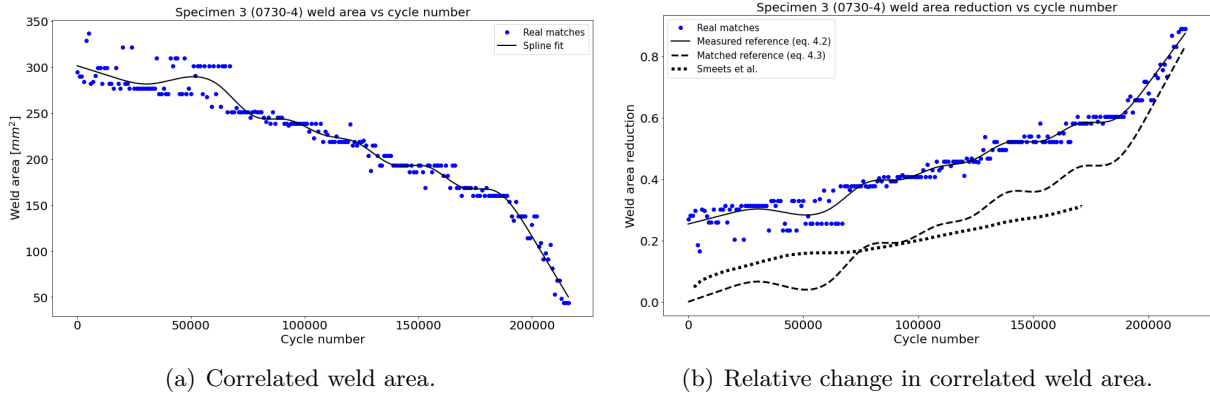


Figure 5.12: DIC to FEM strain field correlation weld area results for specimen 3.

Figure 5.13 shows the weld area evolution based on reaction force correlation. Each dot in the picture corresponds to the reaction force measured during a loading cycle. Overlapped in black are the results of strain field correlation from figure 5.12.

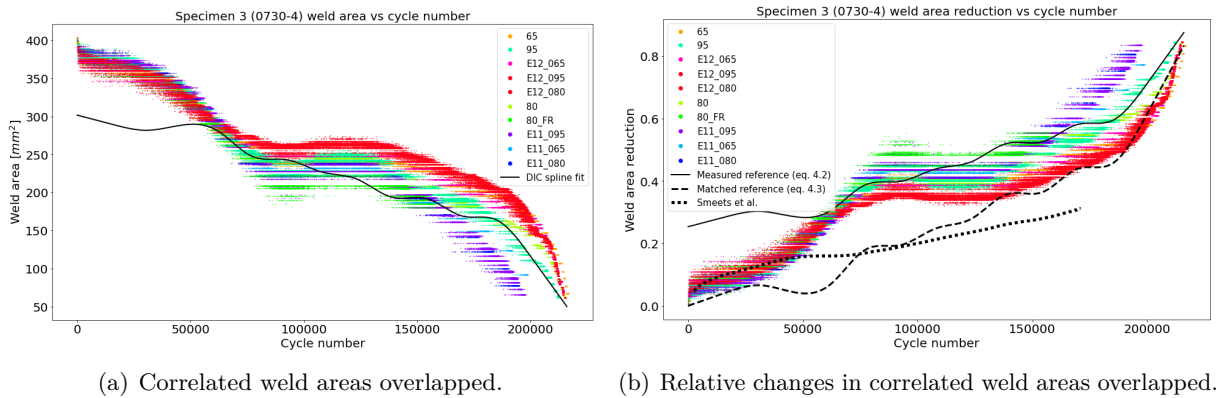


Figure 5.13: DIC to FEM strain field weld area results overlapped with measured reaction force to FEM reaction force correlation results for specimen 3.

At the beginning of the test, where the strain field correlation showed less stability, the estimated weld areas through strain field correlation and through reaction force correlation differ the most. The fact that the estimate through reaction force correlation is higher, considering that at the beginning of the test the method of reaction force correlation is most accurate, would indicate that the matches with the larger areas for the first 5000 loading cycles, represented by the peaks in figure 5.13(a), were more representative of the weld shape. Indeed, looking at figure 5.11(e) and figure 5.11(f), which would correspond to one of those matches with larger weld area, there is more similarity in shape as compared to the match result shown in figure 5.10(f). Figure 5.13(b)

further supports, through relative comparison with the area of the weld area traced by hand, that the weld area through strain field correlation was under-estimated at the start of the test.

The estimated weld area through reaction force correlation is not strictly monotonous. Around loading cycle 9000 there is an increase in estimated weld area. This is because the reaction force measured by the test machine, shown in figure 5.14(a), registered an increase. This is not considered physically realistic, and is likely a measurement error due to a variation in temperature in the laboratory. Testing this specimen took approximately twice as many loading cycles compared to the previously presented ones, and the test ran over night, when the temperature in the laboratory likely dropped and then increased again the following morning.

A second distinguishing feature of figure 5.13 when compared to previously presented results is the larger spread in the weld areas estimated through reaction force correlation. This is because there was more variation in the shapes of the simulated disbonded weld shapes, as the shape of the real weld was more more irregular and was influenced more by the disbonding criteria used to generate the database of simulations. Figure 5.14(b) shows the corresponding relationships between simulated reaction forces, weld areas and disbonding criteria used for simulating this specimen.

In the second half of the fatigue test, there was good agreement between the estimations made by strain field correlation and by reaction force correlation in terms of weld area.

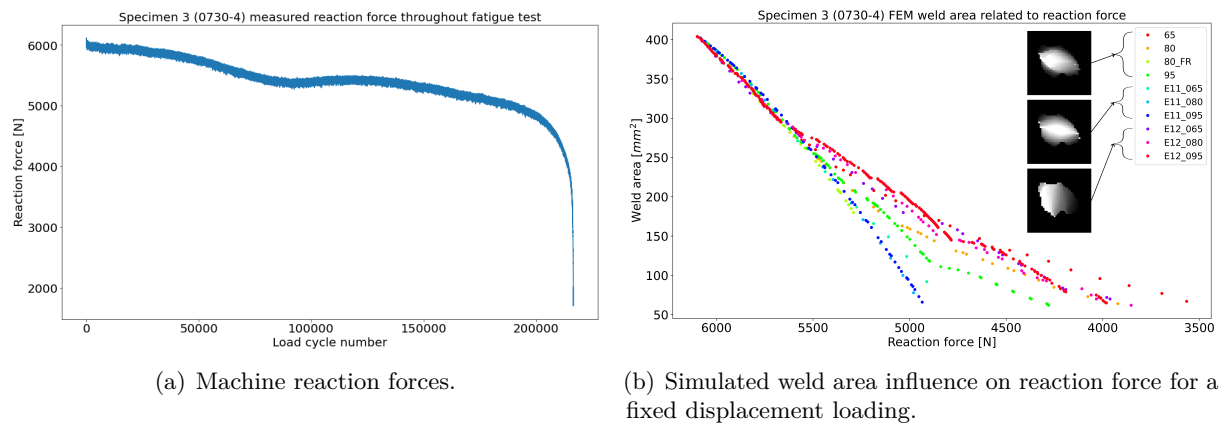


Figure 5.14: Measured reaction forces and simulated dependency between weld area and reaction force for specimen 3.

5.2.2 Results for specimen 4 (0730-24)

The strain field analysis for specimen 4 was of consistent quality, and is presented in detail in appendix F. In this section only the summary of the results of strain field analysis is included below. This specimen is being discussed in this section of specimens showing less agreement between the results of strain field analysis and the results of reaction force matching to showcase an instance when the specimen settling within the first loading cycles affected the effective loading of the specimen for the entire fatigue life test. The results obtained through reaction force correlation are therefore the less accurate ones for specimen 4.

Figure 5.15(a) shows in blue dots the matched weld areas through strain field correlation, and in black a spline fit of the data, which is used for further comparison. Figure 5.15(b) shows the

relative change in estimated weld areas with respect to the area of the weld surface, approximated by the area of the mask traced by hand used to model the weld. As the relative change in area at the start of the experiment is close to 0, the strain field correlation method gave an accurate approximation of the measured weld area.

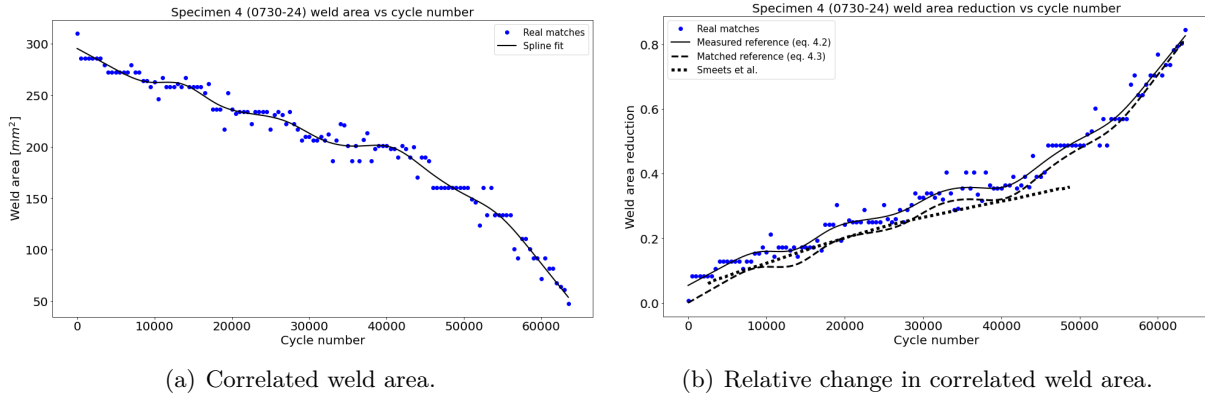


Figure 5.15: DIC to FEM strain field correlation weld area results for specimen 4.

Figure 5.16 shows the weld area evolution based on reaction force correlation. Each dot in the picture corresponds to the reaction force measured during a loading cycle. Overlapped in black are the strain field correlation results from figure 5.15.

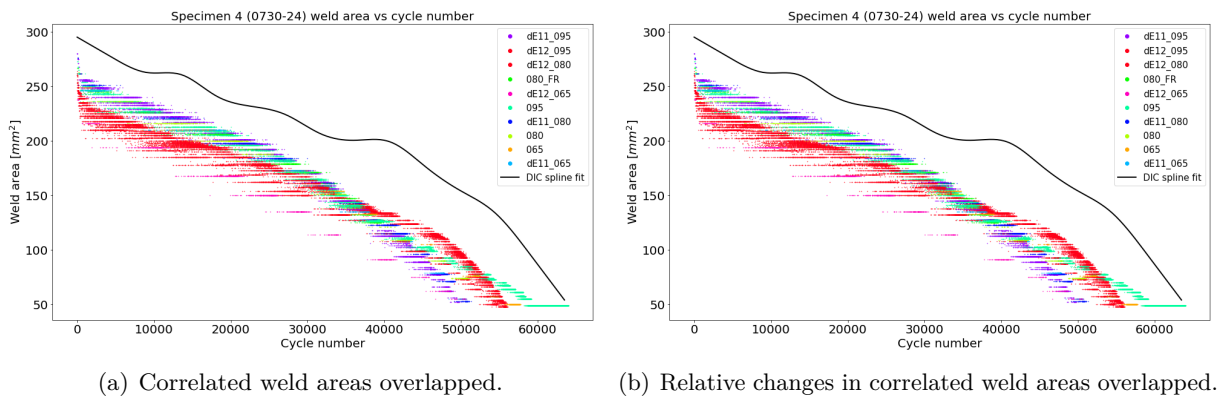


Figure 5.16: DIC to FEM strain field weld area results overlapped with measured reaction force to FEM reaction force correlation results for specimen 4.

The weld area estimated through reaction force matching is consistently lower than that estimated through strain field correlation. This is because at the start of the fatigue test the reaction force dropped quickly in the displacement controlled test, as shown in figure 5.17(a). The larger drop in reaction force than registered previously for the other specimens presented is possibly due to the combined effect of the secondary weld breaking, discussed in appendix F, and the specimen settling within the clamps of the test machine. Having said that, the trend in weld area estimation is very similar to that obtained through strain field correlation, which is a good result. The bottoming out of the weld area estimated through reaction force matching is due to the limit on the lowest area of weld simulated. If the applied loading in the real test is not the same as that used in the simulations, such situations will occur where reaction force correlation reaches

the bounds of the physical areas of the welds. In other words, it is not possible to obtain lower reaction forces through simulation for the given fixed displacement loading, nor is it possible to simulate a higher reaction force than that corresponding to an intact weld at the imposed displacement boundary condition. Figure 5.17(b) shows the simulated relationships between weld areas and reaction forces, for different weld shapes obtained through disbonding the weld according to the different criteria described in section 4.1.

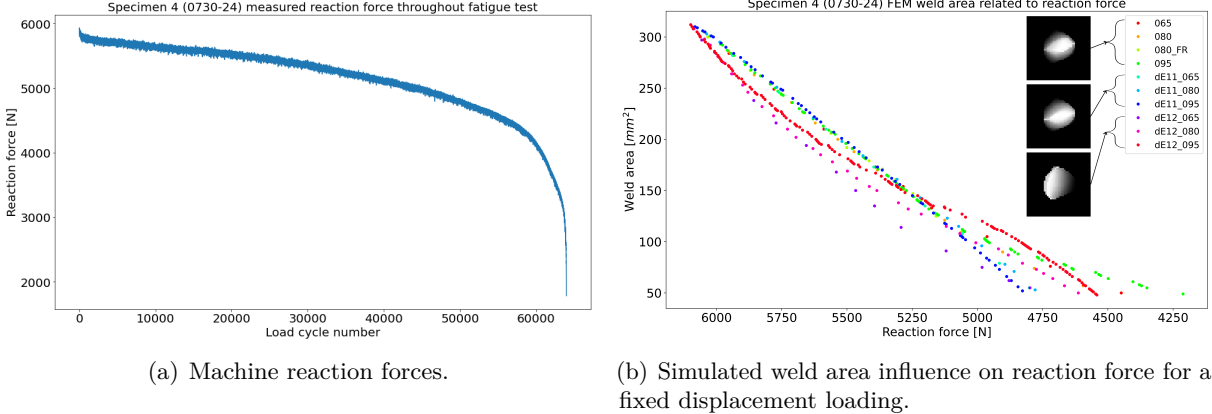


Figure 5.17: Measured reaction forces and simulated dependency between weld area and reaction force for specimen 0730-24.

6 Methodology for multiple weld spot analysis

The multiple weld spot analysis presented in this chapter is an extension of the methodology used to analyze the lap shear specimens containing single spot welds. A collection of finite element simulations is made to approximate the surface strain fields expected to be measured during experiments through digital image correlation. As the methodology of analysis naturally extends to any general ultrasonically welded lap shear joint, the structure of this chapter follows that of chapter 4. Further mentions are only made where relevant to the analysis of the specimens with all spot welds arranged in a vertical column, described in section 6.1.

6.1 Multiple spots fatigue experimental setup

The specimen manufacturing and the experimental setup for the multiple weld spot analysis part of the thesis have been done in collaboration with the authors of [15]. Three types of specimens were attempted, all containing 4 round ultrasonic weld spots: one type with all spots in a column, another type with all spots in a row, and another type with 4 spots in a square. Manufacturing of specimens with all spots in a row was not successful and was abandoned. Figure 6.2 shows the geometry of specimens with 4 spots in a square, which, after many attempts, was manufactured well enough to attempt fatigue testing on it. Unfortunately, the quality of the manufactured welds were still too inconsistent to be able to test the specimens in fatigue under similar loading. Fatigue testing the column specimens spanned multiple weeks with repeated loading increments, which makes the data difficult to analyze, due to having to build a computationally expensive database of reference finite element simulations for each loading condition used in the testing, and the testing of a statistically relevant batch of specimens impractical.

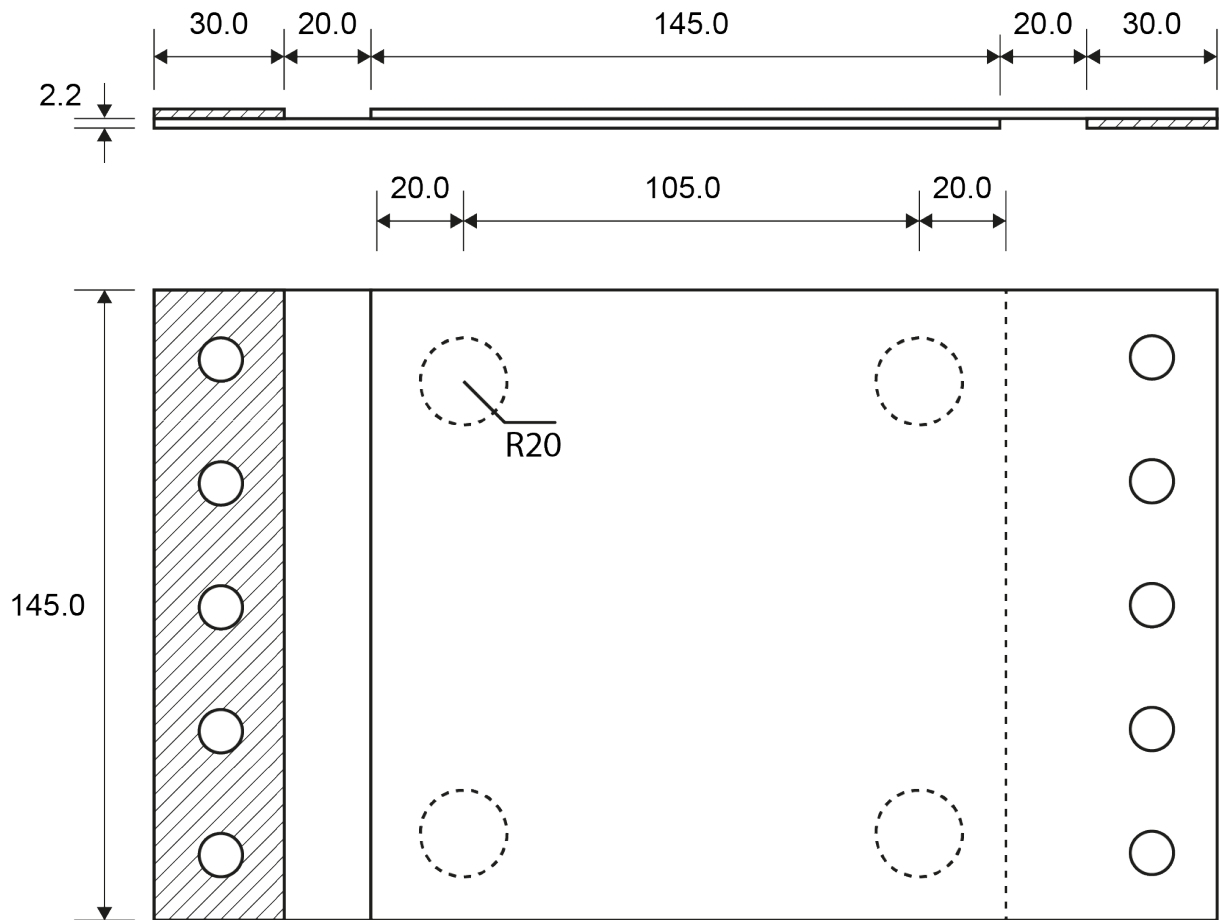


Figure 6.1: Geometry of square specimen successfully manufactured, picture courtesy of the authors of [15].

After significant trial and error with welding parameters, which will be later published by the authors of [14], only the specimens with all weld spots in a column shown in figure 6.2 were successfully manufactured and tested. The analysis of those specimens is presented in this thesis.

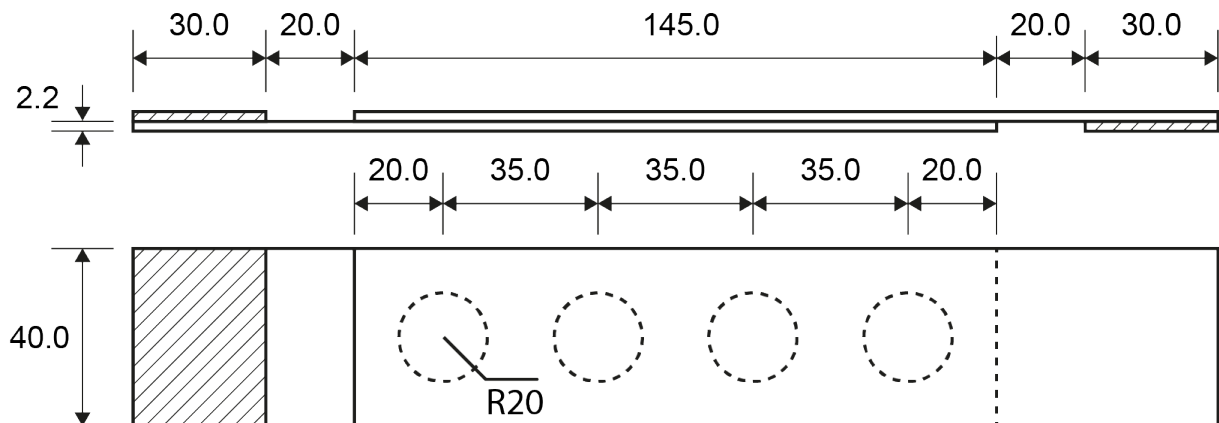


Figure 6.2: Geometry of column specimen successfully manufactured, picture courtesy of the authors of [15].

6.2 Creation of finite element database of simulations

As in section 4.1, a database of FEM simulations of the real lab experiments is compiled, which is to be used for comparing surface strain fields and reaction forces measured during the experiments, to simulated surface strain fields and reaction forces. Care was taken, in line with the discussion in section 4.1, to include as much relevant, possibly realistic variability in the shapes of the welds simulated for each real specimen, while maintaining the computational cost, of building and searching through such a database, limited. The welds of each tested multiple-spot specimen are flipped and mirrored, and omitted from the specimen in each combination possible. Weld spots are omitted to enforce as much variation the fatigue of weld spots outside the regular progressions obtained through sequentially breaking an intact specimen. An example of omission is given in appendix B. A database including such omission will be referred to as an "enhanced database". Furthermore, the database is augmented with fictitious sets of welds representing potential specimens, processed in the same way. Each set of welds is subsequently fatigued using the same criteria described in section 4.1, with the distinction that for this database the criteria are combined randomly at each fatigue cycle to gain a representation of the mean effect of the criteria after fewer simulations. For the analysis of the specimen presented in chapter 7, approximately 8000 finite element simulations were available for comparison. Including more simulations in the data set for that specimen would not bring any significant improvements in the consistency of the results, as the relatively lower quality of the measured strain fields through DIC are the bottleneck in achieving better correlation between simulation and real measurement. Further discussion on the acquired DIC data is included in section 6.3.

6.2.1 Choice of finite elements

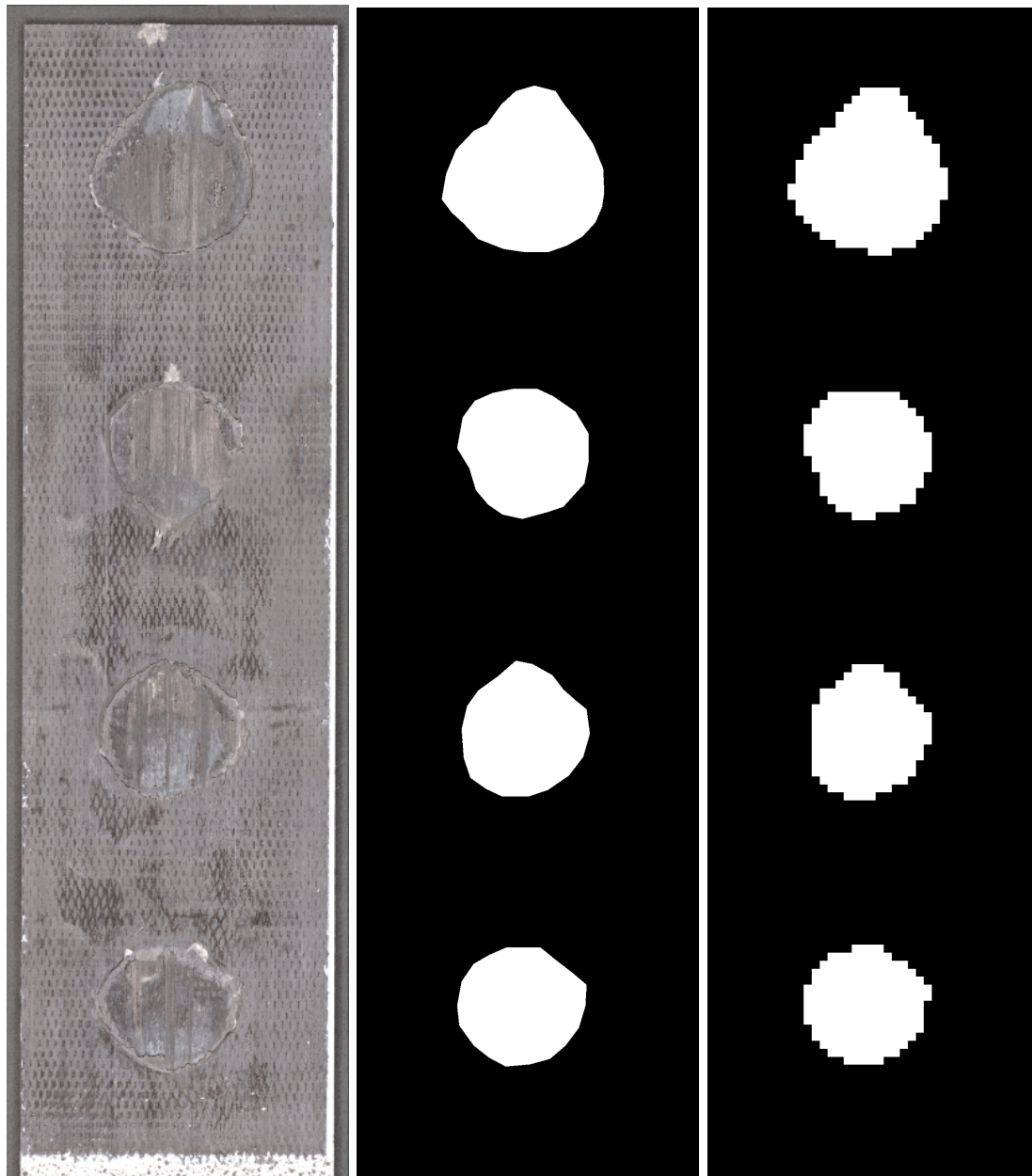
The same finite elements described in section 4.1.1 were used in the simulations of lap shear joints containing multiple weld spots. The advantage of the analysis method presented is that once it is set up, there is comparatively little human effort in adapting it to the analysis of similar experiments.

6.2.2 Choice of boundary conditions

As the boundary conditions of the real tests have not changed between the test campaigns, the same boundary conditions illustrated in figure 4.5 were maintained in the simulations. The discussion of boundary conditions implemented in the simulation, from section 4.1.2, remains relevant.

6.2.3 Numerical representation of weld spots

The same numerical representation of weld spots was maintained from the single spot specimen analysis. The discussion in section 4.1.3 remains relevant. Figure 6.3 shows the process of creating a representation of real welds at mesh nodal locations, through tie constraints.



(a) Specimen 1705-09-12 weld spot. (b) Specimen 1705-09-12 weld spot hand drawn mask (c) Specimen 1705-09-12 weld spot hand drawn mask discretized

Figure 6.3: Weld spot modelling representation through nodal tie constraints.

6.2.4 Finite element implementation

The same finite element implementation described in section 4.1.4 was used. As in section 4.1.4, a favorable comparison between surface strain fields over the overlap area, simulated with Abaqus and displayed in figure 6.4, and simulated with the custom FEM implementation, shown in figure 6.5, can be made. As there is less secondary bending, due to the geometrical configuration of the multiple weld spot specimens analyzed in this report, shown in figure 6.2, the linear-only implementation of the continuum shell elements produces accurate results for a fully welded specimen.

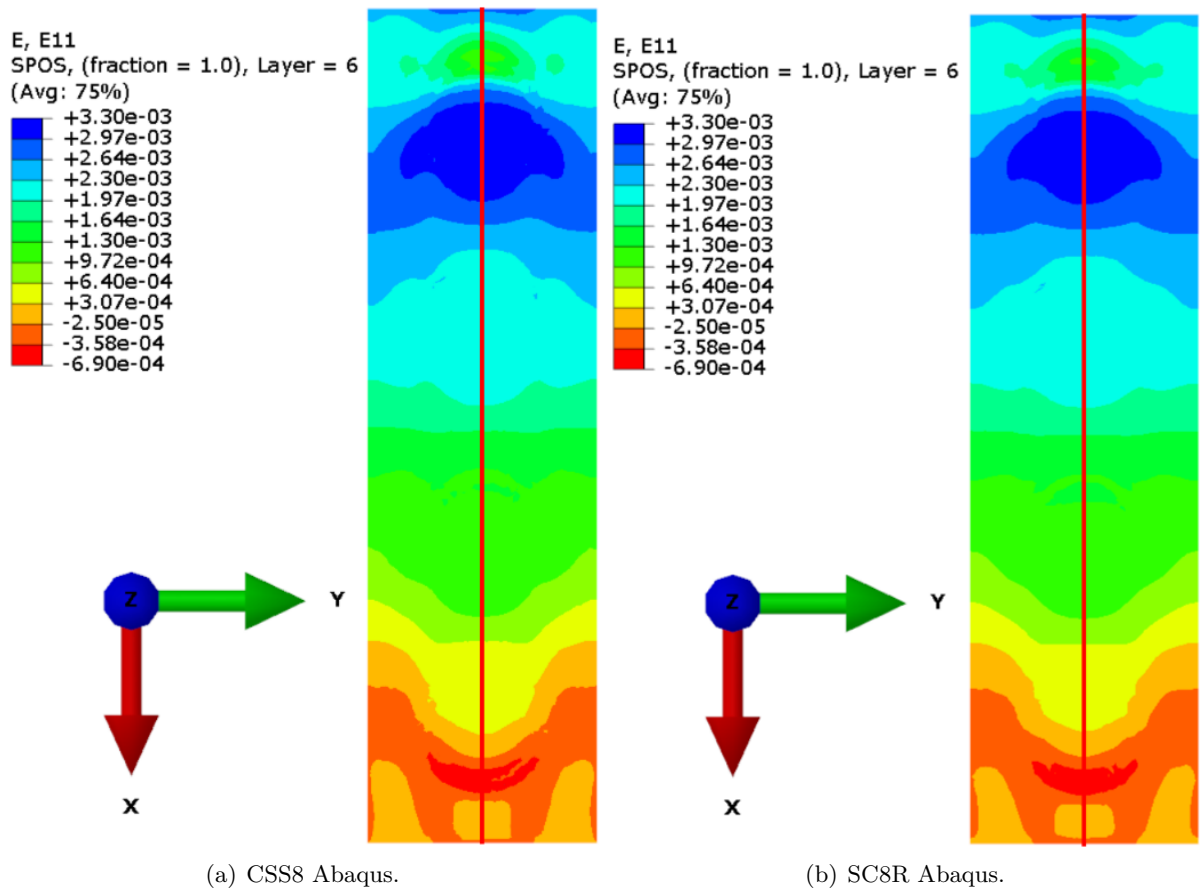


Figure 6.4: Simulated surface strain distributions for a column of perfectly round weld spot with continuum solid shell elements in Abaqus.

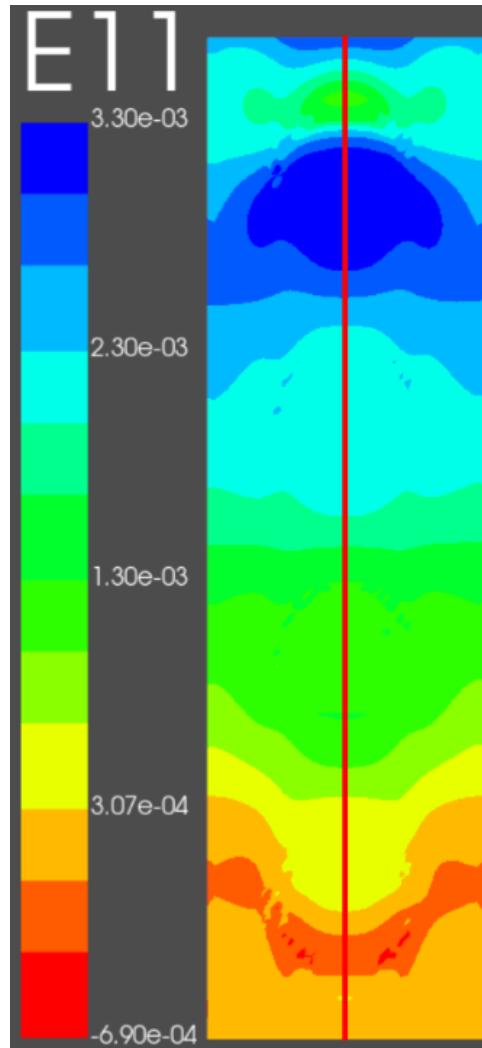


Figure 6.5: Simulated surface strain distribution for a perfectly round weld spot with the custom implementation of continuum solid shell elements.

6.2.4.1 Implementation limitations

As the specimens fatigue and welds break, the accuracy of the solution is expected to decrease slightly due to an increase in secondary bending which is under-estimated by the overly stiff linear continuum shell elements. Having said that, no further adjustment was made to compensate for the potentially less accurate bending behavior towards the end of a fatigue test, because the less precise measured strain fields are limiting the accuracy of correlation more than a slightly less accurate bending curvature estimation. Moreover, a broken weld is not perfectly equivalent to an absent weld. Plastic deformations on the outer surface of the plate remain as a result of the ultrasonic welding process, and the fracture surface includes damage in at least the first layers at the contact between the plates. Those characteristics of damaged specimens have not been modelled and will also have an effect on the surface strain distributions after weld spots have failed. Without accurate modelling of the mechanical properties of ultrasonically welded plates, which currently is not available, it is not possible to accurately include the full effects of damage in a simulation. Even if it were possible, the cost to benefit ratio for this particular application of comparing hypothetically highly accurate surface strain fields to relatively inaccurate measured

strain fields with DIC is not advantageous. Little benefit in damage measurement is expected through more accurate modelling, as the accuracy of real measurements is limited as well.

6.2.4.2 Implementation verification

The good agreement between strain fields simulated with Abaqus and with the custom element implementation of this project, shown in figure 6.4 and in figure 6.5, for the multiple weld spot in a column specimens, stands as further verification for the correctness of the implementation for this particular application.

6.2.5 Choice of meshing technique

The same meshing technique described in section 4.1.1 was used in the simulations of lap shear joints containing multiple weld spots. The mesh resolution of one element per square millimeter and two elements through the thickness of each plate was maintained, in line with the convergence analysis presented in appendix D. Figure 6.6 shows the mesh used to model the plates, and the displacement analysis of a common specimen.

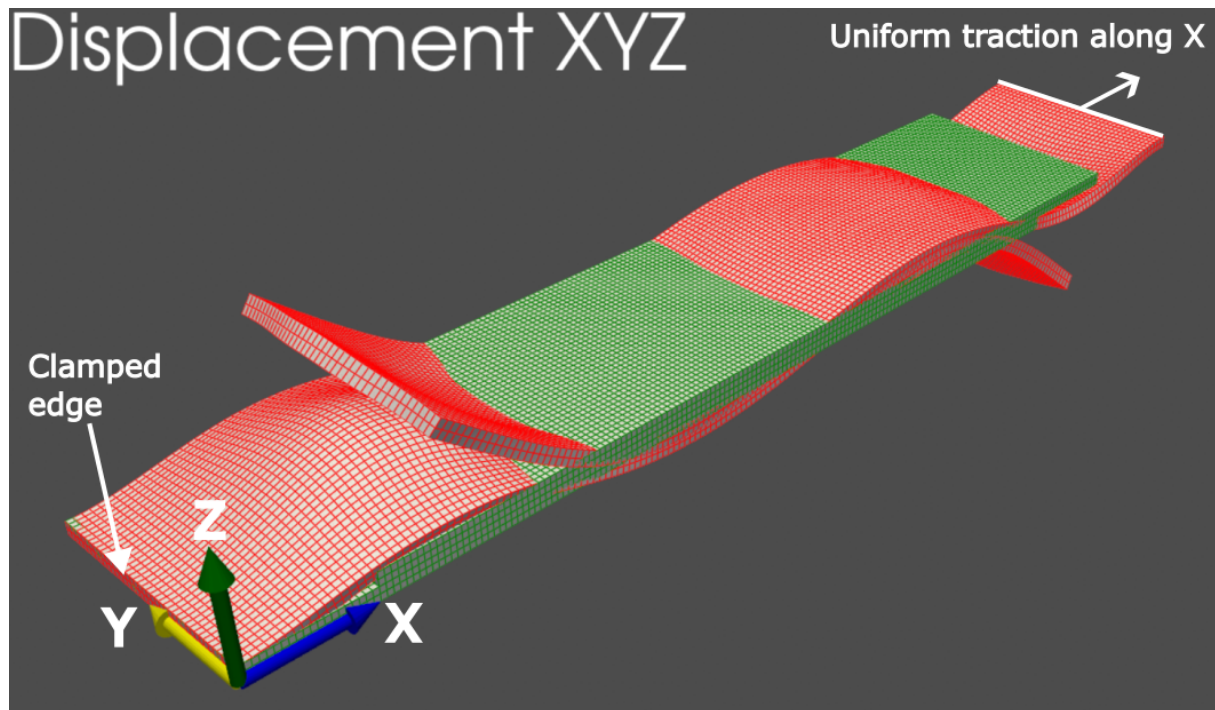


Figure 6.6: Mesh used to model the lap shear test specimens, in its undeformed state in green and in its exaggerated deformed state, which is a result of the simulation, in red.

6.3 DIC to FEM strain field correlation

A square region of interest, as wide as the specimen, is defined around the desired center location of each weld, shown in figure 6.2. The correlation is then done for each section as for the specimens containing a single weld spot, as described in section 4.2. The distinction between the single weld spot correlation and the multiple weld spot correlation is an additional weighing factor when summing up the correlation scores into an overall score for a given specimen comparison. The surface regions, defined by the desired weld locations, where there is more variation in the

strain field, are given a higher score in weighing compared to the correlated areas containing strain fields of lower variation. This way, more importance is given in strain field matching to the locations where there most load transfer. The best results have been obtained with a high relative weight to the areas with high strain variation. To generate the results presented in chapter 7, the correlation score over the region of interest with the highest variation was given a weight of 4, and the correlation score over the regions of interest with the lowest variation a score of 0.1. The scores for the regions in between were interpolated linearly. The simulated weld, which generated simulated strain fields which correlate to the DIC strain fields with the highest total score, is picked as the best match to the real weld.

6.4 Measured reaction force to FEM reaction force correlation

Measured reaction force to simulated reaction force correlation is done the same way as described in section 4.3 for the analysis of single weld spot specimens. The distinctions lie only in the data and not in the methodology. In particular, for specimens containing multiple weld spots, the correlation between reaction force and the area of any particular weld is less strong. There can be many configurations of partly disbonded weld shapes which lead to the same measured reaction force. It is not possible from the reaction force alone to infer which weld spots have degraded. It is possible, however, to use the reaction force as a rough estimation of the total weld area. The more weld spots a specimen will include, the less accurate the estimation of total weld area can be without making assumptions about which spots disbond first. For the case of the specimens with all weld spots in a column, analyzed in this thesis, using the only disbonding criteria and not including any of the enhancement omissions mentioned in section 6.2, shown in appendix B, a relatively clear relation between the total weld area and reaction force is obtained, see figure 6.7. The average weld disbonding pattern, included in the top right corner of figure 6.7, indicates the order in which the spot welds are being disbonded by the damage criteria. The brighter the weld location, the longer it has been present in the simulations.

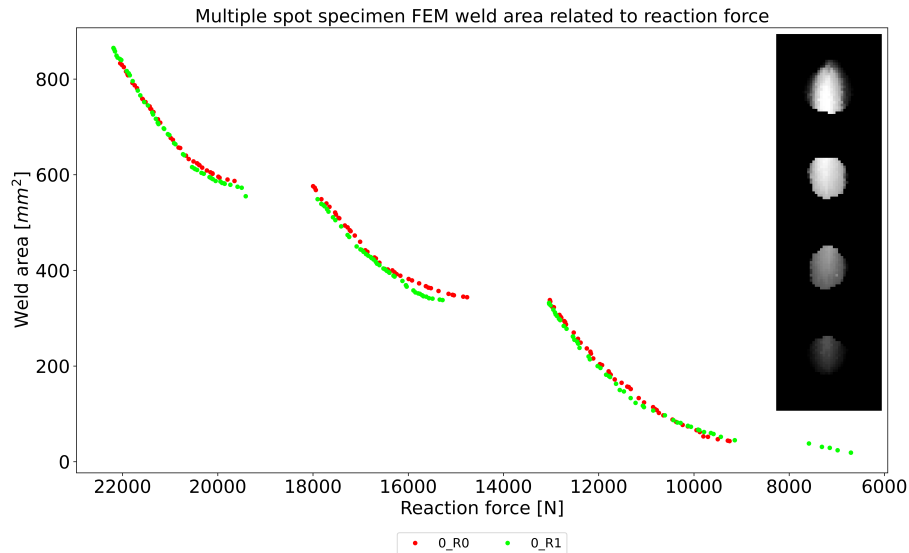


Figure 6.7: Simulated weld area influence on reaction force for a fixed displacement loading.

The low variation in estimated weld area is due to the assumptions made in creating the weld disbonding criteria, namely that disbonding is related to the difference in surface strain between

the welded plates, which must be related to strain within the weld spots. Figure 6.7 only includes two random progressions using the criteria because of the high computational cost of generating more progressions, with low benefit for the comparison as all progressions remain close to the ones shown. If the subsequent omissions of weld spots are included in the database, thus eliminating the influence of the disbonding criteria on the order in which spot welds break, a much wider spread of total weld area for a given reaction force is obtained, shown below in figure 6.8.

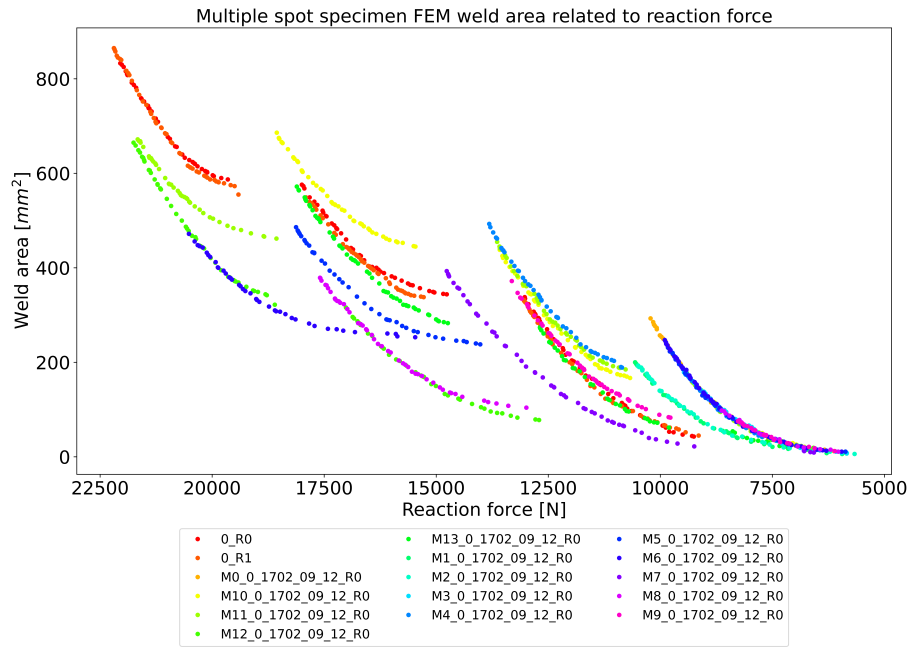


Figure 6.8: Simulated weld area influence on reaction force for a fixed displacement loading.

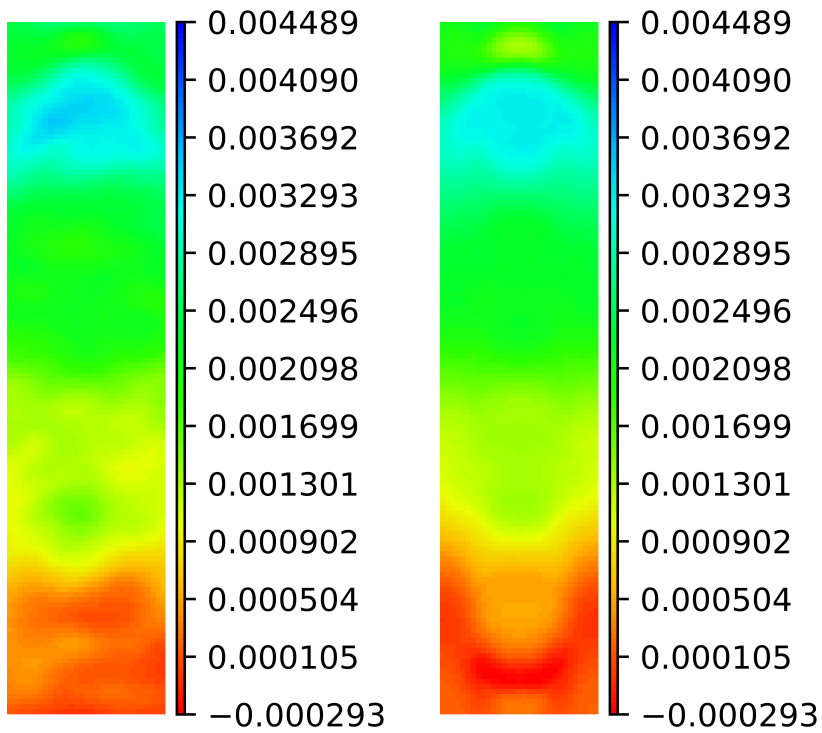
The more weld spots a specimen would have, the wider the spread in weld area a plot such as figure 6.8 would show. Having said that, assuming every possible disbonding mode by omitting relatively lightly loaded welds is not realistic and will reduce the usefulness of the method. As knowledge builds up within the scientific community on the fatigue behavior of ultrasonic welds, through increasing experimental data, assumptions can be made to restrict the disbonding modes considered. Within the scope of this report, the comparison of reaction force matching area estimation to strain field correlation results will be done for two cases: with a database of reaction forces only including the results of disbonding criteria from a mask of the intact specimen, and the enhanced version of the database including the results of disbonding criteria from partial masks of the intact specimen, as shown in appendix B.

7 Results for multiple weld spot analysis

The analysis results of experimental data, collected during fatigue tests of lap shear joints welded with multiple ultrasonic weld spots are presented in this chapter. The methods used for analysis are those presented in chapter 6. In this chapter the results are presented with little qualitative judgment, the discussion being reserved for chapter 8.

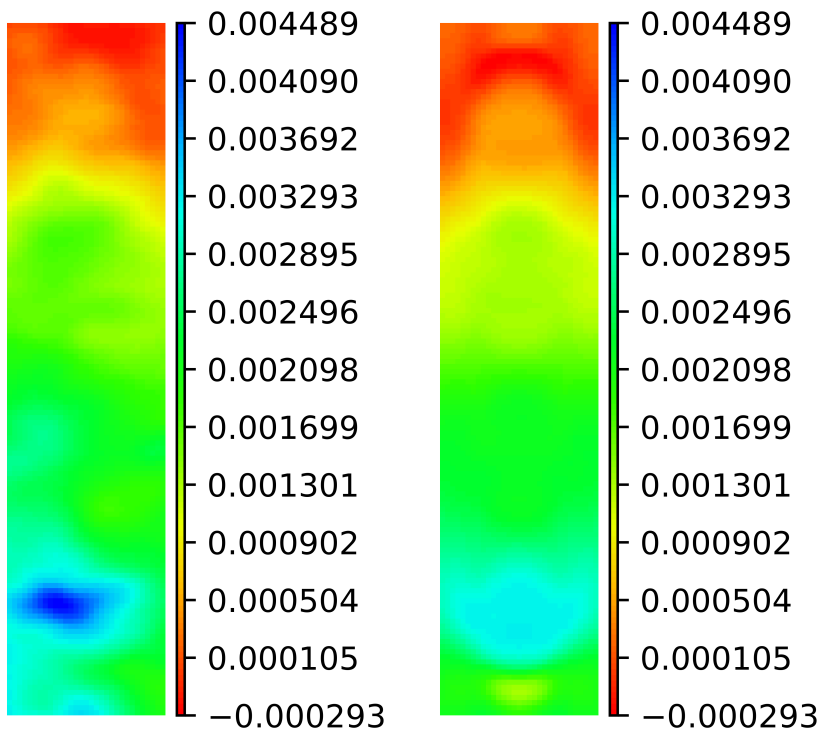
The analysis of specimens containing multiple weld spots generally show less consistency in the results of correlating measured and simulated surface strain fields. This is because the measurements obtained through digital image correlation are less accurate, due to the cameras being positioned further away from the specimen in order to capture the larger overlap area in their field of view. In particular, for the test campaign carried out during this thesis, the DIC system available to be placed on the back side of the specimen was less accurate due to potentially damaged lens mounts. It was very difficult to focus the lenses sufficiently to perform the image correlation, and larger errors are expected from those measurements. In this section, a representative specimen (1705-09-12 for future comparison to [14]) is showcased for which the measurement were of uniform good enough quality throughout the entire overlap outer surface.

In a similar presentation structure to that used to display the results of single weld spot analysis, figure 7.1 shows on the right the surface strain fields on the front and back of the specimen measured with DIC, and on the left the best fit simulated strain fields. In particular on the back face of the specimen the strain field measurements are of lesser quality, showing more variation between subsequent measurement and larger overall deviation from the simulated strain fields. Poorer quality results from the back face DIC system was anticipated from the moment of setting up the experiment, as the system's lenses were very difficult to focus. With a DIC system in better condition it would be possible to achieve more accurate correlation result.



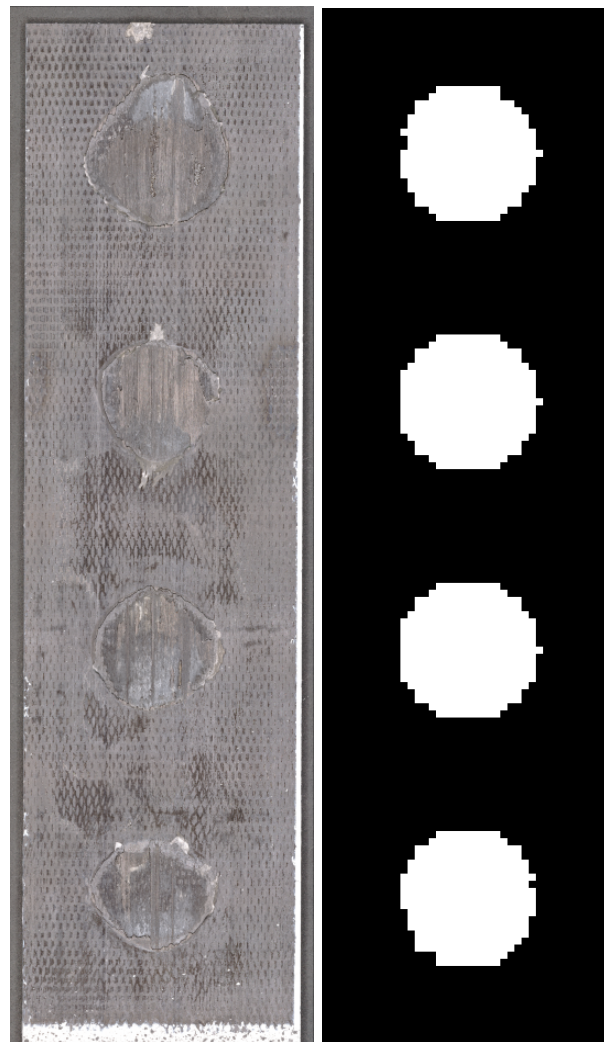
(a) DIC strain field front face

(b) Correlated FEM strain field front face



(c) DIC strain field back face

(d) Correlated FEM strain field back face

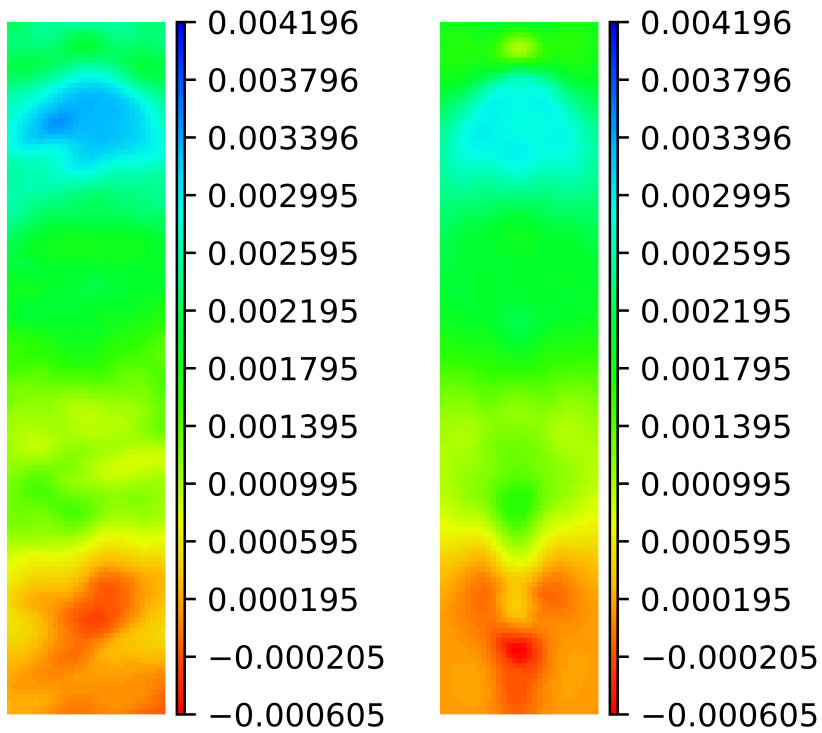


(e) Initial weld surface (f) Correlated weld surface mask, cycle 50

Figure 7.1: DIC to FEM strain field correlation results, loading cycle 50, longitudinal component (E11).

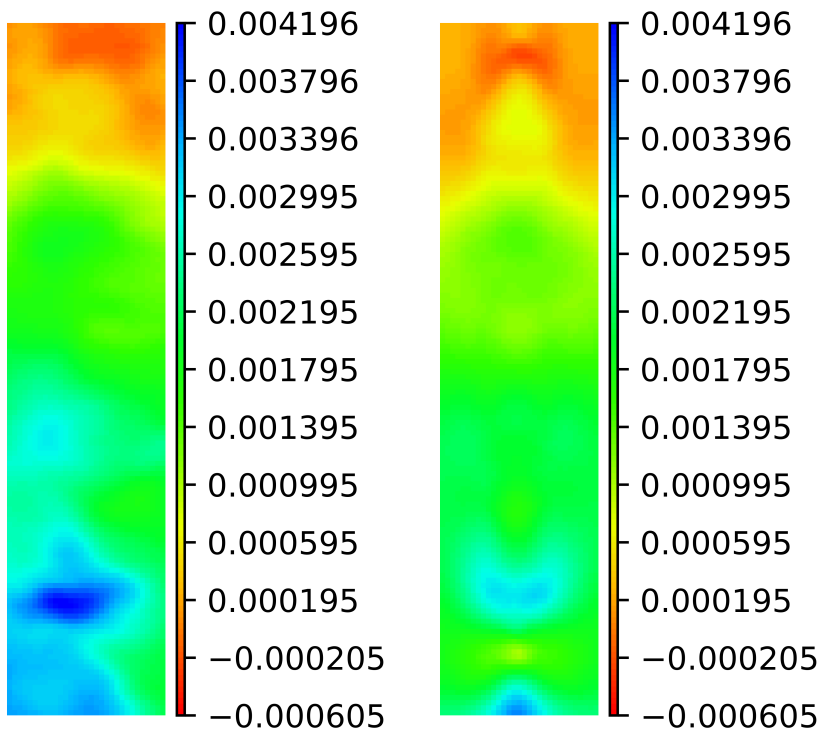
Figure 7.1(f) shows that for the real fracture surface, displayed in figure 7.1(e), a mask with larger weld spots is selected, which is a slightly disbonded version of the mask representing specimens with ideal, perfectly round welds. In an earlier test with a smaller database which only included masks generated from the real specimen, a mask close to the initial mask of the real approximated fracture surface was picked by the correlation algorithm, which would have been a falsely accurate result out of lack of choices. This shows the importance of having a large database of simulated strain fields to reliably test the performance of the strain field correlation method, even though the temptation may be to stop testing once the desired matches are made.

Figure 7.2 shows the matching result after 4500 loading cycles, when the smaller, lower weld spot was close to failure. On the right are the measured strain fields, and on the left the correlated simulated strain fields.



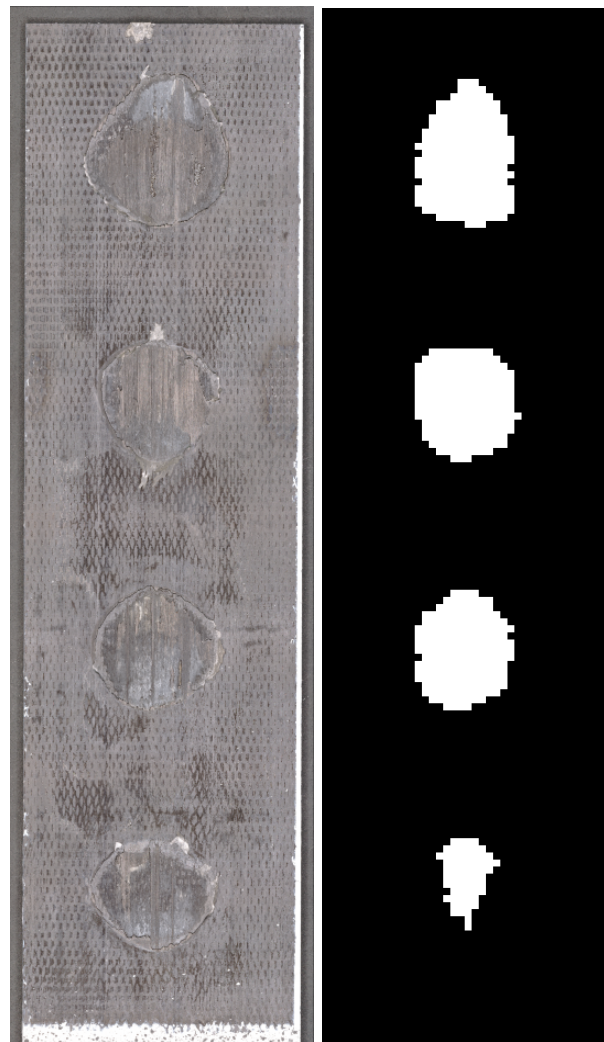
(a) DIC strain field front face

(b) Correlated FEM strain field front face



(c) DIC strain field back face

(d) Correlated FEM strain field back face



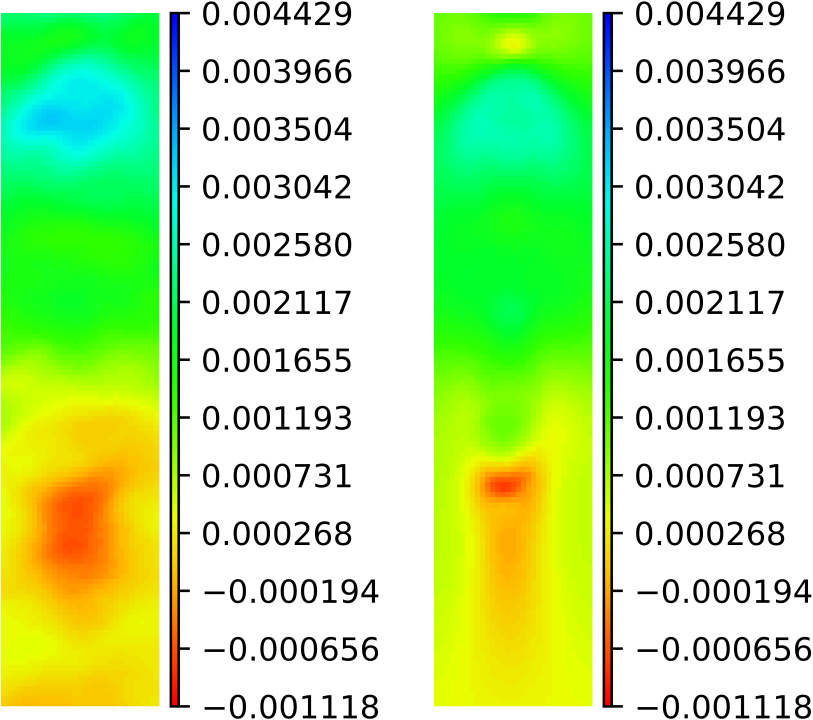
(e) Initial weld surface (f) Correlated weld surface mask, cycle 50

Figure 7.2: DIC to FEM strain field correlation results, loading cycle 4500, longitudinal component (E11).

It can be visually appreciated that the measured and simulated strain fields correspond better than at the start of the test, as the strains measured on the back face of the specimen were more similar to the simulated strains. Figure 7.2(f) shows a fatigued weld mask corresponding to the real mask of the weld, out of all possible other choices the match could have identified. It can be noticed that the smaller outer weld spot, on the bottom of the specimen, presents most damage, which is in line with the intuitive expectation based on the fact that the outer welds are loaded the most, and the stresses will be highest for the smaller weld.

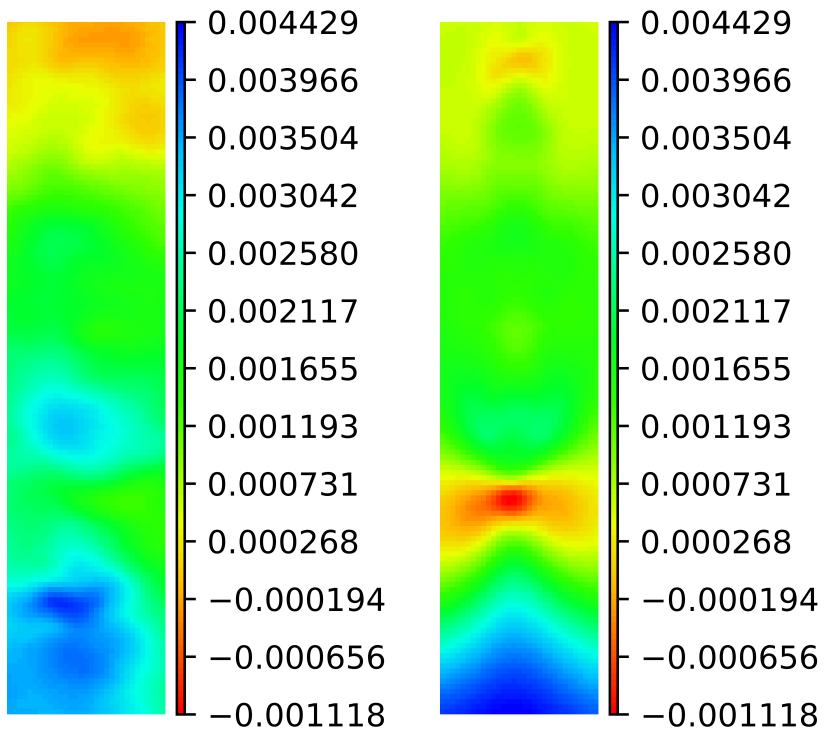
The fact that the bottom most weld failed first is also supported by inspecting visually the relative changes in the measured strain fields. Figure 7.3 shows on the right the measured strain fields after 6000 loading cycles, and on the left the best correlated simulated strain fields. It can be inferred by visual observation of the increase in uniformly strained parts on the lower part of the specimen that that weld had failed. Moreover, on the back side of the specimen shown in figure 7.3(c), the contour of the next weld spot appears on the surface strain field, meaning that

load was then transferred through it.



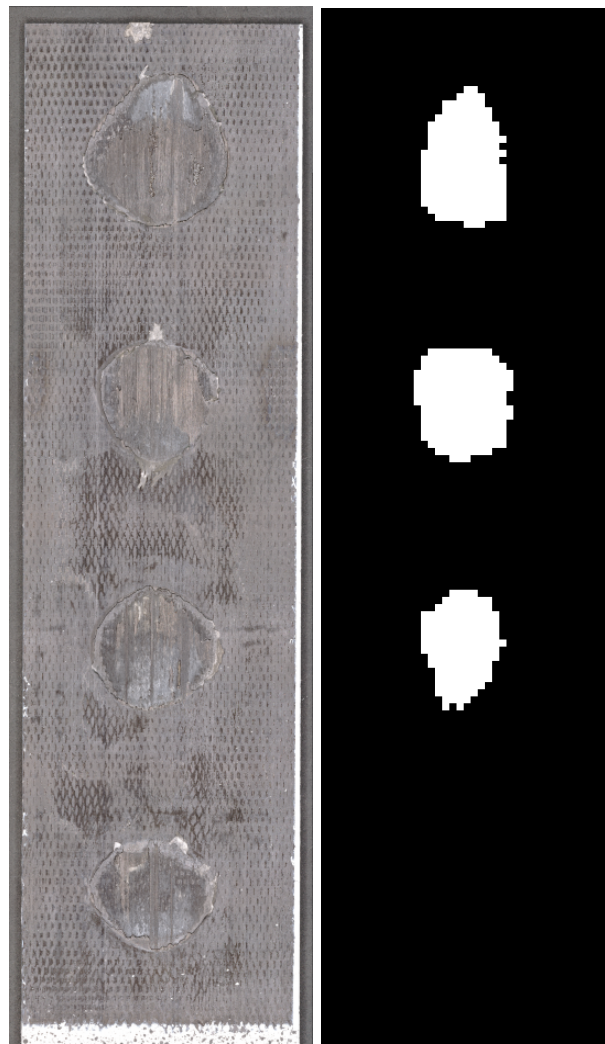
(a) DIC strain field front face

(b) Correlated FEM strain field front face



(c) DIC strain field back face

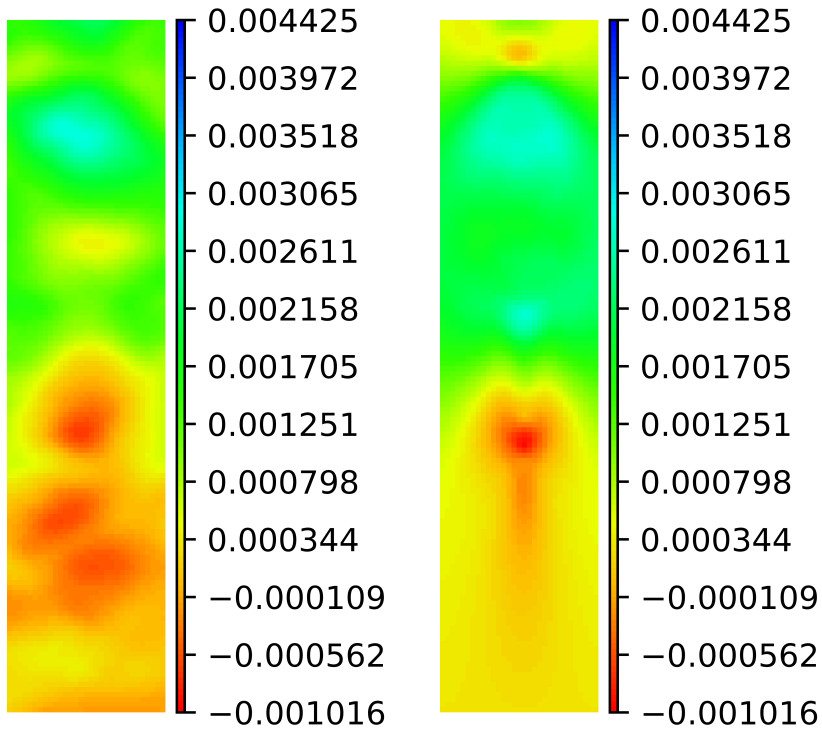
(d) Correlated FEM strain field back face



(e) Initial weld surface (f) Correlated weld surface mask, cycle 50

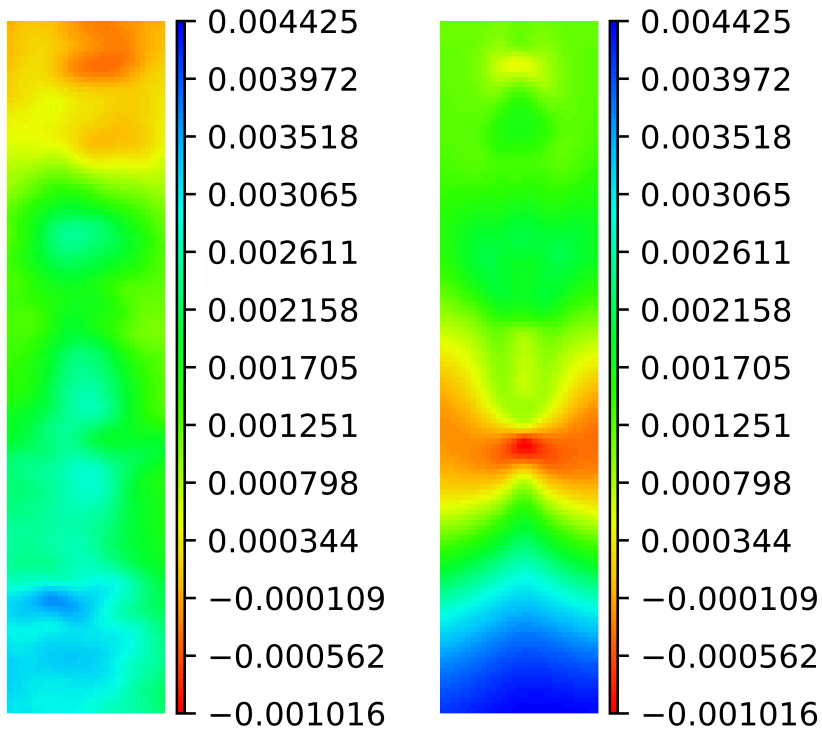
Figure 7.3: DIC to FEM strain field correlation results, loading cycle 6000, longitudinal component (E11).

The broken bottom most weld is indeed reflected by the matched weld mask for the specimen, shown in figure 7.3(f). The fact that a weld spot had failed in between cycle 4500 and 6000 is also supported by a registered drop in reaction force, shown in figure 7.9. A long period of slow fatigue progression over 20000 loading cycles followed, over which the third weld spot failed. The analysis for loading cycle 25050 is presented in figure 7.4, with the measured strain fields on the left and the correlated simulated strain fields on the right.



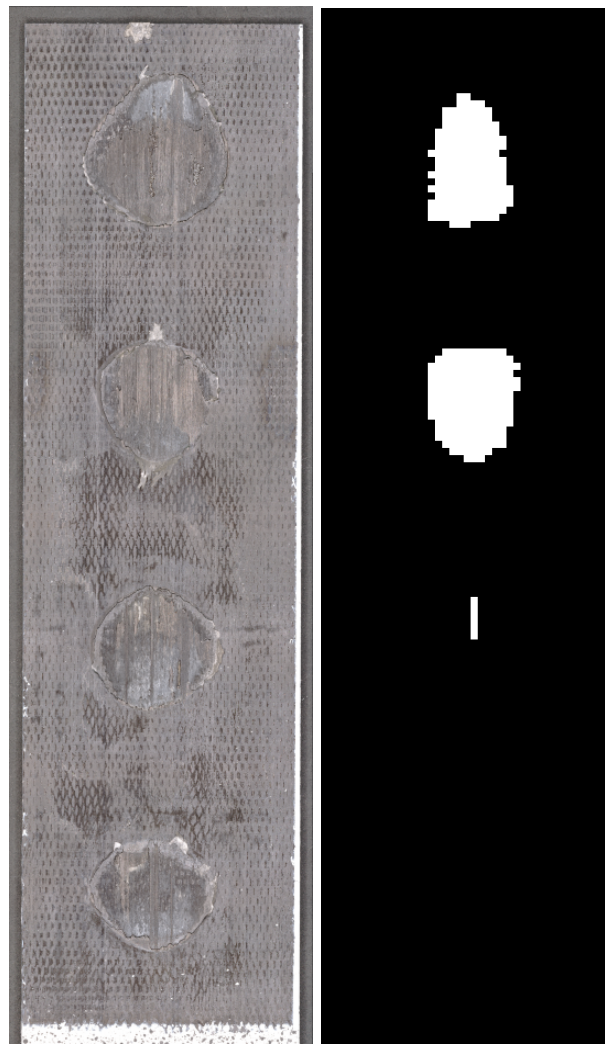
(a) DIC strain field front face

(b) Correlated FEM strain field front face



(c) DIC strain field back face

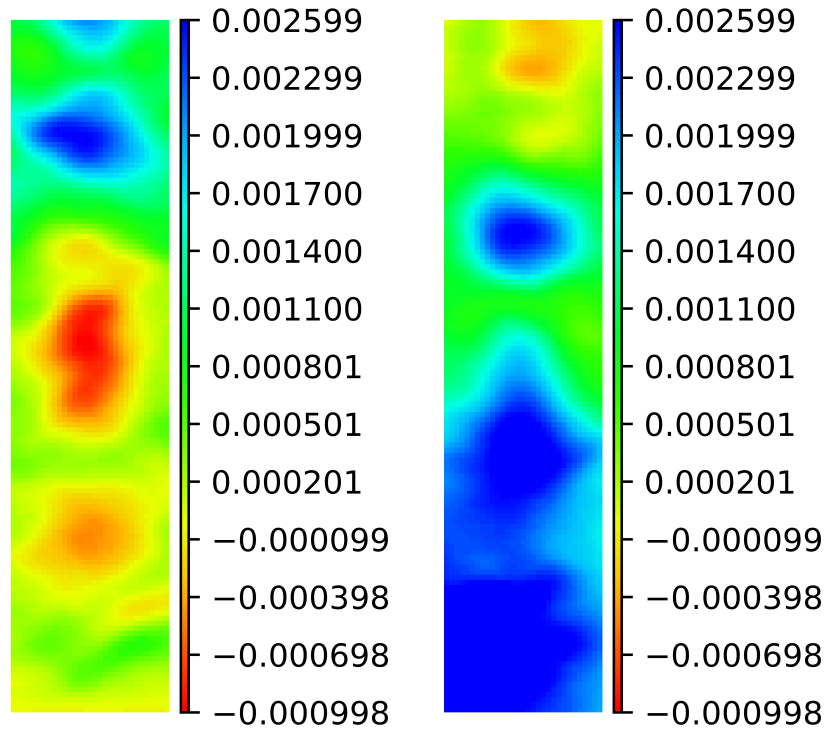
(d) Correlated FEM strain field back face



(e) Initial weld surface (f) Correlated weld surface mask, cycle 50

Figure 7.4: DIC to FEM strain field correlation results, loading cycle 25050, longitudinal component (E11).

Figure 7.4(f) shows indeed the third weld spot almost entirely broken. Figure 7.5 shows the measured strain fields 450 loading cycles later, when the weld spot had completely failed. The measured reaction force also registered a sharp drop at the same time, seen in figure 7.9.



(a) DIC strain field front face.

(b) DIC strain field back face.

Figure 7.5: Strain fields measured through DIC after 25500 loading cycles.

After the third weld spot failed, the strain field correlation with simulations for the remaining two weld spots no longer produced consistent results. This is probably because the noisy strain fields over the failed welds were too influential in establishing correlation between measurement and simulation. The situation can also be expressed in terms of relevant signal to noise ratio. As the weld spots fail, the useful signal over the intact weld spots, relative to the signal over the entire overlapped area, decreases. The weighing criterion when correlating strain fields, based on measured strain field variation, was not efficient in compensating for the large areas of strain less relevant strain fields over broken spot welds, because of the relatively high variation of strain over those areas. This is attributed to measurement noise, and to the damage to the layers of the plates where the welds were located. A more robust method, independent of human interpretation of data, for strain field correlation method capable of delivering more consistent results was not found.

Figure 7.6(a) shows in blue dots the areas of the matched weld masks through strain field correlation over the fatigue life of the specimen. It is apparent that the accuracy of the matches is lower than that observed in the analysis of single spot specimens, primarily because the measured strain fields are less accurate. Oscillations in strain field measurement between subsequent cycles leads to oscillation in weld area categorization. A spline fitting over the data was made, as for the analysis of single weld spot specimens, and is shown in red. This spline is used for further comparison with reaction force matching estimations.

From figure 7.6(b) it can be seen by looking at the red spline that the first weld masks overestimate the area of the real weld, as their area exceeds the area of the initial weld surface, which in

indicated by a negative relative weld area reduction. The dotted black curve in figure 7.6(b) shows the change in damaged weld area relative to the first weld area matched, which is why the values start at 0.

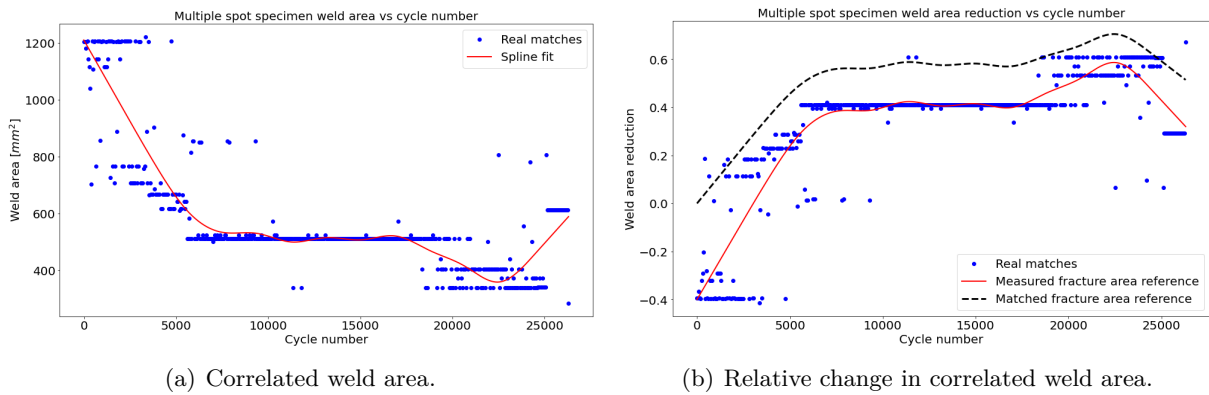


Figure 7.6: DIC to FEM strain field correlation weld area results.

The results obtained through strain field correlation can be compared to the area estimations approximated through reaction force matching, as done before for the single spot analysis. In the case of multiple weld spot specimens, the reaction force comparison to simulated reaction forces is done by using two databases. First the results for the enhanced database, as explained in section 6.4 is used for comparison. The results of reaction force correlation, using the enhanced, more diverse database, are presented in figure 7.7. Color coding is used to keep track of which group of simulations, classified based on the starting conditions shown in appendix B, lead to a given area estimation. The simulated reaction forces for this specimen have already been presented in section 6.4 and are not repeated here.

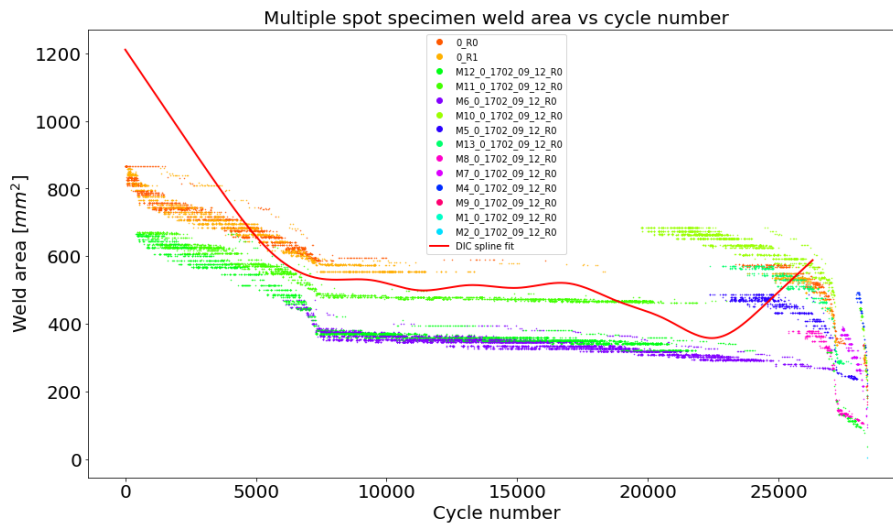


Figure 7.7: Correlated weld area, using the enhanced database of simulations for reaction force correlation.

As expected, because there is a large spread in total weld areas for a given simulated reaction force, the spread in weld area estimation through reaction force matching is high throughout the

fatigue life. Strain field correlation leads to an overestimation of weld area at the beginning of the test, which is not supported by the reaction force matching method. For the majority of the fatigue life however, the estimations overlap. Having said that, after cycle 20000, the area approximation made through strain field analysis dips and then increases again, influenced by the erroneous strain field correlations after the second spot weld failure. A last observation when comparing the results of the two methods is that the DIC data collection stopped early, around the time the third weld spot failed based on the third sharp dip in reaction force. The abrupt drop in reaction force probably caused the DIC system to stop recording data, as if the test had ended.

Figure 7.8 shows the weld disbonding damage progression, relative to the measured area of the fracture surface, and relative to the approximated area of the first correlation result.

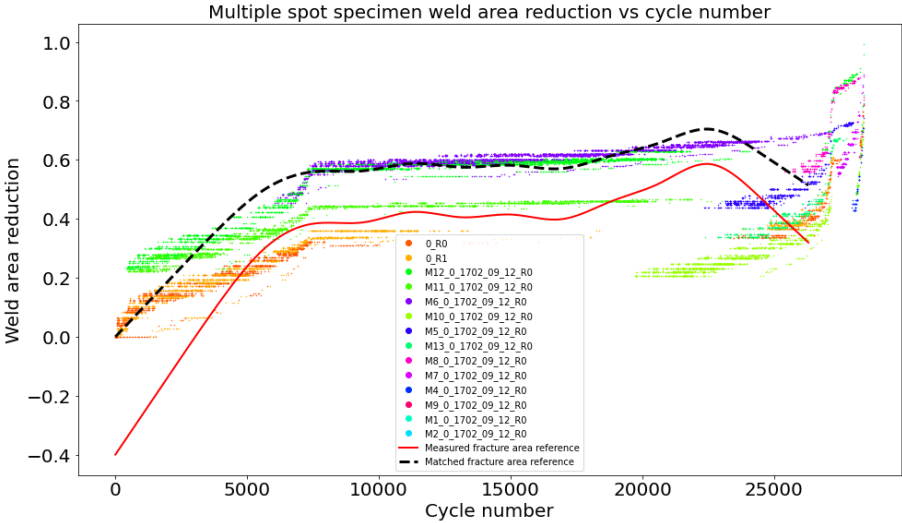


Figure 7.8: Relative change in correlated weld area, using the enhanced database of simulations for reaction force correlation.

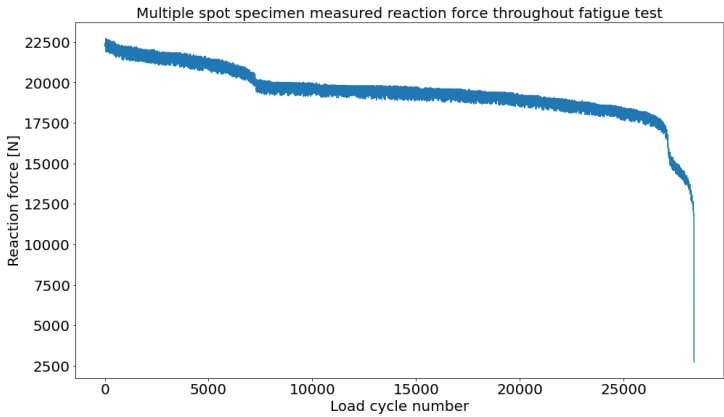


Figure 7.9: Reaction forces measured by the test machine during the fatigue test.

The second reaction force matching analysis presented is based on a smaller database of reaction forces generated from the model of the intact weld by applying the breaking criteria mentioned in section 6.2. It can be seen from figure 7.10 and figure 7.11 that the approximations made

through strain field correlation seem to follow well the approximation made through reaction force matching generated with the breaking criteria only. This agreement supports the validity of the weld disbonding criteria used to create the database of simulations, but is not to be interpreted as a verification because the strain field correlation method did not show satisfactory consistency in characterizing weld area. However, validation through ultrasonic scanning of the specimen at regular intervals throughout the fatigue test could potentially validate the method using the disbonding criteria, together with reaction force matching, to obtain an accurate approximation of the area of each weld spot throughout the fatigue life of a specimen containing multiple weld spots, for the layup used in the column specimens analyzed in this thesis.

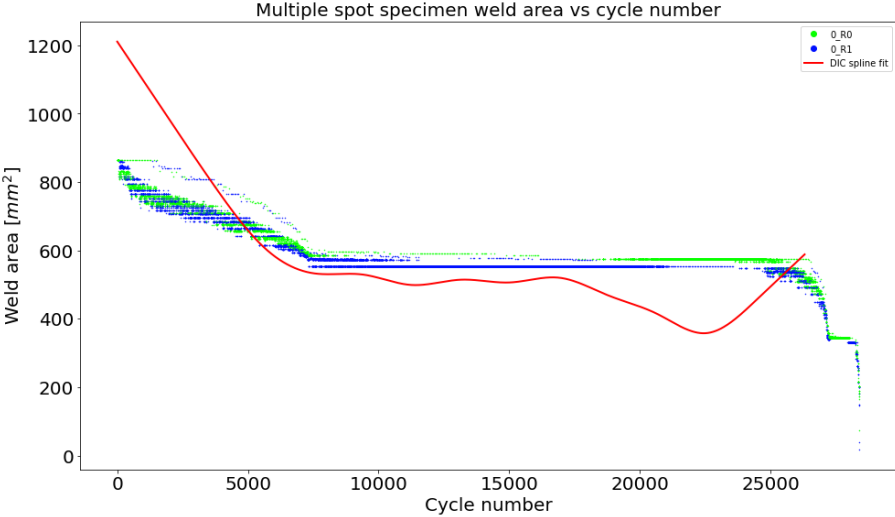


Figure 7.10: Correlated weld area.

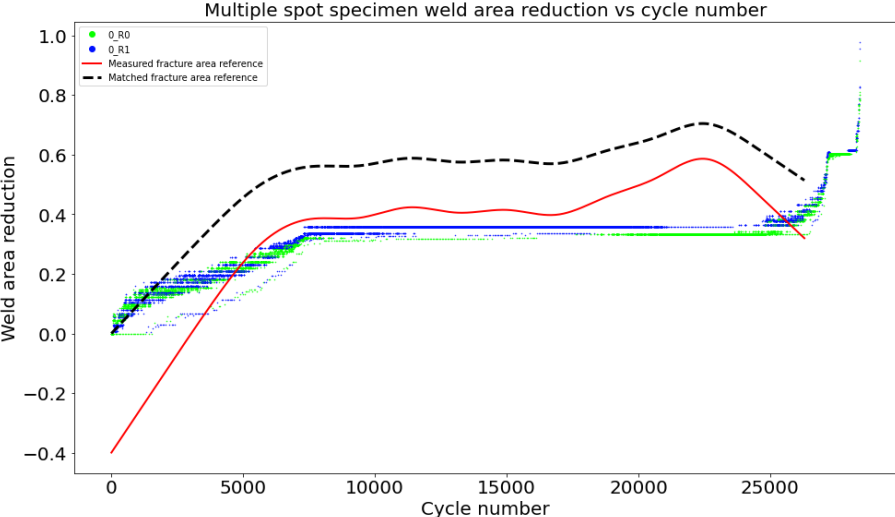


Figure 7.11: Relative change in correlated weld area.

The black dotted line in figure 7.11 shows the damage accumulation relative to the initial correlation result. As the initial weld area approximations through strain field correlation were not accurate, the interpretation of the damage accumulation throughout the entire fatigue life is more difficult. A comparison with the results obtained through the interpretation of reaction

forces is less apparent, as the trends no longer overlap. This is a case in point for the reason why comparing the results to the fixed reference of the measured fracture surface was preferred in this report. When a fixed reference is used for comparison, errors in measurement do not influence subsequent interpretation of results.

8 Discussion of results

The research questions are revisited in this chapter in view of the results obtained through the proposed methodology. The extent to which the methodology is advancing the state of the art is critically evaluated, such that further research can be efficiently defined. The discussion is split into two sections, following the structure of this report: an evaluation of the single weld spot results, and an assessment of the results of multiple weld spot analysis.

8.1 Analysis of single weld spots

The discussion of the analysis of specimens welded through a single weld spot is organized into a section which compares the results obtained in this thesis with the original results of [15], a section about how well the research questions have been addressed, and a section about how useful the results are from a practical perspective.

8.1.1 Comparison of results with previous research

Figure 8.1 gives an overview of the analysis results presented in chapter 5, expressed in terms of relative weld area change. The black dotted lines are the results of the analysis by [14], partly already published in [15]. The dashed black lines are the results of strain field correlation, obtained by comparison to simulated strain fields with the method presented in this report, expressed as disbonding damage accumulation with respect to the first area approximation result. Therefore the black dashed and black dotted lines are to be compared directly, as they have both been expressed with respect to the initial analysis results.

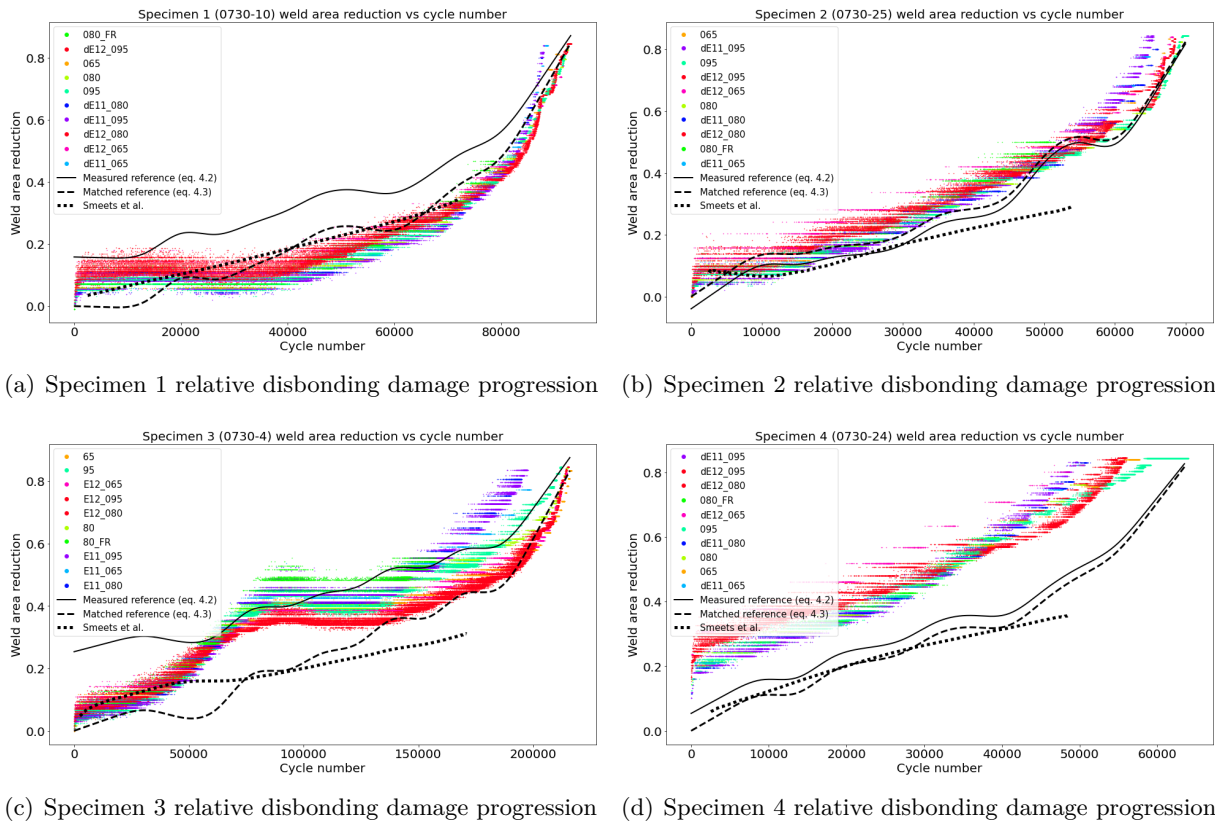


Figure 8.1: Comparison of the relative disbonding damage accumulation between the results obtained by strain field and reaction force correlation, proposed in this field, and the method of strain field analysis proposed by [15].

Any agreement between the analysis method of [15] and the methods presented in this thesis is to be interpreted with caution if detailed modelling is to be based on it, because all results presented are spline fits of scattered data points. It would be possible to draw multiple slightly curved damage progression lines through this measurement spread, which could lead to seemingly slightly better or worse agreement between the methods. Having said that, the curves do show reasonable agreement over all plots. The advantage of the method of strain field interpretation proposed in this report is that it remains consistent towards the end of the fatigue experiment, and it can characterize a larger reduction of weld area than the method of [15] can. The strain field analysis method of [15] seems to produce consistent result until the weld area has reduced by approximately 30%, and fails to capture the last part of the fatigue life when the weld fails at an accelerated rate. By correlating measured strain fields to simulated strain fields, it is possible to approximate the damage accumulation to a larger extent, potentially until the weld area has been reduced by 80%. However, the accuracy of the method at higher damage ratios still needs to be validated by an independent means of measurement, potentially by ultrasonically scanning the specimens towards the end of their fatigue life. The measured strain fields towards the very end of the fatigue life are less similar to the simulated strain fields from the collection of simulations, and the approximated weld area through reaction force analysis is also less accurate as the compliance of the welded joint also depends on the shape of the damaged joint, rather than on the area alone. The results presented in figure 8.1 for the end of the fatigue life are likely to be less accurate than those over which [14] also provides results, and need to be interpreted with skepticism until further validation experimental work is done.

8.1.2 Reflection on research questions

Recall that two research questions have been asked for the analysis of lap shear joints welded through a single ultrasonic weld spot. The first research question asks whether measured surface strain fields could be interpreted to describe the state of fatigue damage in the weld spot, and the second question asked whether the increase in compliance of the lap shear joint could be used as an indicator of damage, for the purpose of providing an independent result useful for verification. The two sections below reflect on each question, based on the results obtained.

8.1.2.1 Surface strain field correlation research question

The first research question asked whether it is possible to use a collection of simulated surface strain fields to interpret measured surface strain fields over the overlap area of an ultrasonically welded lap shear joint, containing a single weld spot. The surface strain field interpretation is to be used as an indirect method of damage state characterization within the ultrasonic weld spot. The level of detail at which the damage state can be described is analyzed in the following paragraphs. The strain field correlation method proposed had the potential to characterize the weld shape at each loading cycle at which a surface strain field measurement was made. Whether the weld shape was indeed captured consistently, or whether only the relative changes in weld areas have proven to be consistently approximated, is discussed below, starting from the lowest level of detail useful for fatigue life modelling, which is the rate of fatigue damage accumulation.

The results obtained, expressed in terms of relative change in weld area, show good agreement with the previous surface strain field analysis method published by [15], which indicates that the method of strain field correlation proposed in this thesis is at least as capable of characterizing relative accumulated disbonding damage in the weld spot. Moreover, the extent of relative disbonding damage approximated through strain field correlation extends beyond that of [15], to the end of the fatigue life. Having said that, the accuracy of the approximation, is to be treated with skepticism until further measurements are made to validate the results, because the measured strain fields correlate less well to the simulated strain fields towards the end of the fatigue life. The extent of damage approximated may be overly influenced by the assumptions made to limit the damage cases included in the database of finite element simulations, and by the assumptions made to simplify the simulations. It may therefore be the case that the damage present in the weld is overestimated at the end of the fatigue life, due to the worse correlation between the measured strain fields and the available simulated strain fields used for comparison. This is because the strain field cross correlation function used tries to match the peaks and valleys in the surface strain fields, which could give a higher correlation score to a more uniform surface strain field when the peaks and valleys in the strain fields no longer align well. A more uniform strain field corresponds to a more damaged weld, leading to an over-estimation of damage towards the end of the fatigue life. It is therefore advised to use a direct form of damage measurement, such as ultrasonic scanning, before further conclusions, about the fatigue damage evolution of ultrasonically welded lap shear joints, are proposed based on indirect strain field interpretation methods presented either in this thesis or in [15].

For specimen 2 and specimen 4, at the start of the fatigue test, the area of the weld approximated through strain field correlation agrees well with the area of the weld measured by the fracture surface. This indicates that the analysis method does have the capability of estimating the area of the weld as well. For area approximations to be accurate, it is required that the measured strain fields, on both sides of the lap shear joint, correlate nearly perfectly to the simulated strain fields. The weld area approximation is more sensitive to the quality of correlation between measured and simulated strain fields, because there are multiple possible weld shapes, of slightly

different areas, which can simulate similar surface strain distributions. The strains diffuse from the welded surface throughout the thickness of the welded plates, which makes it difficult to uniquely identify which weld shape produced a given measured strain field.

The weld shape characterizations have proven to be of less consistency when compared to the overall weld area. The measured surface strain fields can be associated with multiple weld shapes, because the strain diffuses from the surface of the weld through the thickness of the plates. It was observed that consecutive weld shape characterizations are influenced by errors between subsequent measurements, such that consecutive weld shapes do not correspond to a physically consistent evolution. This has been highlighted between the results for two consecutive measurement shown in figure 5.10 and in figure 5.11. The strain field correlation method proposed in this thesis is therefore not well suited for a consistent weld shape characterization, because the results are too sensitive to errors in strain field measurement. Only on average, the weld areas of the weld shape descriptions are consistent with physical damage accumulation.

8.1.2.2 Increase in compliance analysis research question

The second research question for the single weld spot analysis part of this research asked whether it is possible to use the observed increase in compliance of the lap shear joint specimens, to characterize the state of fatigue damage within the weld spot of the specimens, by comparison to simulated increase in compliance associated with weld disbonding. To this end, simulated force-displacement dependencies on spot weld areas were compared to the measured force-displacement curves throughout the fatigue tests. It was observed that initially, starting from an approximately round weld spot, the locations at which the disbonding damage was simulated on the perimeter of the weld, had little influence on the simulated reaction forces. The average reduction in weld area, until approximately half of the weld was disbonded, was observed to have the largest influence on the increase in compliance of the lap shear joint specimens welded through a single weld spot. This observation, based on the collection of simulations made, suggests that the overall increase in compliance of the specimen does indeed correlate well to the extent of damage within the weld spot. The main factors observed to reduce the accuracy of weld area characterization are related to the accuracy with which the real force-displacement curve measurement of the specimen can be made. Specimen settling, noise in the reaction force readings, and influence of temperature contributed to disagreement with weld area characterization made based on strain field correlation. Having said that, the same rates of disbonding damage accumulation were observed, which were also consistent with the results of strain field analysis made by [15]. Compliance increase of the lap shear joints, welded through single ultrasonic weld spots, is therefore proposed as a good indicator of the remaining area of the weld spot within the joint, for damage states not exceeding more than approximately half the weld area.

As the weld area is further reduced, the locations at which the disbonding damage is assumed to accumulate on the perimeter of the weld does influence increasingly more the observed compliance. The overall weld shape is increasingly influenced by the accumulated damage and becomes a contributing factor to the stiffness of the joint. The correlation between weld area and reaction force still remains useful for validating a more accurate result. Accounting for the large settling observed in specimen 4, the area approximations of strain field analysis and of reaction force to area correlation remain overlapped for all specimens, see the overview in figure 8.1.

8.1.3 Applicability of results

Interpreting the results of the analysis of specimens containing a single weld spot adds significant insight into the state of damage of the weld. It would be difficult to interpret the measured strain fields by hand, with more accuracy, to characterize the disbonding damage accumulation. From a practical perspective of trying to have as much accurate information as possible about ultrasonic spot welds failing during fatigue tests, the output of the methods presented in this thesis for single weld spot analysis are of particular value.

8.2 Analysis of multiple weld spots

Since there are no previous references to compare the results of the multiple weld spot analysis to, in the discussion about the multiple weld spot analysis is organized into a reflection about how well the methodology has been able to address the research questions, and into a critical assessment of the practical usefulness of the results.

8.2.1 Reflection on research questions

The research questions for the multiple weld spot part of the thesis asked whether it is possible to use the finite element method to generate a database of simulations that can be used to interpret surface strain fields, measured with digital image correlation, and measured reaction forces at the clamps of the test machine, to characterize the state of damage of the weld spots.

Referring to the first research question, through the method of strain field correlation, only a rough classification about the state of damage in a weld spot was achieved. It is possible to estimate from an average of the matched masks whether a weld spot is intact, severely damaged or completely broken. The results of correlation are not more consistent because the measured strain fields are not accurate enough. It may be possible to improve on the results using a better DIC system on the back side of the specimen in a future test campaign.

A more accurate estimation of the damage state of a weld could be estimated through the method of correlating the measured reaction forces with a set of simulated reaction forces, considered representative for the real specimen through the set of assumptions used to generate it. Good agreement was observed between the weld areas approximated through reaction force matching, starting from the modelled intact real weld, and the weld areas approximated through strain field correlation. It may therefore be the case that for the column specimens tested for this thesis, the weld damaging criteria proposed in section 6.2 are already close to modelling the real order in which the weld spots disbond under fatigue testing. Further validation, by regular ultrasonic scanning of such specimens during fatigue tests, could confirm whether the disbonding criteria used to generate the simulation databases used in this analysis have indeed already captured the sequence of weld spot failure correctly. In that case, it would be possible to estimate roughly the area of each weld spot based on the measured compliance of the specimen, with the insight of correct order of weld disbonding captured when creating the collection of simulated force-displacement curves used as comparison. At this point this is only a speculation however, which could become a research question for subsequent modelling efforts.

8.2.2 Applicability of results

While the results presented in chapter 7 have shown that the method of using a collection of FEM simulations to interpret strain field and reaction force data, for the purpose of characterizing the state of damage in the weld, generalizes with little modification to the analysis of different

weld configurations, the question whether such an analysis is even necessary naturally arises for this particular multiple weld spot specimen configuration tested. While it is encouraging to see that the method of surface strain field correlation provided reasonably accurate results for the specimens tested, those results could have also been inferred directly by manually looking at the strain fields measured with DIC. It is difficult for a computer to analyze imperfect data, but a human brain can observe patterns in visually presented data and infer correlations from it with relative ease. For the case of the welds in column specimens tested, even for tests where the measured strain fields are less accurate, by observing the relative change in strain fields over the experiment it is possible to follow more accurately when the weld spots through which most load was transferred were damaged and when they broke. Considering the work needed to set up the database of simulations for any given configuration of specimens tested, and the care taken at the end of each analysis to check whether the results are in line with the real data, looking at the measured strain fields by hand for a test campaign of 10-20 specimens does not cost much more human effort. It would be entirely possible, therefore, to answer the research questions, for this configuration of weld spots, just by looking at plots of DIC strain fields, which from a practical perspective can deliver results of the same, or even higher quality in term of state of damage characterization per spot weld. The computer-assisted method of analysis does add rough information about the current area of each weld spot, but it is not consistent enough to base future conclusions about accuracy of fatigue modelling on it. Having said that, for other weld spot configurations, the method of analysis through strain field correlation presented in this thesis may add more insight into the current state of a weld during a fatigue test than by directly looking at the progression of measured surface strain fields.

9 Recommendations for future research

Recommendations for future research are made in this chapter to improve the applicability of the results with respect to the research goal of creating high quality validation data for fatigue models of ultrasonically welded lap shear specimens. The recommendations are split into two sections: one for the single spot analysis, and one for the analysis of specimens containing multiple weld spots.

9.1 Single weld spot analysis recommendations

The main recommendation for future research from the single weld spot analysis is to perform another test campaign which shall include regular ultrasonic scanning of the specimens. Validation data is needed for both the methods presented in this thesis, and the method of estimating relative change in weld areas proposed by [15]. Until then, all three methods remain mere speculations, and even good agreement between all three of them is not proposed as sufficient verification, because all measurement methods are indirect. A direct measurement of the weld area at regular intervals throughout the fatigue test, such as through ultrasonic scanning, would provide the validation data needed to gain confidence in the indirect methods of damage characterization.

Further research into the topic could integrate insights from acoustic emission to better localize the damage sites. Ample research is available on the topic, as mentioned in chapter 2. Much of the leading expertise is developed at TU Delft, which facilitates integration of knowledge should this research be continued within the department.

9.2 Multiple weld spot analysis recommendations

The recommendations from the single weld spot analysis are also relevant for the multiple weld spot analysis. Another test campaign is needed, with regular ultrasonic scans of the specimens throughout the fatigue life, to validate whether the weld disbonding criteria, used in creating the set of simulations for comparison in this thesis, already correctly capture the sequence in which weld spots are failing. Acoustic emission could also prove to be valuable for this purpose, as an alternative non-destructive method of localizing damage in the lap shear joint.

The last recommendation made to improve on the results obtained in this thesis is related to the quality of acquired DIC data. More consistent strain fields, with distributions closer to the simulated ones, may be obtained with a more accurate pair DIC systems. The accuracy of the measured strain fields are the bottleneck in the usefulness of results through the automated strain field correlation method proposed in this research.

10 Conclusion

This thesis presented an indirect method of damage accumulation quantification within the welds of ultrasonically spot welded lap shear joints, based on comparing experimental measurements with a collection of finite elements simulations corresponding to different weld damage states. The analysis results for specimens containing a single weld spot showed good agreement with the earlier results published by [15]. The analysis of single ultrasonic weld spots presented in this thesis extends the results beyond those obtained by [15], for the entire fatigue life of the specimens. Moreover, for the analysis of single weld spots, the method showed the capability of characterizing the weld area as well, rather than only the relative change in area.

Strain field interpretation is sensitive to the accuracy of the acquired digital image correlation data. The analysis of strain fields measured over the overlap of the larger specimen containing four ultrasonic weld spots in a column was much less accurate when compared to that of the strain fields measured over the smaller lap shear specimens containing a single weld spot, because the strain field measurements were less precise. The same digital image correlations were used in both test campaigns, but for the larger specimen containing multiple weld spots, the cameras had to be placed further away from the specimen in order to capture the overlapping area within the field of view, leading to a more coarse spatial resolution of results. The strain field analysis could only be used for a rough characterization of damage for each weld spot, into three levels: undamaged, significantly damaged and completely broken. Having said that, it was observed that the database of simulated strain fields corresponding to damaged weld spots contains the correct order of failure of the weld spots. If further experiments could validate this observation, it would mean that the simulations have already captured the correct order of weld spot failure, which is a starting point for further fatigue life modelling of ultrasonically welded lap shear joints.

The recommendation for future research is to conduct a test campaign of fatigue tests to include ultrasonic scanning of the weld spots at regular intervals throughout the fatigue life. Ultrasonic scanning would provide direct measurements of the disbonding damage accumulation within the weld spots. Direct measurements are needed to validate the results of the indirect measurement methods proposed in this thesis and by [15], before indirect methods of measurements are used to validate numerical predictions. Another recommendation is to exploit the usage of acoustic emission as a non-destructive measurement technique, alongside digital image correlation, to localize the accumulation of damage within the ultrasonically welded lap shear joints. Interpretation of surface strain fields has proven to be effective at characterizing the amount of disbonding damage accumulated, and acoustic emission has the potential to localize the damage within the weld spots more accurately.

Bibliography

- [1] C.B.G. Brito et al. “The effects of misaligned adherends on static ultrasonic welding of thermoplastic composites”. In: *Elsevier Composites Part A* (2022).
- [2] Saullo G P Castro. *saullocastro/tudaesasII: 2022.11*. Version 2022.11. Mar. 2022. DOI: 10.5281/zenodo.6395245. URL: <https://doi.org/10.5281/zenodo.6395245>.
- [3] Pierre Duchene et al. “A review of non-destructive techniques used for mechanical damage assessment in polymer composites”. In: *Springer Journal of Materials Science* (2018).
- [4] Bram Jongbloed et al. “Improving the quality of continuous ultrasonically welded thermoplastic composite joints by adding a consolidator to the welding setup”. In: *Elsevier Composites Part A* (2022).
- [5] Bram C. P. Jongbloed et al. “A Study on Through-the-Thickness Heating in Continuous Ultrasonic Welding of Thermoplastic Composites”. In: *Materials* (Nov. 2021).
- [6] S. Klinkel, F. Gruttmann and W. Wagner. “A Continuum Based 3D–Shell Element for Laminated Structures”. In: *Computers and Structures* 71 (1999), pp. 43–62.
- [7] F. Kohler et al. “Static ultrasonic welding of carbon fibre unidirectional thermoplastic materials and the influence of heat generation and heat transfer”. In: *Journal of Composite Materials* (2021).
- [8] Xi Li et al. “Damage accumulation analysis of cfrp cross-ply laminates under different tensile loading rates”. In: *Elsevier Composites Part C: Open Access* (2020).
- [9] G. R. Liu and S. S. Quek. *The finite element method a practical course*. Butterworth-Heinemann, 2003.
- [10] C.A. Meijerman. “Fatigue Behavior of Multi-Spot Welded Joints in Thermoplastic Composites”. MA thesis. Delft University of Technology, 2021.
- [11] L. Vu. Quoc and X. G. Tan. “Optimal solid shells for non-linear analyses of multilayer composites. I. Statics”. In: *Computer methods in applied mechanics and engineering* 192 (2003), pp. 975–1016.
- [12] G. Romhány, T. Czigány and J. Karger-Kocsis. “Failure Assessment and Evaluation of Damage Development and Crack Growth in Polymer Composites Via Localization of Acoustic Emission Events: A Review”. In: *Polymer Reviews* (2017).
- [13] Milad Saedifar and Dimitrios Zarouchas. “Damage characterization of laminated composites using acoustic emission: A review”. In: *Elsevier Composites Part B* (2020).
- [14] E.T.B. Smeets. “Numerical modelling and optimization of multi-spot welded joints”. In press. PhD thesis. Delft University of Technology, 2023.
- [15] Eva Smeets et al. “Measurement of damage growth in ultrasonic spot welded joints”. In: *Composites Meet Sustainability - Proceedings of the 20th European Conference on Composite Materials, ECCM20*. June 2022.
- [16] *Standard Test Method for K-R Curve Determination*. ASTM International.
- [17] *Standard Test Method for Measurement of Fracture Toughness*. ASTM International.
- [18] Richard Szeliski. *Computer vision algorithms and applications*. Springer, 2011.
- [19] Irene Fernandez Villegas and Calvin Rans. “The dangers of single-lap shear testing in understanding polymer composite welded joints”. In: *Philosophical Transactions A* (Jan. 2021).
- [20] Jalal Yousefi et al. “Delamination characterization in composite laminates using acoustic emission features, micro visualization and finite element modeling”. In: *Journal of Composite Materials* (2016).

- [21] Ali Yousefpour, Mehdi Hojjati and Jean-Pierre Immarigeon. “Fusion Bonding/Welding of Thermoplastic Composites”. In: *Journal of Thermoplastic Composite Materials* (2004).
- [22] Tian Zhao. “Sequential Ultrasonic Spot Welding of Thermoplastic Composites - an experimental study on the welding process and the mechanical behavior of (multi-)spot welded joints”. PhD thesis. Delft University of Technology, 2018.
- [23] Tian Zhao et al. “Enhancing weld attributes in ultrasonic spot welding of carbon fibre-reinforced thermoplastic composites: Effect of sonotrode configurations and process control”. In: *Elsevier Composites Part B* (2021).
- [24] Tian Zhao et al. “On sequential ultrasonic spot welding as an alternative to mechanical fastening in thermoplastic composite assemblies: A study on single-column multi-row single-lap shear joints”. In: *Elsevier Composites Part A* (2019).
- [25] Tian Zhao et al. “Towards robust sequential ultrasonic spot welding of thermoplastic composites: Welding process control strategy for consistent weld quality”. In: *Elsevier Composites Part A* (2018).

Appendix A Single Weld Spot Fatigue Evolution Results

A.1 Examples for specimen 0730-10 from [15]

Every weld area reduction criterion mentioned in section 4.1 has a different effect on the shape evolution of the simulated welds. Figure A.1 shows some examples of weld masks from the database for specimen 0730-10.

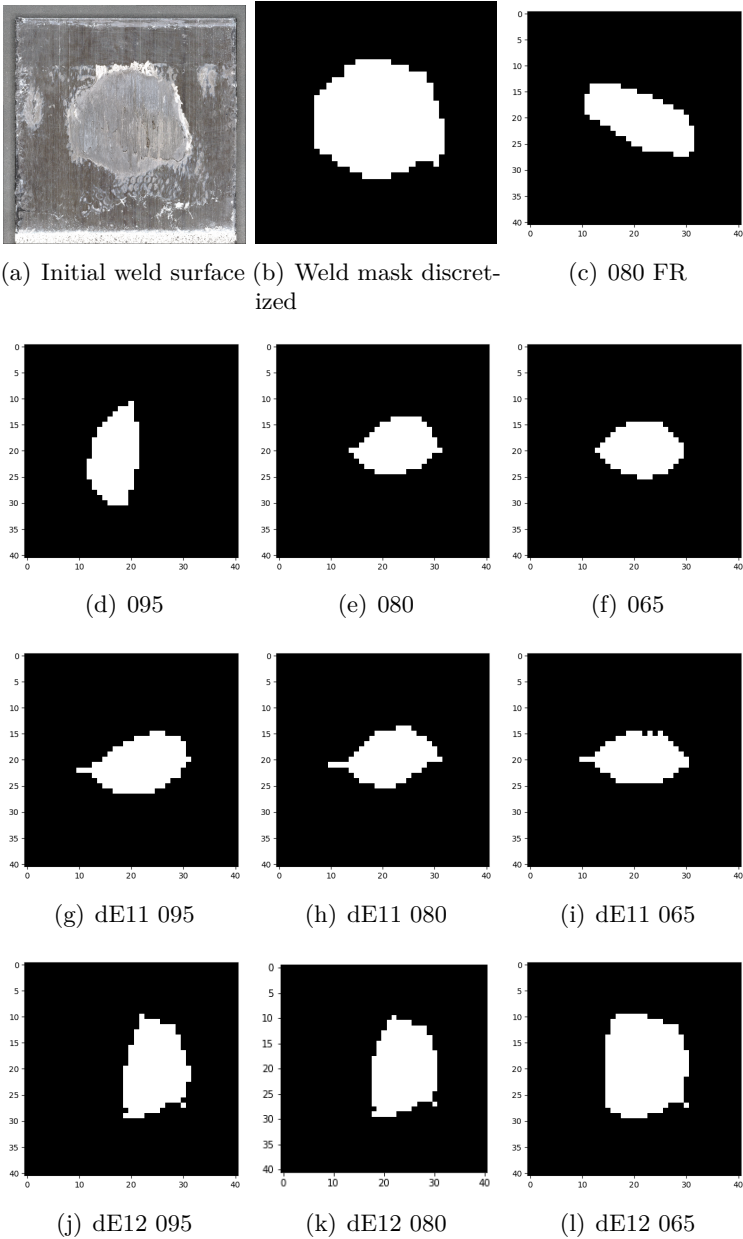
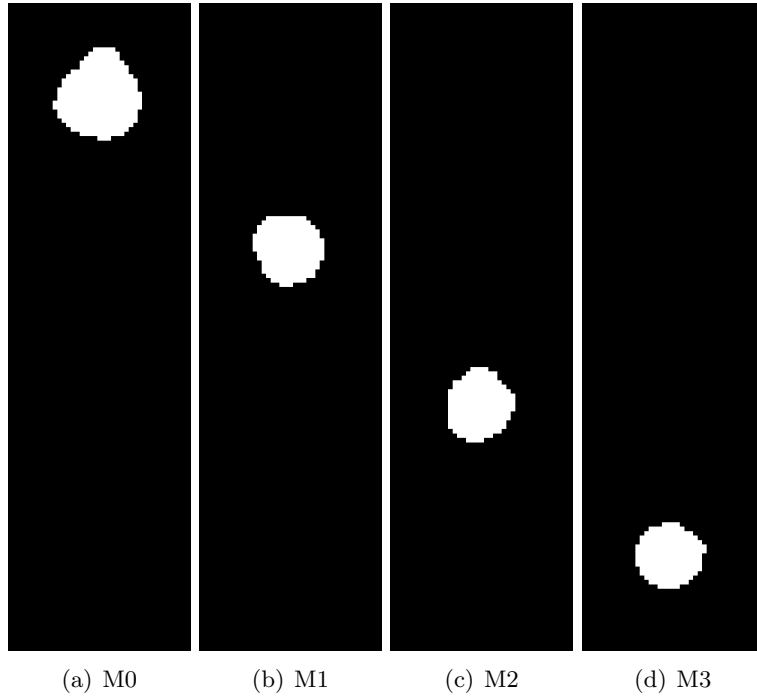
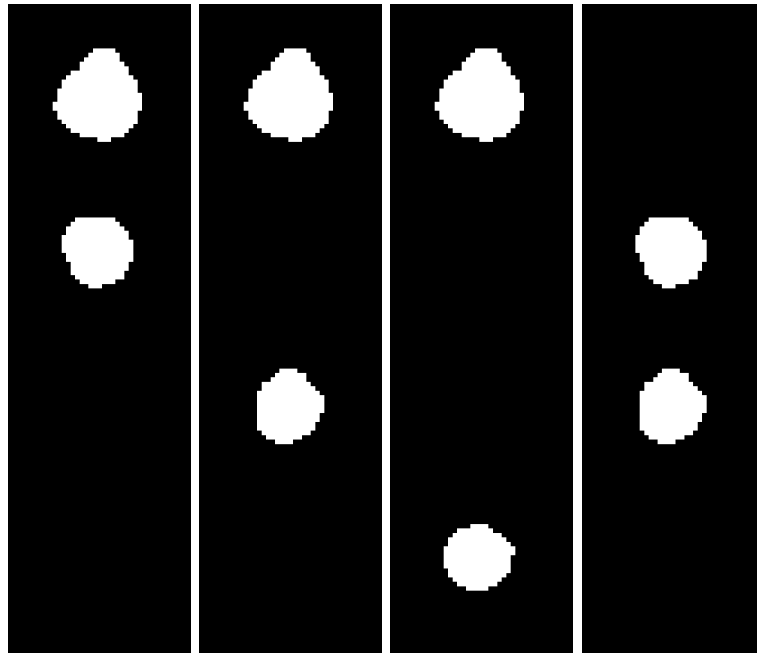


Figure A.1: Various partly broken weld masks from the database of simulations.

Appendix B Multiple Weld Spot Fatigue Evolution Enhancement Masks



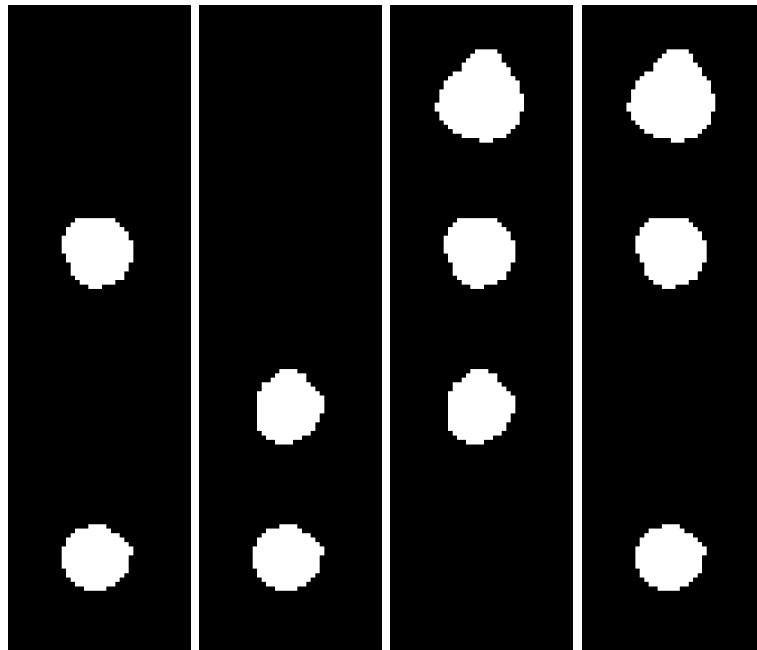


(e) M4

(f) M5

(g) M6

(h) M7



(i) M8

(j) M9

(k) M10

(l) M11

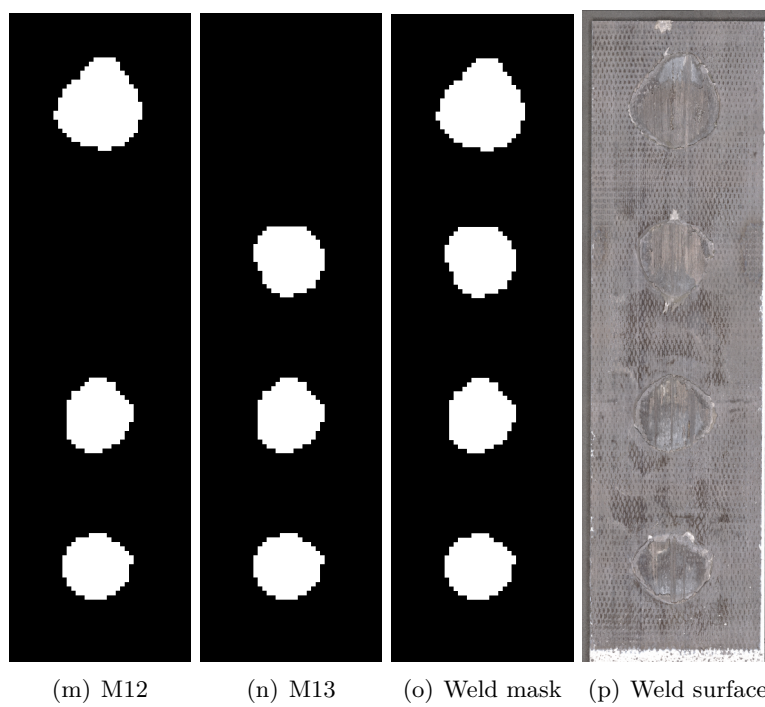


Figure B.0: Weld mask split into all combinations of individual welds.

Appendix C Convergence study of finite element solution, single weld spot

Figure C.2 shows the influence of increasing the number of elements, through the thickness of the plate, on the surface strain distribution. Figure C.3 shows the influence of increasing the number of elements to represent the surface of the plates, on the surface strain distribution. The longitudinal strain component is considered, along the mid-line of the overlap, as shown in figure C.1.

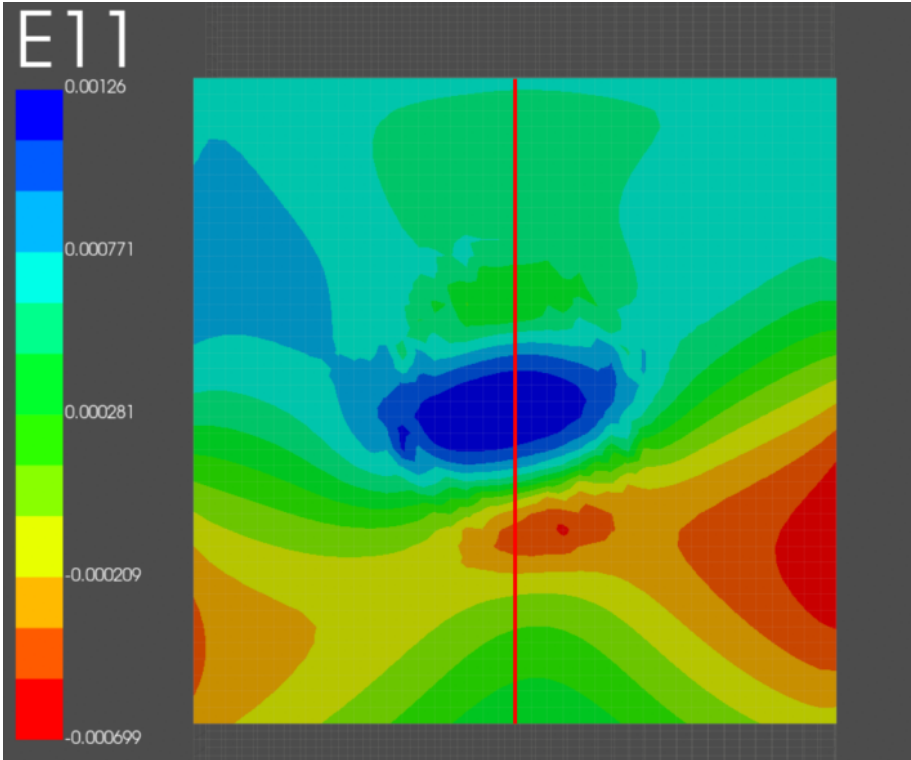


Figure C.1: Surface strain distribution, computed with the custom made finite element implementation. The red line represents the middle of the overlap, where surface strains are compared in the convergence study. 40x40x2 elements per plate over the overlap.

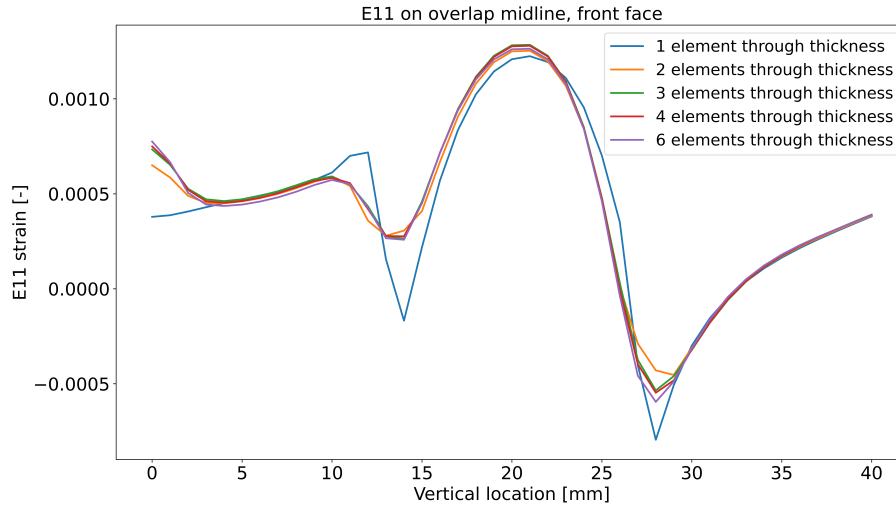


Figure C.2: Influence of increasing the number of finite elements, through the thickness of the plates, on the simulated surface strain distribution at the mid-line of the joint overlap.

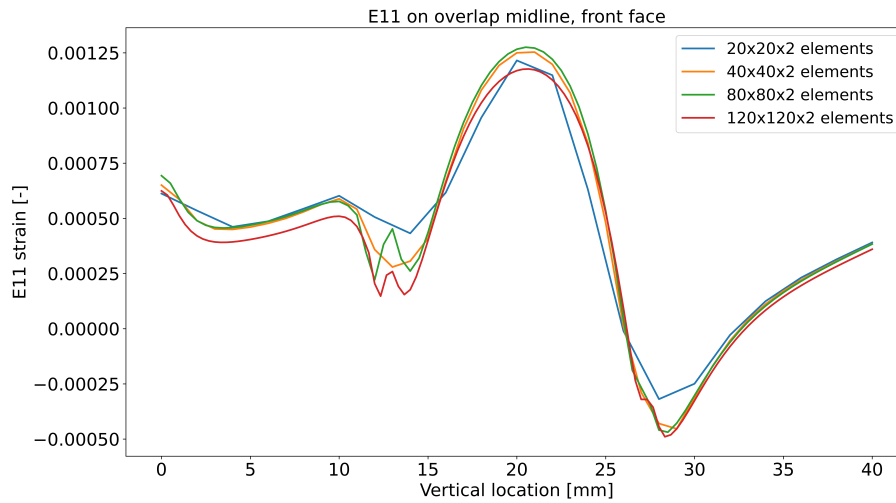


Figure C.3: Influence of increasing the number of finite elements, along the length and width of the plates, on the simulated surface strain distribution at the mid-line of the joint overlap. The legend specifies the number of elements used to represent the plates over the 40x40mm overlap area

Appendix D Convergence study of finite element solution, multiple weld spots

Figure D.2 shows the influence of increasing the number of elements, through the thickness of the plate, on the surface strain distribution. Figure D.3 shows the influence of increasing the number of elements to represent the surface of the plates, on the surface strain distribution. The longitudinal strain component is considered, along the mid-line of the overlap, as shown in figure D.1.

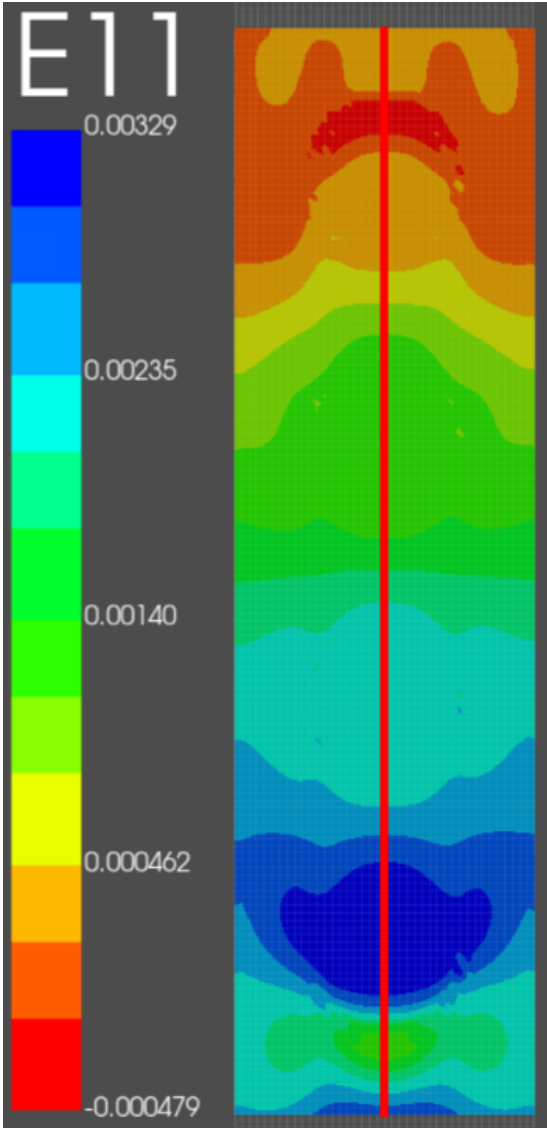


Figure D.1: Surface strain distribution, computed with the custom made finite element implementation. The red line represents the middle of the overlap, where surface strains are compared in the convergence study. 145x40x2 elements per plate over the overlap.

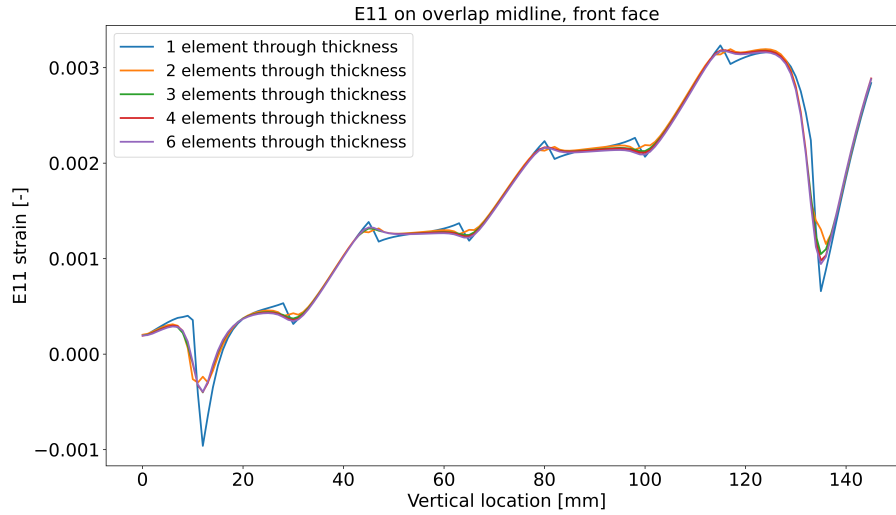


Figure D.2: Influence of increasing the number of finite elements, through the thickness of the plates, on the simulated surface strain distribution at the mid-line of the joint overlap.



Figure D.3: Influence of increasing the number of finite elements, along the length and width of the plates, on the simulated surface strain distribution at the mid-line of the joint overlap. The legend specifies the number of elements used to represent the plates over the 40x40mm overlap area

Appendix E **Single wed spot specimen 2 (0730-25) analysis details**

The left side of figure E.1 shows real measurements of surface strain fields for specimen 2 after 50 loading cycles, and a photograph of the fracture surface. After only 50 loading cycles, when the first set of pictures were taken by the DIC systems, it is expected that the weld shape remained almost identical to the pristine shape of the weld, which can be approximated by the outer contour of the fracture surface. The right side of figure E.1 shows correlated surface strain fields from the database of simulations, and the modelled weld surface which created them.

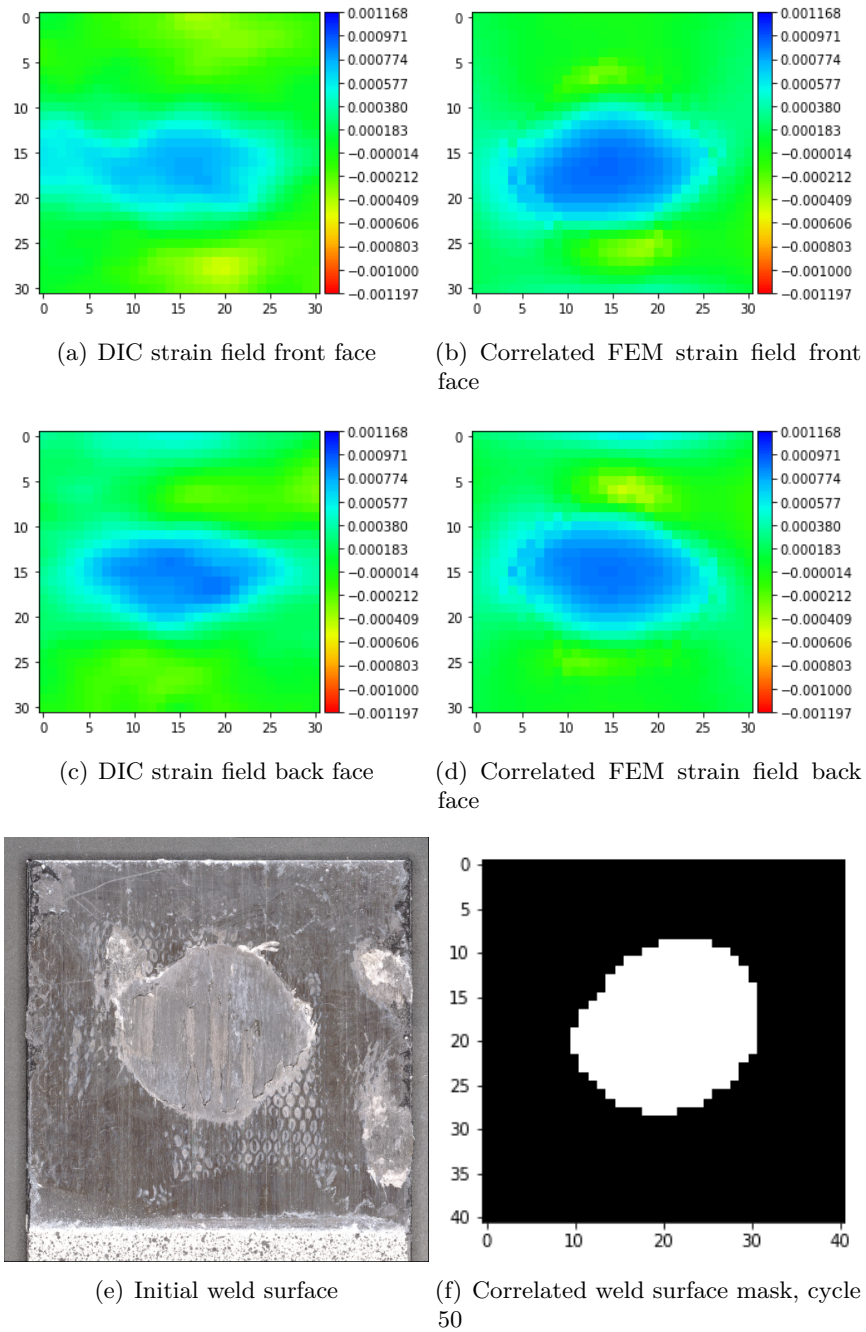


Figure E.1: DIC to FEM strain field correlation results for specimen 2, loading -cycle 50, longitudinal component (E11).

The measured strain field on the front face of the specimen, shown in figure E.1(a), is elongated towards the edge of the specimen. This may be caused by the secondary welds visible on the right side in figure E.1(e). Secondary welds were not accounted for when building the database of reference simulated strain fields. There is no simulation in the reference database that has a closer matching surface strain distribution.

The left side of figure E.2 shows real measurements of surface strain fields for specimen 2 after 2500 loading cycles, and a photograph of the fracture surface to aid in assessing the matched

result. The right side of figure E.2 shows correlated surface strain fields from the database of simulations, and the modelled weld surface which created them.

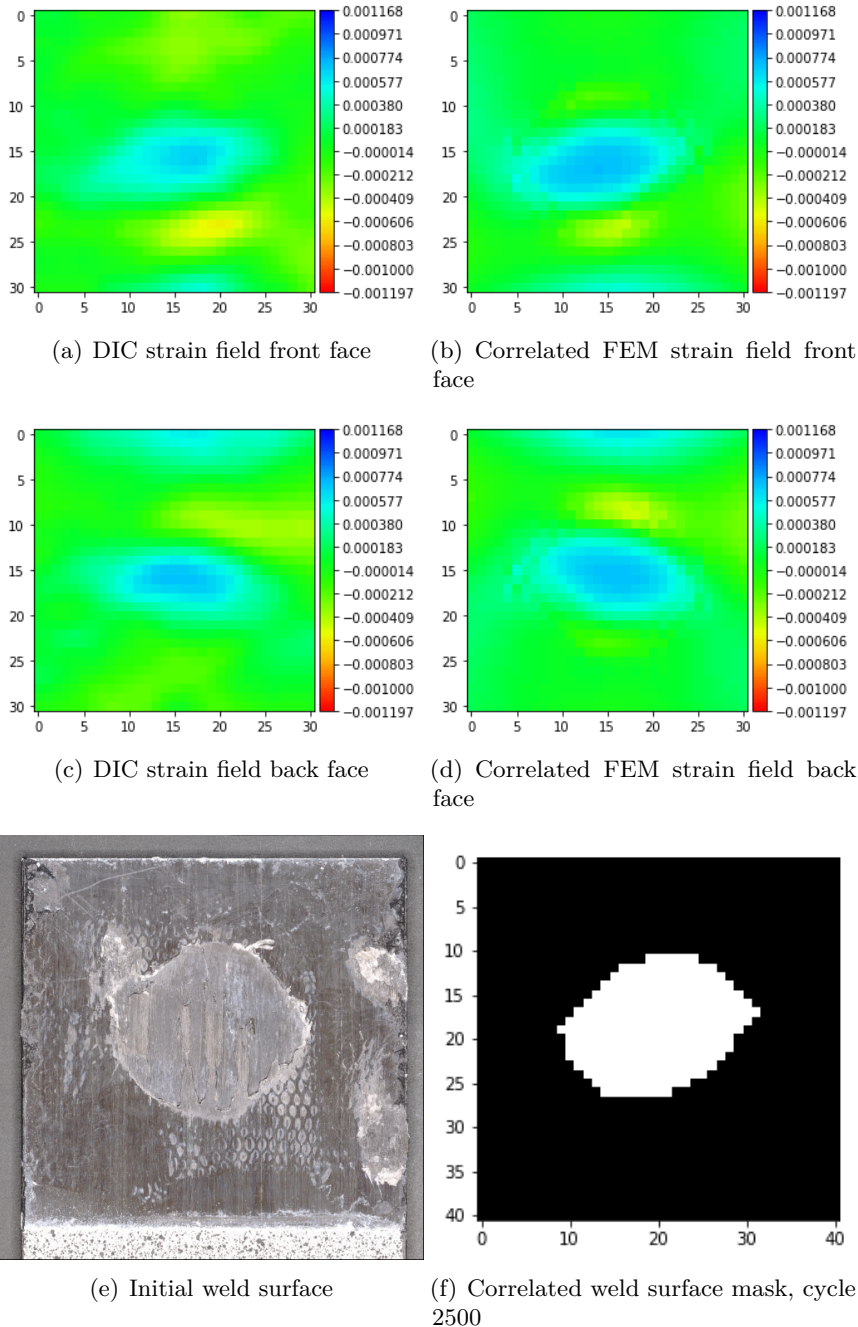


Figure E.2: DIC to FEM strain field correlation results for specimen 0730-25, loading cycle 2500, longitudinal component (E11).

By the 2500th loading cycle, the (usually weaker) secondary welds were very likely broken, which is the reason why the surface strain field no longer shows that unique elongation towards the side measured on the front face of the specimen. The correlated simulated strain fields show slightly larger strains, which may also be because the finite element simulations did not account for the presence of secondary welds at the start of the test. After the secondary welds broke,

the compliance of the real specimen increased, leading to a reduction in loading, as the test was displacement controlled.

Appendix F **Single wed spot specimen 4 (0730-24) analysis details**

The left side of figure F.1 shows real measurements of surface strain fields for specimen 4 after 50 loading cycles, and a photograph of the fracture surface. After only 50 loading cycles, when the first set of pictures were taken by the DIC systems, it is expected that the weld shape remained almost identical to the pristine shape of the weld, which can be approximated by the outer contour of the fracture surface. The right side of figure 5.9 shows correlated surface strain fields from the database of simulations, and the modelled weld surface which created them.

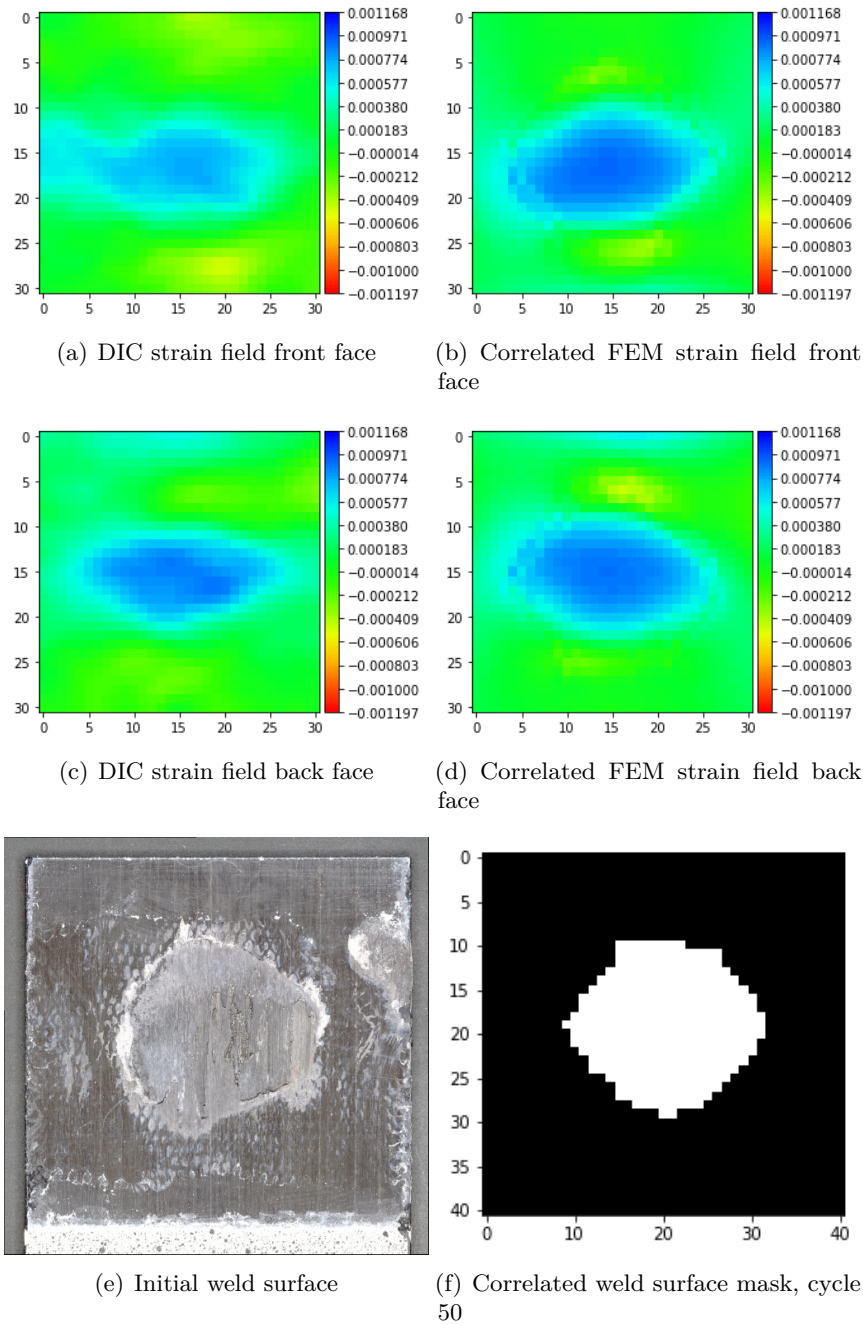


Figure F.1: DIC to FEM strain field correlation results for specimen 0730-24, loading cycle 50, longitudinal component (E11).

Similarly to the fracture surface of specimen 2, specimen 4 shows the presence of a secondary weld on the right side, seen in figure F.1(e). This secondary weld could be the reason why the first measured strain field on the front face of the specimen, shown in figure F.1(a), displays a similar elongation towards the side of the specimen as that shown in figure E.1(a) for specimen 2. Secondary welds have not been accounted for in the database of simulations, which could be the reason why none of the simulations display similar strain distributions.

The left side of figure F.2 shows real measurements of surface strain fields for specimen 4 after

2500 loading cycles, and a photograph of the fracture surface to aid in assessing the matched result. The right side of figure F.2 shows correlated surface strain fields from the database of simulations, and the modelled weld surface which created them.

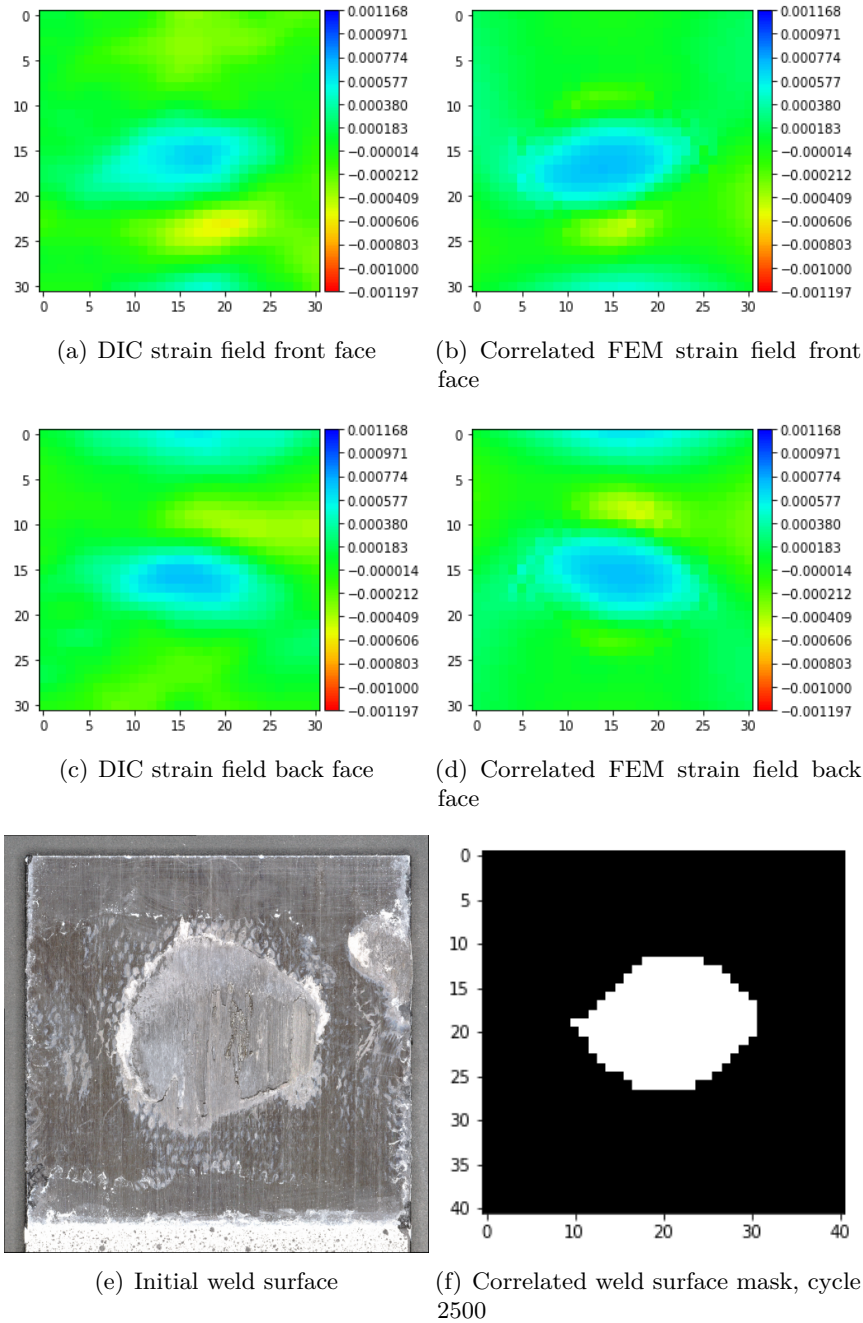


Figure F.2: DIC to FEM strain field correlation results for specimen 0730-24, loading cycle 2500, longitudinal component (E11).

Similarly to the discussion about specimen 2 in appendix E, by the 2500th loading cycle, the relatively weaker secondary weld had likely broken, which is why the surface strain field measured on the front side of the specimen no longer shows the elongation towards the specimen edge. Following a similar argument, about the load on the real specimen being lower after the secondary

weld broke, as in appendix E, the measured surface strains are slightly lower than the simulated ones because the loading used in the simulations was higher.